

Water Vapour in the Upper Troposphere and Lower Stratosphere

Proceedings of Water Vapour in the
Upper Troposphere and Lower Stratosphere Workshop,
Lancaster University, England
5th to 7th July 2005



Sponsors:
Upper Troposphere Lower Stratosphere Ozone Programme
Clouds, Water Vapour and Climate Programme

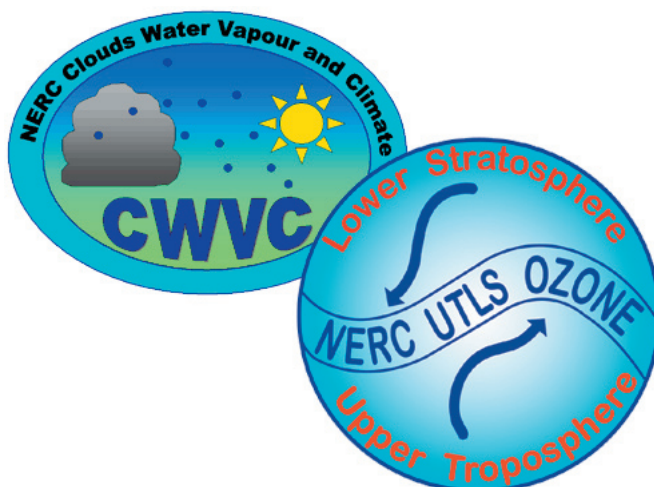
Foreward

Atmospheric water vapour measurements have been made by a variety of techniques for many years, but substantial uncertainties still remain (e.g. poor geographical coverage of radiosondes and poor vertical resolution of satellite observations). However, because water vapour plays such a dominant role in thermodynamic and radiative processes in the atmosphere, a good knowledge of its distribution is essential. For example, a major uncertainty lies in the precise nature of the water vapour feedback which occurs as the climate system seeks to respond to radiative forcing. Improved analysis and interpretation of existing measurements is a priority in order to improve our knowledge of water vapour distributions.

This collection of extended abstracts summarise presentations from a workshop on 'Water Vapour in the Upper Troposphere and Lower Stratosphere' held at Lancaster University on 5th to 7th July 2005. The papers cover a number of themes (Variability and Trends in the Upper Troposphere Lower Stratosphere (UTLS); Ice Supersaturation and the Relationship to Cloudiness; Observation Techniques; Radiation and Climate; Chemical Impacts; and Stratosphere-Troposphere Exchange) which underline the scientific importance of water vapour in many atmospheric processes.

This meeting attracted over 55 attendees including several overseas scientists, and as such it was apparent that improved understanding of atmospheric water vapour is a significant component of several UK research projects. The vitality of the meeting was assisted by six keynote speakers, Karen Rosenlof (NOAA), K. Gierens (DLR-Oberpfaffenhofen), Geraint Vaughan (University of Manchester), John Harries (Imperial College), Martyn Chipperfield (University of Leeds) and Peter Haynes (University of Cambridge). Thanks go to the Natural Environment Research Council's Upper Troposphere Lower Stratosphere Ozone (UTLS OZONE) and Clouds Water Vapour and Climate (CWVC) programmes for sponsoring this workshop.

Dr Keith Bower, Professor John Harries, Professor Robert Harwood, Professor Roderic Jones,
Miss Rebecca Penkett, Dr Helen Rogers and Professor Keith Shine
The Organising Committee



Organising Committee

Dr Keith Bower, Clouds, Water Vapour and Climate Programme, University of Manchester, England
Professor John Harries, Science and Atmospheric Physics Group, Imperial College, University of London, England
Professor Robert Harwood, Department of Meteorology, University of Edinburgh, Scotland
Professor Roderic Jones, Department of Chemistry, University of Cambridge, England
Miss Rebecca Penkett, Upper Troposphere Lower Stratosphere Ozone Programme, University of Cambridge, England
Dr Helen Rogers, Upper Troposphere Lower Stratosphere Ozone Programme, University of Cambridge, England
Professor Keith Shine, Department of Meteorology, University of Reading, England

Participants

Dr Steven Baughcum
Boeing Company, USA

Dr Keith Bower
University of Manchester, England

Dr Piero Cau
University of Reading, England

Dr Martyn Chipperfield
University of Leeds, England

Dr Hannah Clark
Meteo France, France

Miss Holly Coleman
Met Office, UK, England

Dr Olivier Dessens
University of Cambridge, England

Miss Louise Eden
University of Cambridge, England

Miss Annette Faux
Lancaster university, England

Dr Federico Fierli
ISAC - CNR, Italy

Mr William Flynn
University of Cambridge, England

Mr Tom Gardiner
National Physical Laboratory, England

Dr Anne Garnier
Service d'Aéronomie, CNRS, France

Dr Alan Geer
University of Reading, England

Dr Klaus Gierens
DLR Inst. for Atmospheric Physics, Germany

Mr Paul Gordon
Lancaster University, England

Prof. Joanna Haigh
Imperial College, England

Prof. John Harries
Imperial College, England

Prof. Bob Harwood
University of Edinburgh, Scotland

Prof. Peter Haynes
University of Cambridge, England

Dr Darren Hayton
Cardiff University, Wales

Dr Franz Immler
Alfred Wegener Institute for Polar and Marine Research, Germany

Mr Viju Oommen John
University of Bremen, Germany

Dr Roderic Jones
University of Cambridge, England

Dr ManojJoshi
Met Office, UK, England

Miss Elizabeth Kennett
Imperial College, England

Mr Sergey Khaykin
Central Aerological Observatory, Russia

Prof. David Lee
Manchester Metropolitan University, England

Dr Ling Lim
Manchester Metropolitan University, England

Dr Alexander Lukyanov
Central Aerological Observatory, Russia

Dr A. Rob MacKenzie
Lancaster University, England

Mr Paul Madden
Rolls Royce Plc, England

Dr Virginie Marècal
Laboratoire de Physique et Chimie de l'Environnement, CNRS, France

Dr Mark McCarthy
Met Office, UK, England

Dr John Methven
University of Reading, England

Ms Beatriz Monge Sanz
University of Leeds, England

Miss Nicola Patmore
Imperial College, England

Dr Edward Pavelin
Met Office, UK, England

Miss Rebecca Penkett
NERC UTLS OZONE, University of Cambridge, England

Dr Jean-Pierre Pommereau
Service d'Aéronomie, CNRS, France

Dr Hugh Pumphrey
University of Edinburgh, Scotland

Dr Gaby Rädcl
University of Reading, England

Dr Chuansen Ren
Lancaster University, England

Dr Howard Roscoe
British Antarctic Survey, England

Dr Karen Rosenlof
NOAA Aeronomy Laboratory, USA

Mrs Kate Samuelson
Lancaster University, England

Ms Harjinder Sembhi
University of Leicester, England

Mr Alex Shillings
University of Cambridge, England

Ms Andrea Stenke
DLR Institute for Atmospheric Physics, Germany

Dr David Stevenson
University of Edinburgh, Scotland

Mr Martin Streibel
European Ozone Research Coordinating Unit, University of Cambridge, England

Dr Claudia Stubenrauch
Laboratoire de Météorologie Dynamique, CNRS, France

Mr Tuomo Suortti
Finnish Meteorological Institute, Finland

Prof. Geraint Vaughan
University of Manchester, England

Dr Alison Waterfall
Rutherford Appleton Laboratory, England

Mr Lloyd Watkin
Cardiff University, England

Dr Jim Whiteway
York University, Toronto, Canada

Programme

Tuesday 5 July 2005

		Rapporteur: Tom Gardiner	Chair: Bob Harwood
Variability	K. Rosenlof	NOAA, USA	Changes in Stratospheric water vapour: Observations, uncertainties and possible mechanisms
	M. McCarthy	UKMO, Hadley Centre	Variability and trends in tropical upper tropospheric relative humidity
	E. Kennet	Imperial College	Lifetime of atmospheric water vapour
	P. Cau	University of Reading	Low humidity in the tropical and subtropical atmosphere
	A. Stenke	DLR, Germany	Simulated trends of water vapour in the UTLS between 1960 and 1999
	H. Pumphrey	University of Edinburgh	Upper troposphere / lower stratosphere data from the EOS MLS instrument on Aura.
	H. Roscoe	British Antarctic Survey	The lower stratospheric water vapour trend, 1950s to 1970s, revisited
	<i>Discussion</i>		

Wednesday 6 July 2005

		Rapporteur: Andrea Stenke	Chair: John Harries
Ice Supersaturation	K. Gierens	DLR, Germany	Ice supersaturation and the relationship to cloudiness
	J. Whiteway	York University, Canada	Measurements of humidity, turbulence and microphysics in middle latitude tropical cirrus
	C. Ren	Lancaster University	Tropical cirrus cloud modelling and tests in field campaigns
	F. Immler	Alfred Wegener Institute, Germany	Cirrus clouds and ice supersaturated regions observed by lidar and radiosonde
	G. Rädcl	University of Reading	Ice supersaturation and persistent contrail occurrence over Reading, UK
	A. Faux	Lancaster University	World War II bomber contrails: A study of aviation effects on climate
	C. Stubenrauch	CNRS, France	Thin cirrus and upper tropospheric humidity from TOVS Path-B: Natural variability and the impact of air traffic on cirrus coverage
	<i>Discussion</i>		

Wednesday 6 July 2005

Rapporteur: Gaby Radel			Chair: Rod Jones
Observations	G. Vaughan	University of Manchester	Recent Developments in observational techniques
	F. Fierli	ISCAC-CNR, Italy	Cloud and aerosol detection by balloon-borne lidar & laser back scattersonde in the UTLS during the HIBISCUS Campaign: Optical and dynamical properties
	T. Gardiner	National Physical Laboratory	Trace water vapour measurement and calibration
	S. Khaykin	Central Aerological Observatory, Russia	FLASH-B Lyman-alpha hygrosone for the UTLS: Instrument design, observations and comparison
	T. Suortti	Finish Meterological Institute	Preliminary results of the homogeneity assessment of the Vaisala radiosonde humidity records
	H. Sembhi	University of Leicester	Tropical tropopause layer water vapour and clouds observed by the MIPAS instrument
	V.O. John	University of Bremen, Germany	Analysis of upper tropospheric humidity measurements by microwave sounders and radiosondes
	<i>Discussion</i>		
Rapporteur: Hugh Pumphrey			Chair: Rob MacKenzie
Radiation and Chemistry	J. Harries	Imperial College	Observations and analysis of far IR emission and cooling in the upper troposphere
	W. Zhong	Imperial College	Radiative heating rates in tropical cirrus clouds
	J. Haigh	Imperial College	Solar influences on dynamical coupling between the stratosphere and troposphere
	<i>Discussion</i>		

Thursday 7 July 2005

Rapporteur: Hugh Pumphrey			Chair: Rob MacKenzie
Chemical Impacts	M. Chipperfield	University of Leeds	Water Vapour in the lower stratosphere: Issues and modelling studies
	O. Dessens	University of Cambridge	Potential impacts on the UTLS of water vapour emission from a supersonic fleet
	<i>Discussion</i>		
Rapporteur: Alison Waterfall			Chair: Keith Bower
Stratosphere Troposphere Exchange	P. Haynes	University of Cambridge	Trajectory-based studies of dehydration in the tropical tropopause region
	A. Lukyanov	Central Aerological Observatory, Russia	Trajectory studies of water vapour transport in the UTLS during the LAUTLOS campaign
	N. Patmore	Imperial College	A trajectory based investigation of tropopause moistening over the Asian summer monsoon
	V. Marécal	CNRS, France	UTLS water vapour budget from mesoscale simulations in the frame of the HIBISCUS project
	D. Stevenson	University of Edinburgh	A multimodel intercomparison of present day and near future global tropospheric ozone distributions, budgets and radiative forcing
	<i>Discussion</i>		

Contents

Variability	7
Changes in Stratospheric Water Vapour: Observations, Uncertainties and Possible Mechanisms: K.H. Rosenlof	8
Variability and Trends in Tropical Upper Troposphere Relative Humidity: M. McCarthy	12
Temperature Dependence of Atmospheric Moisture Lifetime: E.J. Kennett	14
Low Humidity in the Tropical and Subtropical Atmosphere: P. Cau	16
Simulated Trends of Water Vapour in the Upper Troposphere and Lower Stratosphere between 1960 and 1999: Results from a Transient Model Simulation with the CCM E39/C: A. Stenke	17
Upper Troposphere / Lower Stratosphere Data from the EOS MLS Instrument on Aura: H.C. Pumphrey	19
The Lower Stratospheric Water Vapour Trend, 1950s to 1970s, Revisited: H.K. Roscoe	20
Rapporteur's Summary: T. Gardiner	22
Ice Supersaturation	24
Ice Supersaturation and the Relationship to Cloudiness: K. Gierens	25
Tropical Cirrus Clouds Modelling and Tests in Field Campaigns: C. Ren	28
Cirrus Clouds and Ice Supersaturated Regions Observed by Raman Lidar and Radiosondes: F. Immler	29
Ice Supersaturation and Persistent Contrail Occurrence over Reading, UK: G. Rädcl	31
World War II Bomber Contrails: A Study of Aviation Effects on Climate: A. Faux	32
Thin Cirrus and Upper Tropospheric Humidity from TOVS Path-B: Natural Variability and Impact of Air Traffic on Cirrus Coverage: C.J. Stubenrauch	33
Rapporteur's Summary: A. Stenke	35
Observations	37
Recent Developments in Observational Techniques: G. Vaughan	38
Cloud and Aerosol Detection by Balloon-borne Lidar and Laser Backscatterometer in the UTLS during the HIBISCUS Campaign: Optical and Dynamical Properties: F. Fierli	40
Trace Water Vapour Measurements and Calibration: T. Gardiner	41
FLASH-B Lyman-Alpha Hygrometer for Upper Troposphere Lower Stratosphere: Instrument Design, Observations and Comparison: S. Khaykin	43
The Homogeneity of the Vaisala Radiosonde Humidity Records (Preliminary Results): T. Suortti	44
Tropical Tropopause Layer Water Vapour and Clouds Observed by the MIPAS Instrument: H. Sembhi	46
Analysis of Upper Tropospheric Humidity Measurements by Microwave Sounders and Radiosondes: V.O. John	47
Rapporteur's Summary: G. Rädcl	48
Radiation and Chemistry and Chemical Impacts	50
Observations and Analysis of Far IR Emission and Cooling in the Upper Troposphere: A Progress Report: J E Harries ..	51
Solar and Volcanic Influences on the Polar Annular Modes: J. Haigh	53
Water Vapour in the Lower Stratosphere: CCM Studies of Increased H₂O: M. Chipperfield	55
Emissions of Water Vapour from a Supersonic Fleet: Impact on the UTLS: O. Dessens	58
Rapporteur's Summary: H. Pumphrey	60
Stratosphere Troposphere Exchange	62
Trajectory-Based Studies of Dehydration in the Tropical Tropopause Region: P.H. Haynes	63
Trajectory Studies of Water Vapour Transport in the Upper Troposphere and Lower Stratosphere during the LAUTLOS Campaign: A. Lukyanov	66
A Trajectory-Based Investigation of Tropopause Moistening in the Asian Summer Monsoon Region: N. Patmore	68
Upper Troposphere Lower Stratosphere Water Vapour Budget from Mesoscale Simulations in the frame of the HIBISCUS Project: V. Marécal	69
The Influence of Future Climate Change on Tropospheric Ozone: D.S. Stevenson	71
Rapporteur's Summary: A. Waterfall	72

Variability

Changes in Stratospheric Water Vapour: Observations, Uncertainties and Possible Mechanisms

K.H. Rosenlof
NOAA Aeronomy Laboratory, Boulder, Colorado, USA

Introduction

Determining whether long-term increases in stratospheric water vapor have occurred is important given its radiative and chemical significance. Previous studies [Rosenlof et al., 2001; Oltmans et al., 2000] have shown an overall increase in stratospheric water vapor, of a magnitude sufficient to explain as much cooling in the lower stratosphere as ozone loss does [Forster and Shine, 1999]. The magnitude of the apparent increase in stratospheric water vapor is larger than what would be expected from the known tropospheric increase in methane, oxidation of which provides a significant chemical source of water vapor in the stratosphere [Oltmans et al., 2000]. Assessing what changes have occurred in stratospheric water vapor is important due to the potential impact on both radiative [Oinas et al., 2001; Smith et al., 2001; Langematz et al., 2003] and chemical [Evans et al., 1998; Tabazadeh et al., 2000; Dvortsov and Solomon, 2001; Stenke and Grewe, 2005] processes. Determining the cause for past changes in stratospheric water vapor is needed to assess what future changes may be expected.

Estimating water vapour trends

Stratospheric water vapour measurements have not been taken continuously at any one location or with any one technique for an extended period of time. It turns out to be quite difficult to determine past trends. Figure 1 shows several sets of water vapour data at northern hemisphere mid-latitudes. Although, as noted Kley et al. [2000], there is an overall increase when one looks at instrumental records separately, there is a problem with simply combining all the data into one time series, as there are uncertainties in the measurements on the order of the trends. Kley et al. [2000] also noted disagreements between different instruments on the order of 10-30%, with percentage differences the largest in the hygropause region. These differences exceeded the stated instrumental uncertainties for the individual instruments. Current measurements show significant differences between measurement systems persist; Figure 2 shows comparisons from 4 measurement days. Two of the days show significant differences (January and November 2004), while agreement is better for the January 2000 and September 2004 cases, although there is still a 1-ppmv spread in measurements in the lower stratosphere.

Although it would be useful to know past trends in stratospheric water vapour from a global perspective, sufficient data only exist since the launch of specialized satellites. To examine global changes in stratospheric water vapor, it is possible to use the UARS HALOE record that starts in the early 1990s [Russell et al., 1995]. To infer earlier changes, we can compare the global record since the early 1990s to that taken in Boulder, Colorado (at 40°N) with research quality frost point balloon measurements [Oltmans, 1985]. Using other satellite measurements, for example SAGE and LIMS, we can examine seasonal and spatial variability of stratospheric water vapor, but cannot do trend analysis.

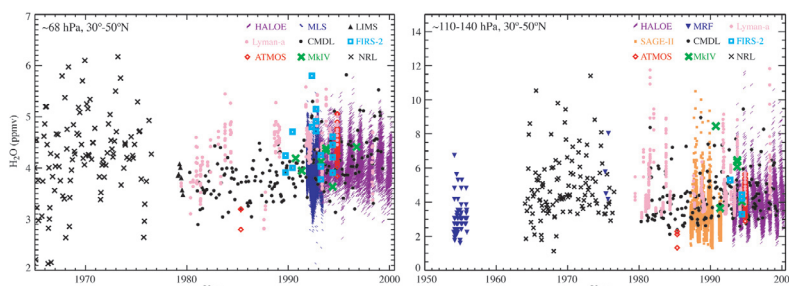


Figure 1: The left panel shows data from in situ and remote samplers at 68 hPa, while the right panel shows the same for the layer 110-140 hPa. Both panels are for Northern Hemisphere mid latitudes. These data show upward trends in different data sets through the mid 1990s, then a leveling off.

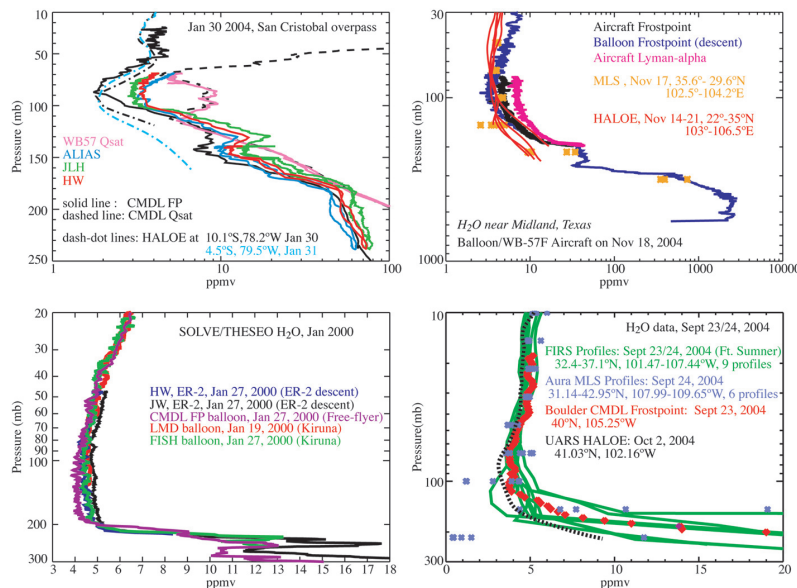


Figure 2: Comparison between water vapour profile measurements. Top left is in the tropics; top right and bottom right are in the mid latitudes; bottom left is at high latitudes.

Figure 3 shows global trends estimated from the HALOE record. Above 10 hPa, there are hemispheric differences in the linear changes of water and methane, with the Northern Hemisphere water vapour increasing at a greater rate than the Southern Hemisphere. There is a compensating offset with the methane changes, with greater decreases in the Northern Hemisphere above 10 hPa. The straight correlation coefficient for the methane and water vapor linear fit coefficients in the altitude region 1-10 hPa is -0.898; an area-weighted correlation is -0.917. Figure 4 shows the anomaly time series for $2xCH_4+H_2O$ for the layer 1-10 hPa. Individual monthly averages are shown as symbols, a layer averaged smoothed line is also shown. The quantity $2xCH_4+H_2O$ shows an increase for the period 1992 to 1996 (-0.4 ppmv), then a leveling off. The large constituent change at the beginning of the record appears to be a combination of a change in circulation strength, in that methane decreases and water increases, and a change in the net transport of $2xCH_4+H_2O$ into the middle and upper stratosphere [Rosenlof, 2002]. Figure 5 shows a comparison of HALOE and Boulder CMDL data. Overall, agreement is rather good, with some deviation after 2002 in the upper level. The reason for the difference is not understood at this time [Randel et al., 2004].

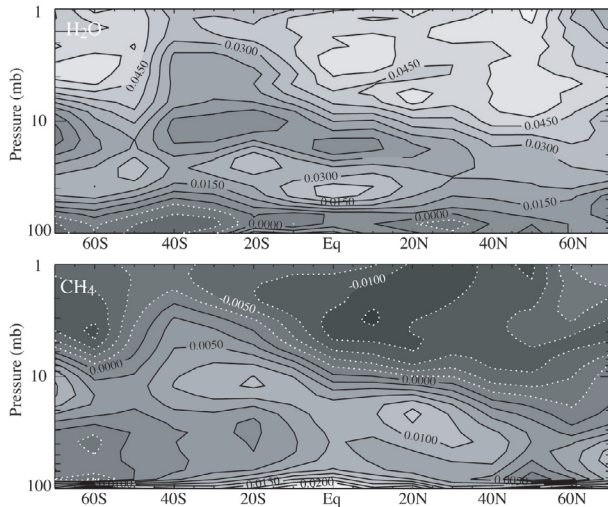


Figure 3: Linear changes (ppmv/yr) for the period April 1992 through April 2001 for HALOE water vapor (top panel), and methane (bottom panel). At most latitudes, linear changes are not significant below 70 hPa. Figure from Rosenlof [2002].

fraction of air that enters the stratosphere by bypassing the coldest part of the tropics, possibly associated with changes in the summertime monsoon.

An examination of the first possibility, a change in tropical temperatures, yields a trend of the wrong sign. Figure 6 shows an average of cold-point and 100 hPa temperatures from 65 operations radiosonde stations. Note that for both traces on the plot, there has been an apparent decrease since 1980, with the cold-point downward trend of $-0.09(\pm 0.01)$ deg/yr. Surface methane has changed (Figure 7), but not enough to explain the water vapor trends implied by the Northern Hemisphere mid latitude historical record (of $\sim 1\%/yr$). There may have been a change in the efficiency of methane oxidation [Röckmann et al., 2004]. But, even assuming complete efficiency in the methane increase, the net sum of what are believed to be the relevant processes does not add up. In short:

- $\Delta H_2O_{midlat(1980-2000)}$ $\sim +1$ ppmv
- $\Delta 2CH_4_{global\ surface}$ $\sim +0.25$ ppmv
- $\Delta tropical\ cold-point\ qsat$ ~ -1.5 ppmv

The changes do not balance, and it is possible that there have been some stratospheric circulation changes [Rosenlof, 2002] or changes in the monsoon circulation impacting stratospheric entry of water vapor. Modeling will be needed to fill in the gaps, as there is not sufficient continuous global stratospheric water and methane data over the 1980-present period.

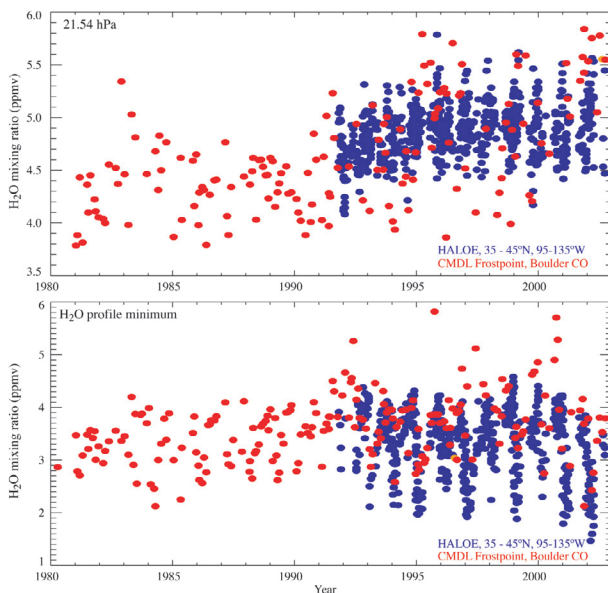


Figure 5: Time series of HALOE data filtered to be near Boulder (blue) and CMDL frost point balloon data at Boulder (red) in the middle stratosphere (top) and at the hyropause.

Figure 6: Temperatures at the cold point (black) and 100 hPa (red) for 65 operational radiosonde stations between 20°S and 20°N.

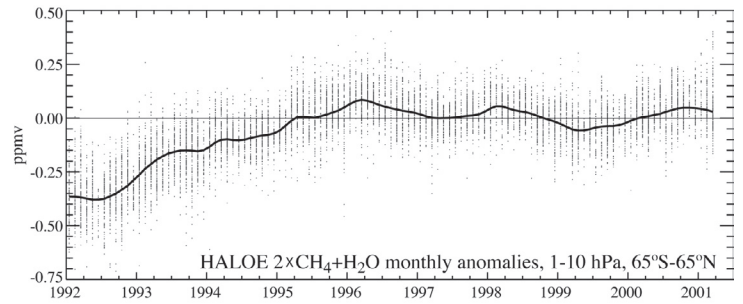


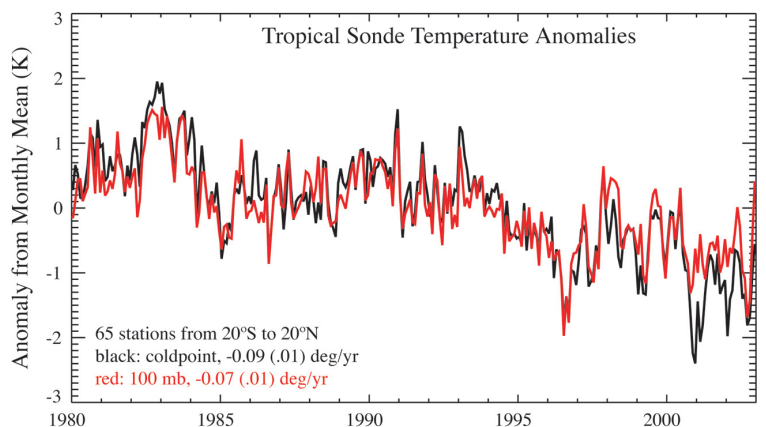
Figure 4: Time series of monthly anomalies for HALOE $2 \times CH_4 + H_2O$. Points are plotted for all measurements between 1 and 10 hPa and 65°S to 65°N latitude. The solid line is a 3-month median smooth of the monthly anomalies.

Mechanisms

Assuming a long-term increase in stratospheric water vapor exists, it is interesting to examine possible reasons for such an increase. On long-time scales, possible drivers could be 1) a change in tropical near tropopause (cold-point) temperatures; 2) a change in the surface methane source; 3) a change in circulation that either alters the flux of methane into the stratosphere or the length of time that individual parcels remain in the stratosphere; or 4) a change in the

Recent changes in stratospheric water vapour

An interesting recent phenomenon is a decrease in stratospheric water vapour that has persisted since late 2000. Shown in Figure 8 are water vapour anomalies in the tropical lower stratosphere. Note the low values starting in the end of 2000, and persisting to the present. Figure 9 shows water vapour plots for two satellite instruments in the tropics and from a polar observing satellite at high latitudes in both hemispheres. The decreases are apparent for both tropical observations, and also at high northern latitudes. There is also evidence for the late 2000 decrease in the CMDL data shown in the bottom panel of Figure 5. The feature appears quite robust. It is apparently a consequence of a drop in tropical temperatures that is seen in the tropical radiosonde cold-point temperatures (Figure 6, black line) but not evident in the 100-hPa temperatures as well (Figure 6, red line).



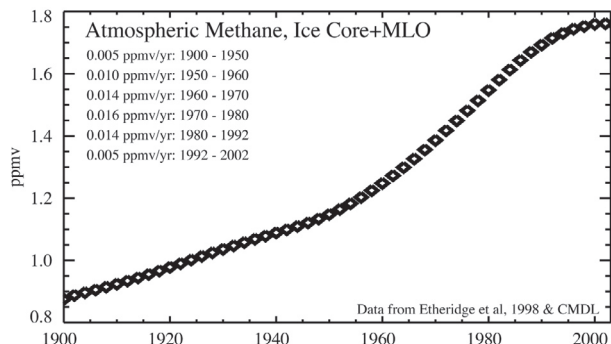


Figure 7: Historical surface methane record from ice core observations reported in Etheridge et al. [1998] extended with global averages from CMDL.

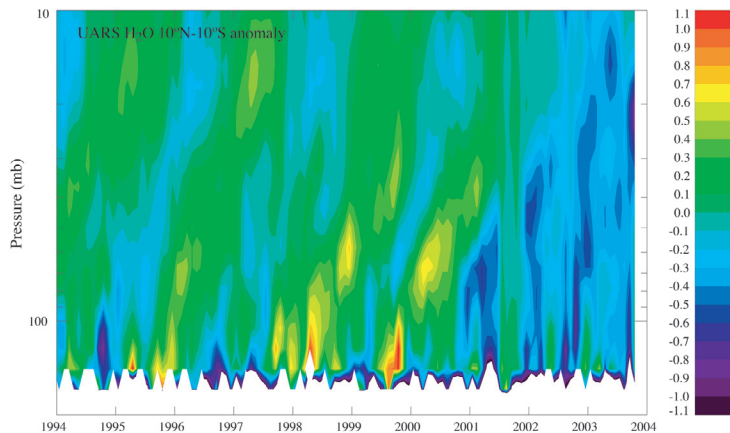


Figure 8: Tropical anomalies in HALOE water vapour. Note the change in character at the end of 2000.

Figure 10 shows the tropopause temperatures from the NCAR-NCEP reanalysis and the tropical 82-hPa HALOE water vapour data. There is a high degree of lag correlation, with water vapour lagging temperature by 1-2 months. The drop in water vapour near the end of 2000 is -0.5 ppmv. The drop in NCEP tropopause temperatures is $1-1.5^\circ$. The UARS-UKMO assimilation also shows a similar feature (Figure 11), with a drop in tropical temperatures over a narrow altitude region (70 - 150 hPa) of $1-2^\circ$. The saturation vapour mixing ratio for a temperature of 192K at 90 hPa is ~ 5 ppmv. Dropping the temperature by 1K then gives a value of ~ 4.3 ppmv. A $1-2^\circ$ temperature drop does a reasonable job at explaining the observed water vapour decrease at the end of 2000.

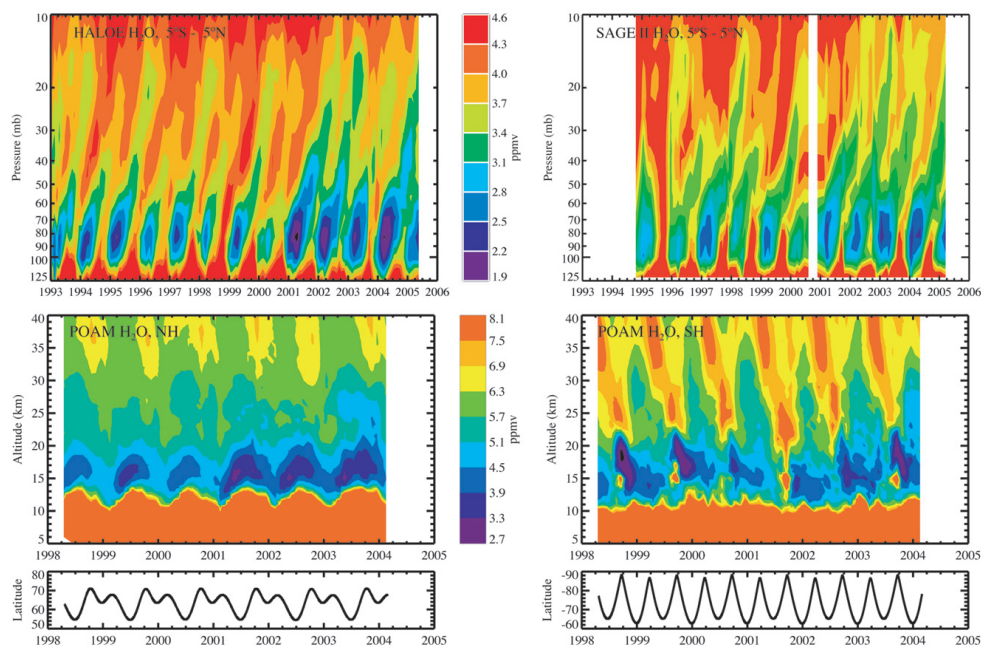


Figure 9: Tropical water vapour from HALOE (top left) and SAGE II (top right). High-latitude water vapour from POAM in the Northern Hemisphere (bottom left) and Southern Hemisphere (bottom right).

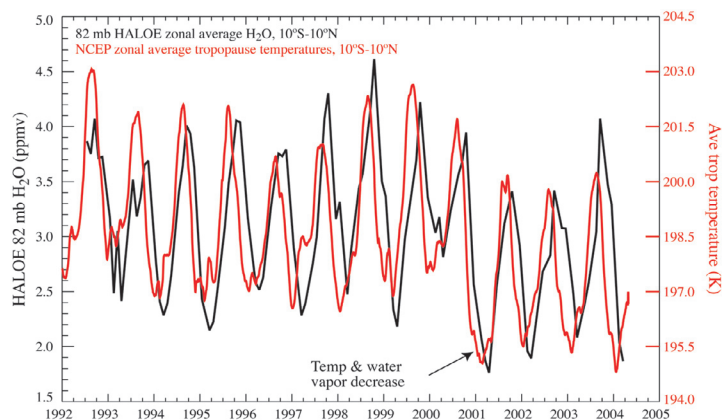


Figure 10: Time series of 82 hPa HALOE water vapour in the tropics (black) and NCEP tropical tropopause temperatures (red). Both are zonally averaged. Note the ~ 2 month time lag between the two traces, and the high correlation. At the end of 2000 there is a drop in both tropical tropopause temperatures, and lower stratospheric tropical water vapour.

Summary

There is evidence for an increase in stratospheric water vapour over the period 1980-1996, and a little change between 1996-2000, then a significant decrease after late 2000. Reasons for the 1980-1996 increase are not well understood. The decrease at the end of 2000 is apparently due to changes in temperature near the tropical tropopause. What is not yet understood is the driving mechanism for the temperature decrease.

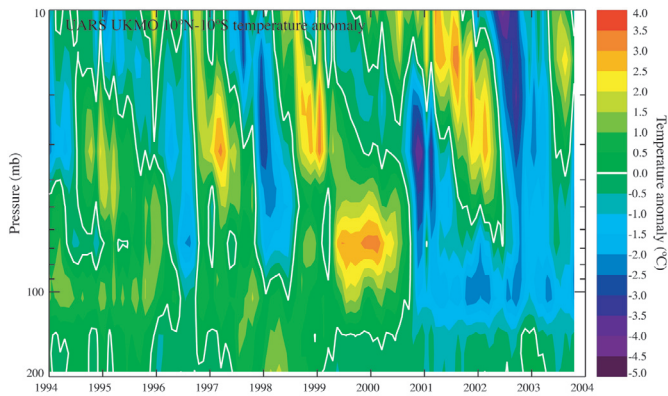
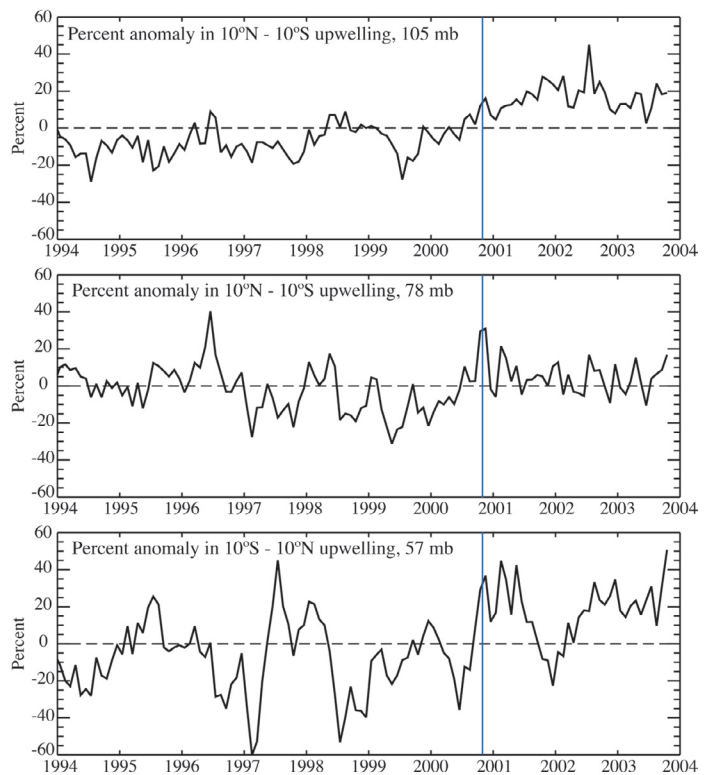


Figure 11: UARS UKMO assimilation temperatures anomalies in the tropics ($^{\circ}\text{C}$). The zero contour is shown with the thick white line. Note the narrow altitude region of temperature decrease starting the end of 2000.

Figure 12: Time series of the anomaly (taken from 10-year monthly averages) in the tropical (10°S - 10°N) upwelling mass flux at 3 levels: near the tropopause at 105 hPa (top), at 78 hPa (middle) and at 57 hPa (bottom). Estimates were made using a radiative heating calculation with UKMO temperatures and UARS constituents as input. The blue line notes where significant changes in tropical water vapour occurred.



References

- Dvortsov, V.L. and S. Solomon, Response of the stratospheric temperatures and ozone to past and future increases in stratospheric humidity, *J. Geophys. Res.*, 106, 7505-7514, 2001.
- Etheridge, D.M., L.P. Steele, R.J. Francey and R.L. Langenfelds, Atmospheric methane between 1000 AD and present: Evidence of anthropogenic emissions and climatic variability, *J. Geophys. Res.*, 103, 15979-15993, 1998.
- Evans, S.J., R. Toumi, J.E. Harries, M.P. Chipperfield and J.M. Russell III, Trends in stratospheric humidity and the sensitivity of ozone to these trends, *J. Geophys. Res.*, 103, 8715-8725, 1998.
- Forster, P. M. de F. and K.P. Shine, Assessing the climate impact of trends in stratospheric water vapor, *Geophys. Res. Lett.*, 29, 2002.
- Kley, D., J.M. Russell III and C. Phillips, 2000, SPARC assessment of upper tropospheric and stratospheric water vapour, WCRP #113, WMO/TD #1043, SPARC Report #2.
- Langematz, U., M. Kunze, K. Kruger, K. Labitzke and G.L. Roff, Thermal and dynamical changes of the stratosphere since 1979 and their link to ozone and CO_2 changes, *J. Geophys. Res.*, 108, 4027, doi:10.1029/2002JD002069, 2003.
- Nedoluha, G.E., R.M. Bevilacqua, R.M. Gomez RM, B.C. Hicks, J.M. Russell III and B.J. Connor, An evaluation of trends in middle atmospheric water vapor as measured by HALOE, WYMS, and POAM, *J. Geophys. Res.*, 108, 4391, doi:10.1029/2002JD003332, 2003.
- Oinas, V., A.A. Lacis, D. Rind, D.T. Shindell and J.E. Hansen, Radiative cooling by stratospheric water vapor: big differences in GCM results, *Geophys. Res. Lett.*, 28, 2791-2794, 2001.
- Oltmans, S.J., Measurements of water vapor in the stratosphere with a frost point hygrometer, in: *Measurement and Control in Science and Industry, Proc. 1985 International Symposium on Moisture and Humidity*, Washington D.C., Instrument Society of America, 251-258, 1985.
- Oltmans, S.J., H. Vömel, D.J. Hofmann, K.H. Rosenlof and D. Kley, The increase in stratospheric water vapor from balloonborne, frostpoint hygrometer measurements at Washington, D.C., and Boulder, Colorado, *Geophys. Res. Lett.*, 2, 3453-3457, 2000.
- Randel, W.J., F. Wu, S.J. Oltmans, K. Rosenlof, G. E. Nedoluha, Interannual changes of stratospheric water vapor and correlations with tropical tropopause temperatures, *J. Atmos. Sci.*, 61, 2133-2148, 2004.
- Röckmann, T., J.-U. Groöß and R. Müller, The impact of anthropogenic chlorine emissions, stratospheric ozone change and chemical feedbacks on stratospheric water, *Atmos. Chem. Phys.*, 4, 693-699, 2004.
- Rosenlof, K.H., Transport changes inferred from HALOE water and methane measurements, *J. Met. Soc. Japan*, 80, 831-848, 2002.
- Rosenlof, K.H., S.J. Oltmans, D. Kley, J.M. Russell, E.W. Chiou, W.P. Chu, D.G. Johnson, K.K. Kelly, H.A. Michelsen, G.E. Nedoluha, E.E. Remsburg, G.C. Toon and M.P. McCormick, Stratospheric water vapor increases over the past half-century, *Geophys. Res. Lett.*, 28, 1195-1198, 2001.
- Russell III, J.M., L.L. Gordley, J.H. Park, S.R. Drayson, D.H. Hesketh, R.J. Cicerone, A.F. Tuck, J.E. Frederick, J.E. Harries and P.J. Crutzen, The Halogen Occultation Experiment, *J. Geophys. Res.*, 98, 10,777-10,797, 1993.
- Smith, C.A., J.D. Haigh and R. Toumi, Radiative forcing due to trends in stratospheric water vapour, *Geophys. Res. Lett.*, 28, 179-182, 2001.
- Stenke, A. and V. Grewe, Simulations of stratospheric water vapor trends: Impact on stratospheric ozone chemistry, *Atmos. Chem. Phys.*, 5, 1257-1272, 2005.
- Tabazadeh, A., M.L. Santee, M.Y. Danilin, H.C. Pumphrey, P.A. Newman, P.J. Hamill and J.L. Mergenthaler, Quantifying denitrification and its effect on ozone recovery, *Science*, 288, 1407-1411, 2000.

Variability and Trends in Tropical Upper Troposphere Relative Humidity

M. McCarthy

Met Office, Hadley Centre for Climate Prediction and Research, England

Our ability to diagnose the variability of tropospheric humidity over large space and time scales is severely hampered by the lack of a globally complete, long term set of high quality observations. As a result there is still considerable uncertainty in future climate projections because of the uncertainty relating to water vapour and cloud feedbacks.

Here we review variability and trends in UTRH in the tropics from an inter-satellite bias-corrected Upper Tropospheric Relative Humidity (UTRH) product from the High Resolution Infra-Red Sounder (HIRS) channel 12 [Bates et al., 2001], and a selection of radiosonde humidity records. These are compared with an ensemble of runs of version HadAM3 of the Hadley Centre atmosphere-only climate model forced with observed Sea Surface Temperatures (SST).

Climatology and Inter-annual Variability

The magnitude and distribution of systematic biases between the HIRS UTRH and HadAM3 equivalent weighted UTRH can be reasonably well explained by a known dry-bias in HIRS resulting from the necessary cloud-clearing [Lanzante and Gahrs, 2000], and known overestimation of the overturning tropical circulation in HadAM3 [Pope et al., 2000]. Comparison with radiosondes in the tropical Pacific suggest that the free troposphere in the model is cooler and wetter with a weaker trade stable layer, than the observations would suggest.

From Figure 1 we see that there is high correlation between the model and observations in regions where the model predicts strong association to the external forcing on inter-annual time scales. Elsewhere the model suggests that the variability is largely unpredictable stochastic noise, and accordingly shows little relation to the observations.

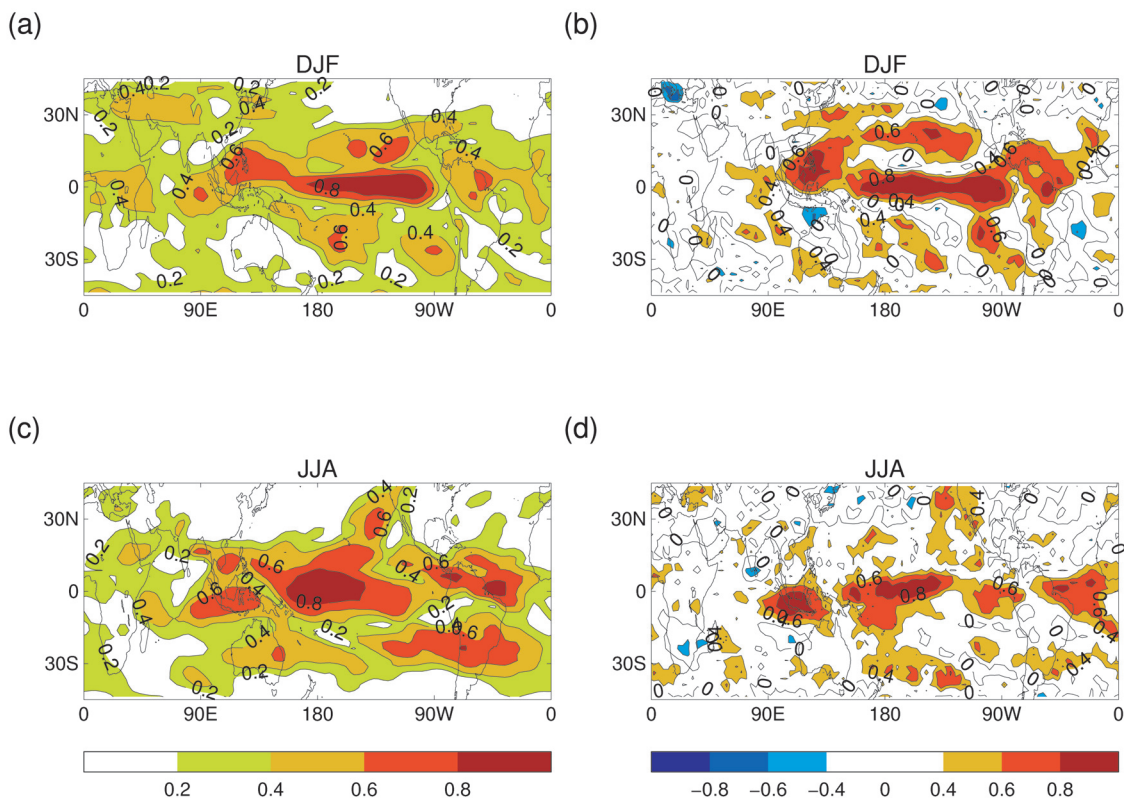


Figure 1: Fraction of inter-annual variance related to external forcing in HadAM3 in (a) December - February (DJF) and (c) June-August (JJA). Field correlation between HadAM3 and HIRS UTRH for (b) DJF and (d) JJA. Observed Sea Surface Temperature (SST) records are the dominant forcing in the HadAM3 ensemble. Model data have been converted to a UTRH equivalent from a weighted average of the relative humidity profile.

Linear Trends

Figure 2 shows linear trends in zonal mean UTRH from HIRS and HadAM3. While the trend in the global or tropic-wide UTRH are close to zero in both observation and model, the observations suggest there have been significant changes in regional UTRH in that time.

Intuitively one might interpret an increase in UTRH near the equator and decreases in the subtropics as relating to an intensification of the tropical Hadley circulation [Chen et al, 2002]. Closer inspection however reveals that the equatorial and subtropical trends are not contemporaneous (not shown) and therefore do not fit with this simple interpretation. Despite the attempt at inter-satellite calibration there is no comprehensive assessment of the uncertainty in these trend estimates beyond the statistical fit uncertainty. The sharpest increases in UTRH near the equator also coincide with a poorly characterised satellite transition over the NOAA-9 period in the latter half of the 1980s.

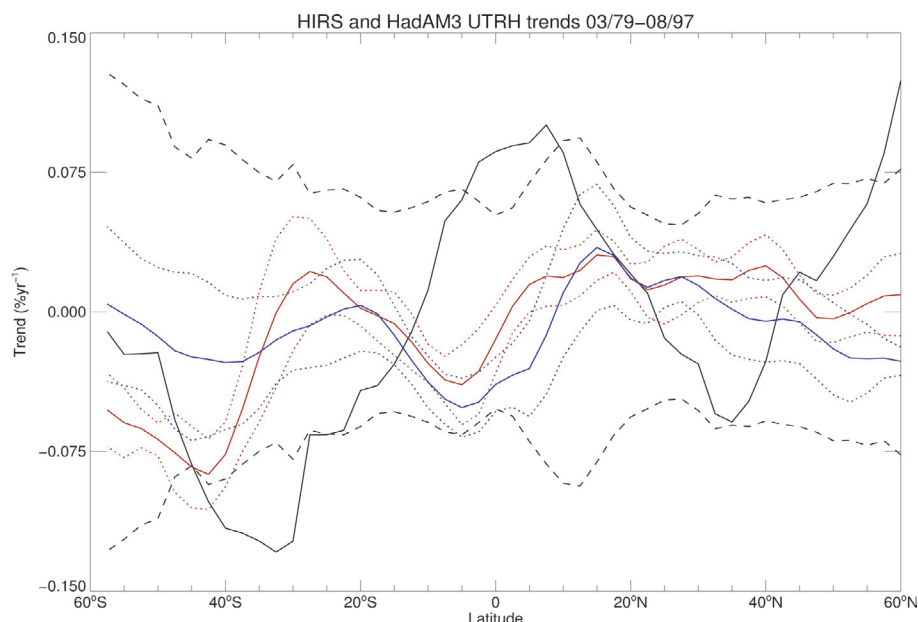


Figure 2: Trends in zonal mean UTRH from HIRS (black), HadAM3 forced with SST and natural forcings, i.e. solar and volcanic (blue), and HadAM3 forced with SST, natural, and anthropogenic, i.e. greenhouse gases, ozone, and sulphate aerosols (red). Dotted lines represent one standard deviation of the ensemble spread for the model data. Dashed lines indicate the 95% significance level for the HIRS data.

A selection of high-quality tropical island radiosonde sites in the West Pacific have also been assessed for linear trends over the period 1973-1995, when no major changes to instrumentation were introduced. At 300hPa, HadAM3 shows linear trends in water vapour mixing ratio three times the magnitude of the radiosondes in these locations. Although the observational uncertainty needs to be better constrained it is unlikely that observational uncertainty alone can explain the model-observation discrepancy.

Uncertainties

In order to fully characterise the uncertainty in long-term climate data records we need to consider the structural uncertainty, i.e. the uncertainty that arises through fundamental methodological choices made in the data set creation. In other words we ask the question, how sensitive are trend estimates to the bias-correction procedures employed?

There is evidence that this structural uncertainty is the largest source of error for climate change detection in the upper atmosphere [Thorne et al., 2005]. It is important that we obtain multiple realisations of data sets using independently developed homogenisation techniques. Humidity observations require at least the level of scrutiny as has been afforded the Microwave Sounding Unit (MSU) measurements of tropospheric and stratospheric temperature.

While most models show little decadal variability in relative humidity and outgoing longwave radiation, lapse rate and water vapour feedbacks are not consistent between models [Allan et al., 2002]. HadAM3 finds trends of greater than 0.4K per decade in tropical upper tropospheric temperatures for 1979-1998, and associated trends in water vapour mixing ratio of 5% per decade maintaining UTRH at a constant level. Temperature trends estimated from radiosondes and some Microwave Sounding Unit records suggest the possibility of little or no warming since 1979.

Summary

We cannot comprehensively validate simulations of recent climate change in the upper troposphere. No existing observational data sets support the profile of change in HadAM3. Uncertainties in historical water vapour data sets may yet prove to be too large for trend detection. Ongoing analysis of the radiosonde and Infra-Red sounders are required, with an emphasis on quantifying their structural uncertainty. Continuation of these records into the future is also required.

The future observing network should be multi-variate, fully integrated, long term and committed to the GCOS monitoring principles. More intelligent design of the network could greatly improve climate monitoring capabilities, and at the least improve instrument calibration, going into the future.

References

- Allan, R.P., V. Ramaswamy and A. Slingo, A diagnostic analysis of atmospheric moisture and clear-sky radiative feedback in the Hadley Centre and GFDL climate models, *J. Geophys. Res.*, 107(D17), 4329-4335, 2002.
- Bates, J.J., D.L. Jackson, F.M. Breon and Z.D. Bergen, Variability of tropical upper troposphere humidity 1979-1998, *J. Geophys. Res.* 106, 32271-32281, 2001.
- Chen, J., B.E. Carlson and A.D. Del Genio, Evidence for strengthening of the tropical general circulation in the 1990s, *Science*, 295, 841-844, 2002.
- Lanzante, J.R. and G.E. Gahrs, The clear-sky bias of TOVS upper-tropospheric humidity, *J. Clim.*, 13, 4034-4041, 2000.
- Pope, V.D., M.L. Gallani, P.R. Rowntree and R.A. Stratton, The impact of new physical parametrizations in the Hadley Centre climate model - HadAM3, *Climate Dyn.* 16, 123-146, 2000.
- Thorne, P.W., D.E. Parker, J.R. Christy and C.A. Mears, Uncertainties in climate trends: lessons from upper-air temperature records, *Bull. Am. Meteorol. Soc.*, in press, 2005.

Temperature Dependence of Atmospheric Moisture Lifetime

E.J. Kennett and R. Toumi
Physics Department, Imperial College, London, England

Precipitation largely feeds on moisture already in the column [Trenberth, 1998], which suggests that the atmospheric moisture budget can be described by a first order loss process, characterised by a lifetime. In this study, we use the European Centre for Medium-Range Weather Forecasts 40-year Reanalysis (ERA40) dataset in order to investigate the temperature dependence of atmospheric moisture lifetime. We also independently derive lifetimes based on aircraft microphysical measurements in cirrus clouds. We find that the most rapid loss of moisture and a corresponding minimum in water vapour scale height occurs near the -40°C level.

The continuity equation for atmospheric moisture can be expressed as:

$$\partial W/\partial t = -\mathbf{v}\cdot\nabla W - \lambda W$$

where W is total water, \mathbf{v} is the velocity vector, λ is the local rate coefficient for first order loss in W , and $1/\lambda$ is the local atmospheric moisture lifetime. Atmospheric moisture lifetime is found to vary significantly with temperature in the column. For example, over the Indian monsoon region ERA40 shows lifetimes within the column varying by greater than a factor of 4 (Figure 1). Globally, the shortest lifetimes occur at temperatures of about -40°C , with mean lifetimes of just over a day at this level (Figure 2). Lifetimes derived independently from aircraft measurements in cirrus clouds confirm a maximum in the loss rate coefficient λ at -40°C , with a dramatic decrease in λ as the temperature falls below this value (Figure 3). This can be understood to result from changes in the rate of nucleation of ice combined with a reduction in ice particle size with decreasing temperature. In particular at about -40°C , there is a transition in nucleation mechanism and ice particle size due to the absence of supercooled water below this temperature.

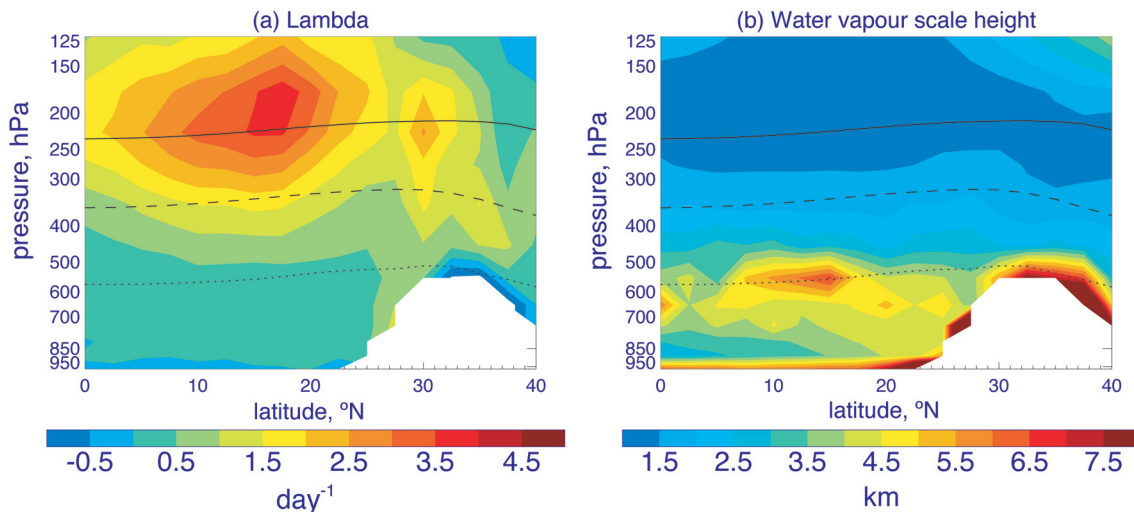


Figure 1: Vertical profile of ERA40 JJA 1979-1998 mean (a) λ and (b) water vapour scale height, averaged across the zonal band $90\text{-}95^{\circ}\text{E}$. Negative λ values correspond to regions of strong turbulent mixing, which is not included in the analysis. Regions below the surface are masked in white. The 0°C , -23°C and -45°C temperature contours are shown as dotted, dashed and solid black lines respectively.

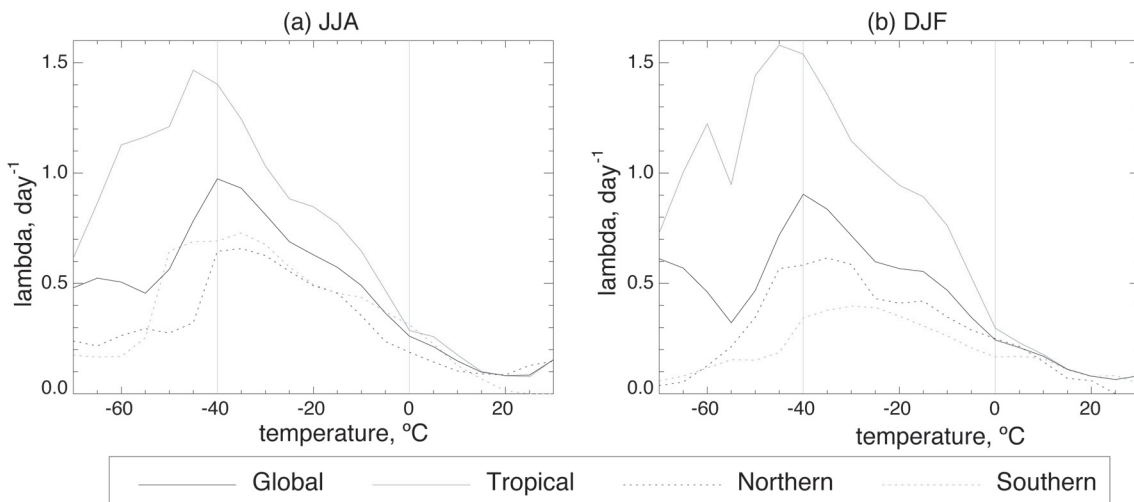


Figure 2: Temperature dependence of λ for (a) June, July and August; and (b) December, January and February, in ERA40 1979-1998. Plotted are mean values, for positive monthly λ values only, in each 5°C temperature interval, globally and for tropical ($30^{\circ}\text{S}\text{-}30^{\circ}\text{N}$), northern (30°N to 90°N) and southern (30°S to 90°S) latitudes.

A similar temperature dependence is observed in water vapour scale height in ERA40, with the lowest water vapour scale heights globally coinciding with the -40°C isotherm (Figure 4). At -40°C , there is a shift in behaviour from constant relative humidity at higher temperatures, to increasing relative humidity as the temperature falls below this value. Folkins et al. [2002] proposed a simple explanation for the increase in relative humidity at upper levels, however this would not predict the -40°C temperature dependence found here, which holds globally and appears to originate from cloud microphysics. The variability of atmospheric moisture lifetime with temperature is found to be a fundamental microphysical control on the distribution of water vapour.

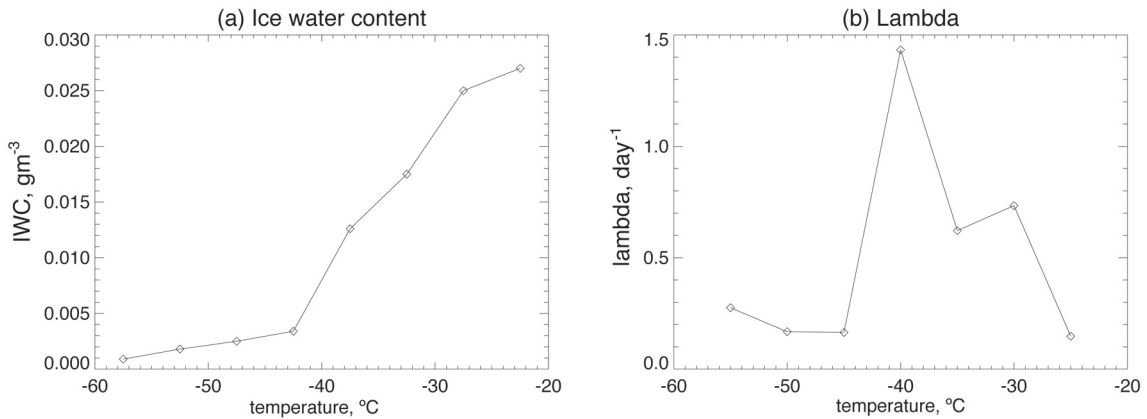


Figure 3: Temperature dependence of (a) ice water content (IWC) and (b) λ calculated from aircraft measurements in cirrus clouds [Heymsfield and Platt, 1984]. λ was calculated using the empirical relationship for precipitation rate R ($\text{kgm}^{-2}\text{s}^{-1}$) = $\text{IWC}1.17/1000$ [Heymsfield, 1977].

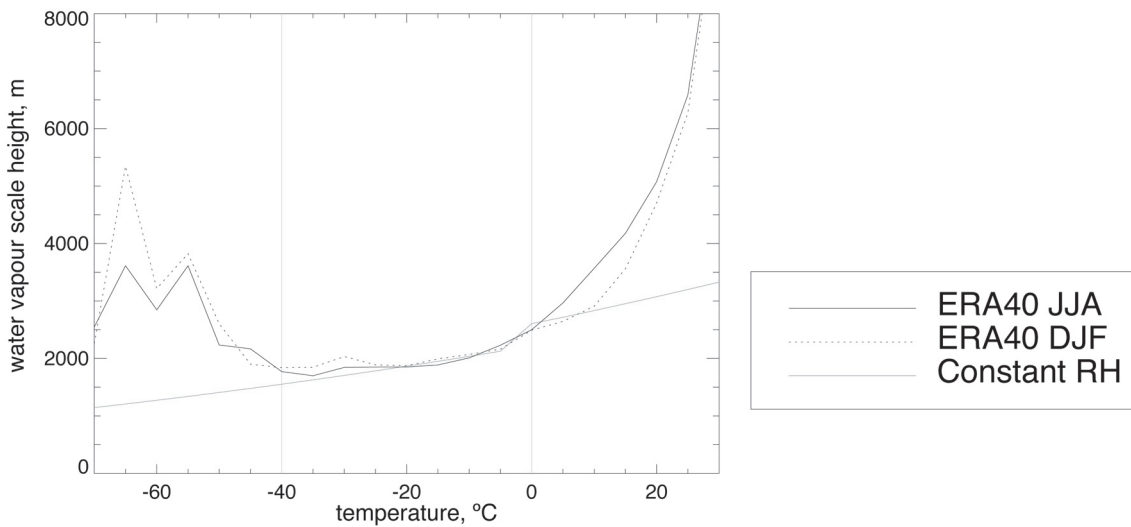


Figure 4: Temperature dependence of water vapour scale height in ERA40 for June, July and August (JJA) and December, January and February (DJF) 1979-1998. Mean values in each 5°C temperature interval globally are plotted. The theoretical relationship for constant relative humidity (RH) is shown.

References

- Folkins, I., K.K. Kelly and E.M. Weinstock, A simple explanation for the increase in relative humidity between 11 and 14 km in the tropics, *J. Geophys. Res.*, 107, art-4736, 2002.
- Heymsfield, A.J., Precipitation and development in stratiform ice clouds; A microphysical and dynamical study, *J. Atmos. Sci.*, 34, 367-381, 1977.
- Heymsfield, A.J. and C.M.R. Platt, A parameterisation of the particle-size spectrum of ice clouds in terms of the ambient-temperature and the ice water-content, *J. Atmos. Sci.*, 41, 846-855, 1984.
- Trenberth, K.E., Atmospheric moisture residence times and cycling: Implications for rainfall rates and climate change, *Climatic Change*, 39, 667-694, 1998.

The aim of this investigation is to study the origin of dry air arriving in the tropical and subtropical troposphere during winter, and we present here the results obtained using a climatology for the month of January 1993. The main motivation behind this study lays on the relative transparency of dry air masses to IR radiation, and the impact they may have in increased green-house gas scenarios for the tropics and the subtropics.

Time from last condensation (τ)

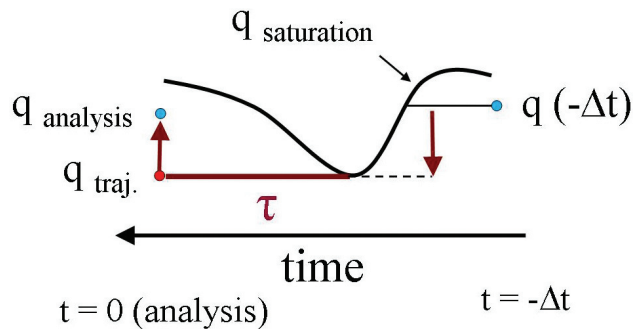


Figure 1: The assignation of specific humidity, q , to a back trajectory.

24-day back trajectories were "released" daily from a regular grid covering all of the tropics and the subtropics from 38°N to 38°S. 16 vertical levels were considered, from 950-200 hPa. We define the origin of dry air as the last condensation event experienced along the trajectory. To identify this event, we note that without mixing, re-moistening or condensation, the specific humidity q would be constant along the trajectory. Each trajectory is assigned the specific humidity at time $-\Delta t$ (see Figure 1). The value is carried forward along the trajectory unless it exceeds saturation. In this case condensation occurs and the value of humidity is set to the saturation value. The last time the value of humidity is set in this way is used to define the origin of dry air and we call τ the time between last condensation event and the arrival on the release grid.

We choose to define dry air masses those that have a relative humidity (RH) lower than 20% at arrival grid, a value that is determined using ERA40 analysis. In figure 2 we show the histogram of τ for all trajectories (upper line) and for dry trajectories only (lower line). Nine plots are shown, corresponding in the vertical to upper (400-200 hPa), middle (700-450 hPa) and lower (950-750 hPa) troposphere, and to southern tropics (38°S to 13°S), equatorial region (13°S to 13°N) and northern tropics (13°N to 38°N). The vertical line in each plot corresponds to the median of the distribution. The plots show an about exponential decay of the number of condensation events with τ above the median. For dry parcels the histograms tend to zero for short values of τ , since an air mass with RH of 20% cannot have been saturated recently. The median is less than 5 days in the upper northern troposphere and as large as 11 days in the lower equatorial troposphere. The chosen trajectory length of 24 days is sufficient for almost all air parcels to experience condensation.

Histograms of τ

latitude and pressure in the arrival grid
dry event is defined by $RH_{analysis} < 20\%$

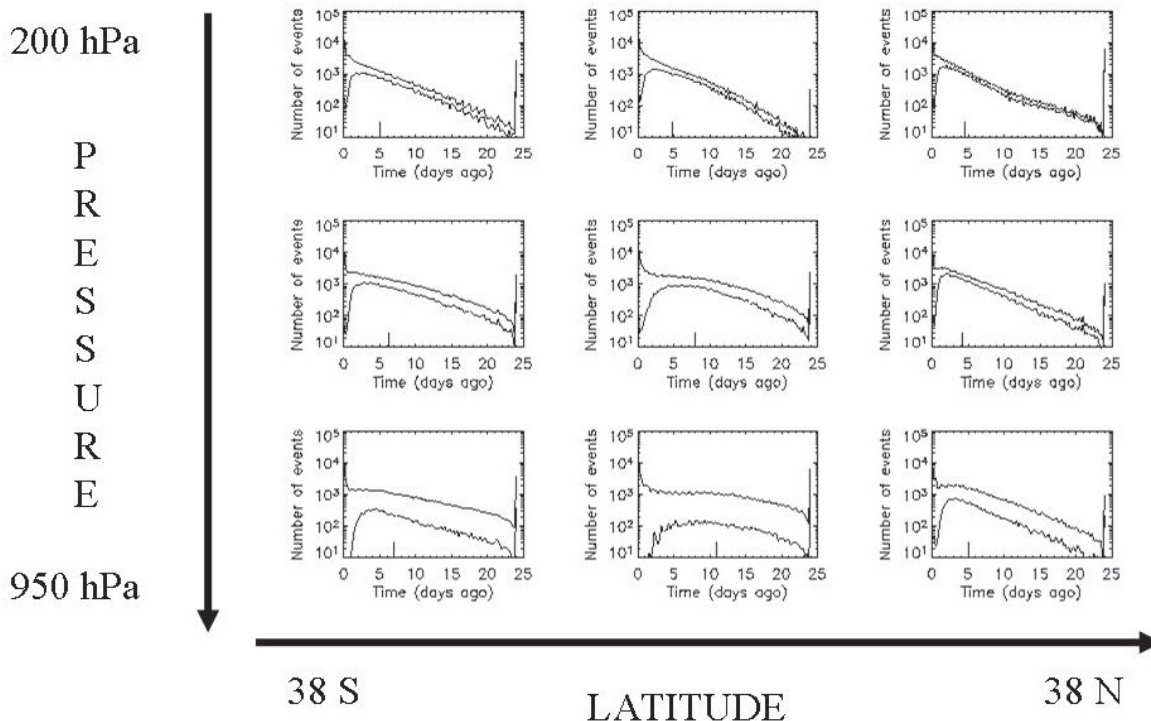


Figure 2: Histograms of the time since last condensation for air parcels arriving in the nine regions (see text). All trajectories (upper line) and dry trajectories only (lower line) are shown.

Figure 3 shows the origin of dry air arriving in the nine regions considered above. The position of the grid points that define each region is also shown, and the contours correspond to the density of condensation events occurring at a given latitude and pressure and leading to dry air at one of those grid points.

Number density of condensation events

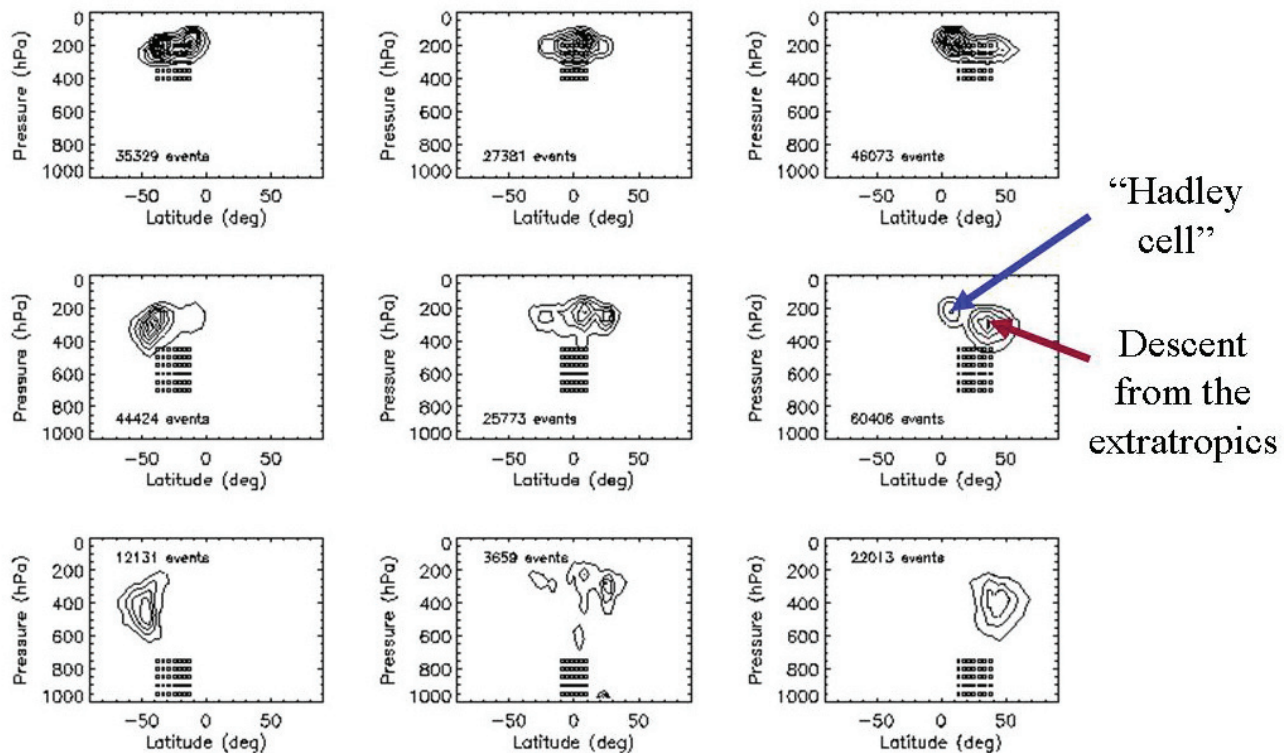


Figure 3: Number density of condensation events associated with air arriving in the nine regions (see text).

In the lower troposphere dry air mainly descends from its origins in the extratropics. Moving up in the troposphere a contribution associated with condensation in the tropics and the descending branches of the Hadley circulation, becomes important. Descent associated with Walker circulations is responsible for the few dry air masses observed in the lower equatorial troposphere. This agrees with the high value of median τ in this last region, because of the long time needed to descend by radiative cooling within the tropics from the upper troposphere into the lower equatorial troposphere.

Simulated Trends of Water Vapour in the Upper Troposphere and Lower Stratosphere between 1960 and 1999: Results from a Transient Model Simulation with the CCM E39/C

A. Stenke, V. Grewe and M. Dameris

Institut für Physik der Atmosphäre, Deutsches Zentrum für Luft- und Raumfahrt, Oberpfaffenhofen, Germany

Water vapour is the most important climate gas. Moreover, it is a controlling factor of climate feedback processes. Therefore, the understanding of the variability of water vapour in the UTLS is essential for the understanding of the climate system. While long-term changes (trends) of UTLS water vapour are a topic of ongoing debate [e.g., Randel et al., 2004], various aspects of the observed interannual variability are well understood. Here, we present results of a transient model simulation with a coupled chemistry-climate model of the troposphere and stratosphere, which includes several external forcings in order to reproduce the main climate interactions involving water vapour, ozone and other species between 1960 and 1999. A key question of this study is the deterministic behaviour of a non-linear model system to external forcings: Are models which include climate-chemistry interactions and climate variability patterns able to reproduce the observed water vapour variations in the upper troposphere and lower stratosphere?

The coupled chemistry-climate model E39/C [Hein et al., 2001] is a derivative of the ECHAM4 climate model, with an enhanced vertical resolution (≈ 700 m) at tropopause levels. Its chemistry module CHEM includes the most relevant stratospheric and tropospheric ozone related homogeneous chemistry as well as heterogeneous reactions on polar stratospheric clouds and sulphate aerosols. In the present model simulation several external forcings are considered in order to reproduce the temporal development of the atmosphere between 1960 and 1999 as realistic as possible. The anthropogenic influence is represented by specifying the

atmospheric concentrations of the most relevant greenhouse gases CO_2 , N_2O and CH_4 , and of chlorofluorocarbons according to IPCC [2001]. The natural forcings considered in this simulation are the QBO, chemical and direct radiative effects of the major volcanic eruptions of Agung (1963), El Chichon (1982) and Mount Pinatubo (1991), as well as the 11-year solar cycle. The Quasi-Biennial Oscillation is forced in the model by a linear relaxation of the simulated zonal winds in the tropical stratosphere towards a time series of observed zonal wind profiles at the equator. The influence of the 11-year solar cycle on the modelled photolysis rates is parameterised according to the intensity of the 10.7 cm radiation of the sun. The prescribed sea surface temperatures follow the global HadISST1 data set of observed SSTs provided by the United Kingdom Met. Office Hadley Centre, including ENSO-related SST anomalies. Chemistry, dynamics, and radiation are interactively coupled to allow for all kinds of feedback processes. A detailed description of the experimental set-up can be found in Dameris et al. [2005].

In this simulation, observed climate variability features are indeed reproduced. In agreement with MLS water vapour observations [Newell et al., 1997], tropical upper tropospheric water vapour in the model simulation is closely related to the ENSO-index. Generally, El Niño-years (positive ENSO-index) are associated with positive water vapour anomalies in the tropical upper troposphere, and vice versa. Despite this overall correlation between ENSO-index and water vapour, single years of the model simulation show a contrary behaviour, e.g. 1993/94. Along with a simulated warming, the tropical upper troposphere additionally exhibits a continuous water vapour increase since the middle of the 1970s.

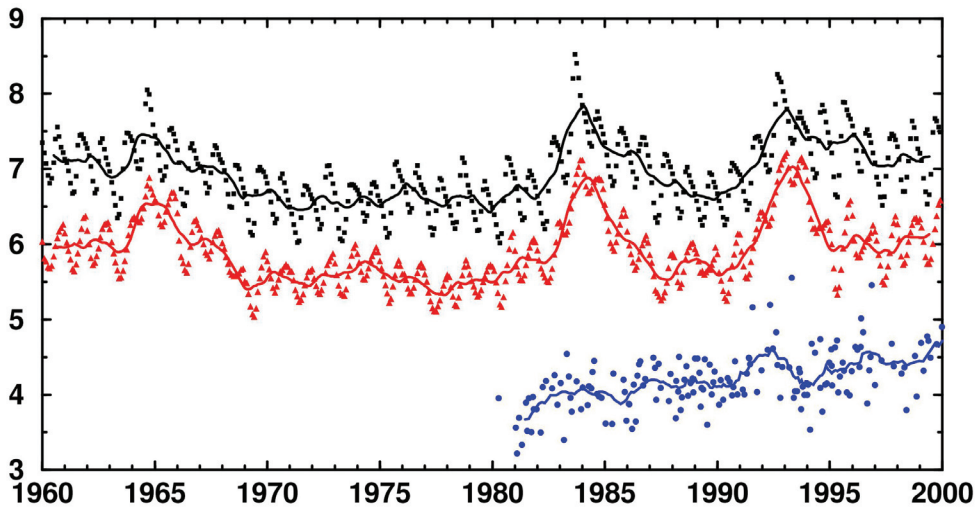


Figure 1: Time series of modelled monthly mean water vapour mixing ratios at 50 hPa, 40°N (black) and 40°S (red), respectively, and of water vapour soundings with the CMDL frostpoint hygrometer at Boulder, CO (blue) [Oltmans et al., 2000, data kindly provided by H. Vömel, NOAA/CMDL, Boulder, Colorado, USA].

seventies (Figure 1). From 1980 on, a clear increase in lower stratospheric water vapour is simulated. The simulated water vapour increase between 1980 and 1999 (+0.029 ppmv/yr) is of the same order of magnitude as observed in balloon measurements at Boulder, Colorado, USA (+0.044 ppmv/yr). Enhanced chemical water vapour production due to increasing methane emissions explains only about 30% of the simulated water vapour trend. The simulated water vapour content in the lower stratosphere shows a close link to modelled temperatures at the tropical tropopause. A cooling of the tropical tropopause during the first decade of the simulation period leads to a decrease of the entry-value and a reduction of lower stratospheric water vapour. During the last 20 years of the present simulation the model results show a warming of the tropical tropopause. This temperature increase seems to disagree with radiosonde observations, which indicate a cooling of the tropical tropopause [Zhou et al., 2001]. This simulated temperature increase at the tropical tropopause and the resulting increase of the entry-value accounts for approximately two thirds of the modelled water vapour trend in the lower stratosphere. Obviously, temperature changes in the upper troposphere and lower stratosphere, i.e. at the tropical cold point tropopause, play a key role in controlling stratospheric water vapour in the model. These temperature variations in turn are controlled by a number of parameters, not only sea surface temperatures, but also volcanic eruptions, stratospheric ozone depletion, and tropospheric ozone increase. The reasons for the temporal development of simulated tropical tropopause temperatures are still unclear. Based on currently available model results we speculate, that the changes of the tropopause temperature are a consequence of solar activity fluctuations.

References:

- Dameris, M., V. Grewe, M. Ponater, R. Deckert, V. Eyring, F. Mager, S. Matthes, C. Schnadt, A. Stenke, B. Steil, C. Brühl and M.A. Giorgetta: Long-term changes and variability in a transient simulation with a chemistry-climate model employing realistic forcing, *Atmos. Chem. Phys. Discuss.*, 5, 2297-2353, 2005.
- Hein R., M. Dameris, C. Schnadt, C. Land, V. Grewe, I. Köhler, M. Ponater, R. Sausen, B. Steil, J. Landgraf and C. Brühl: Results of an interactively coupled atmospheric chemistry-general circulation model: comparison with observations, *Ann. Geophys.*, 19, 435-457, 2001.
- Newell, R.E., Y. Zhu, W.G. Read and J. W. Waters: Relationship between tropical upper tropospheric moisture and eastern tropical pacific sea surface temperature at seasonal and interannual time scales, *Geophys. Res. Lett.*, 24, 25-28, 1997.
- Oltmans, S. J., H. Vömel, D. J. Hofmann, K. H. Rosenlof, and D. Kley: The increase in stratospheric water vapor from balloonborne frostpoint hygrometer measurements at Washington, D.C., and Boulder, Colorado, *Geophys. Res. Lett.*, 27, 3435-3456, 2000.
- Randel, W.J., F. Wu, S.J. Oltmans, K.H. Rosenlof and G.E. Nedoluha: Interannual changes of stratospheric water vapor and correlations with tropical tropopause temperatures, *J. Atmos. Sci.*, 61, 2133-2148, 2004.
- Zhou, X., M. A. Geller, and M. Zhang: Cooling trend of the tropical cold point tropopause temperatures and its implications, *J. Geophys. Res.*, 106, 1511-1522, 2001.

As shown in Figure 1, the time series of simulated water vapour in the lower stratosphere exhibits three pronounced peaks, which are caused by a short-term heating of the tropical tropopause after the volcanic eruptions. Furthermore, tropical lower stratospheric water vapour shows a nearly biannual oscillation, which is directly associated with the Quasi-Biennial Oscillation. The simulated Quasi-Biennial Oscillation-related water vapour anomalies amount approximately ± 0.25 ppmv, which agrees very well with HALOE observations [± 0.3 ppmv, Randel et al., 2004]. During the first 10 years of the simulation period the water vapour content in the lower stratosphere shows a remarkable decrease, followed by nearly constant values during the

Upper Troposphere / Lower Stratosphere Data from the EOS MLS Instrument on Aura

H.C. Pumphrey, M.J. Filipiak and R.S. Harwood
School of GeoSciences, University of Edinburgh, Scotland

Introduction

The EOS Microwave Limb Sounder was launched on 15 July 2004 and has operated continuously since late August 2004. In this paper we describe briefly the measurements made by the instrument in the Upper Troposphere / Lower Stratosphere region.

The scientific objectives of MLS are:

1. To track the recovery of the Ozone layer (by tracking Cl and Br chemistry and resolving issues in Hydrogen chemistry)
2. To understand aspects of how composition affects climate, (specially via H₂O in the upper troposphere).
3. To quantify aspects of pollution in the upper troposphere (mostly via O₃ and CO).

The MLS technique is tried and tested for item 1, much less so for items 2 and 3.

MLS is a small radio telescope, with a 1.5m dish antenna [Waters et al., 2005]. The field of view is scanned mechanically across the Earth's limb every 24 seconds. The radiation received is detected by five radiometers and analysed by over 30 filter banks. Standard retrieval theory is used to estimate profiles of temperature (T) and of the mixing ratio of a variety of molecules [Livesey et al., 2005]. Of these, only T, H₂O, O₃ and CO are useful in the upper troposphere. An additional measurement that is made in the upper troposphere is the ice water content (IWC). Most quantities are retrieved on fixed pressure levels, with 6 levels per pressure decade (approximately one level every 2.7 km).

Aura is in a polar orbit, with MLS looking forward from the satellite. The 3495 scans made every day provide coverage from 82°S to 82°N with profiles spaced every 140 km along the measurement track. There are 14.5 orbits per day, so resolution across the track is on the order of 25° of longitude.

Water Vapour

MLS measures water vapour using the 183.3 GHz spectral line. The data in appear to be of good quality and significant progress has been made in their validation [Froidevaux et al., 2005]. Data are usable down to 316 mb.

Carbon Monoxide

MLS measures CO using a spectral line at 230.5 GHz. The signal from CO in the upper troposphere is very small compared to the signal from nearby O₃ lines, so great care is needed in retrieving the profiles and using them. Early results are in press [Filipiak et al., 2005].

Ozone

MLS measures Ozone using a spectral line near 235.6 GHz and other strong lines in the same spectral region. (There are also filter banks located on Ozone lines at 206 GHz and 660.5 GHz but these are not strong enough to provide a measurement in the upper troposphere.)

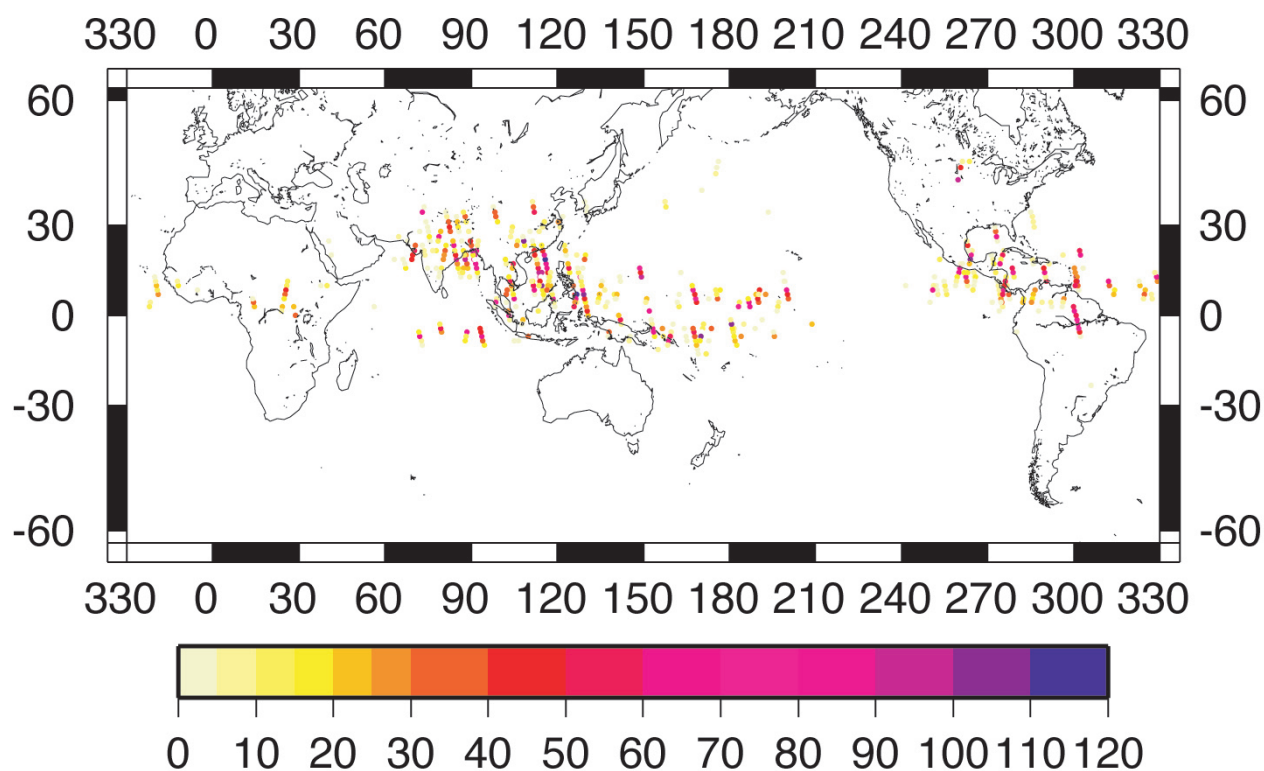


Figure 1: MLS Water vapour at 147 mb for 26-30 June 2005

Ice-Water Content

IWC is retrieved in a multi-step process. First, the state of the cloud-free part of the atmosphere is estimated, and the expected radiances calculated from it. Then the difference between the expected and measured radiances is taken, giving a quantity called the cloud-induced radiance. The IWC is then estimated from this quantity. Most MLS profiles have an IWC of 0. Profiles with significant IWC are concentrated in regions of deep convection.

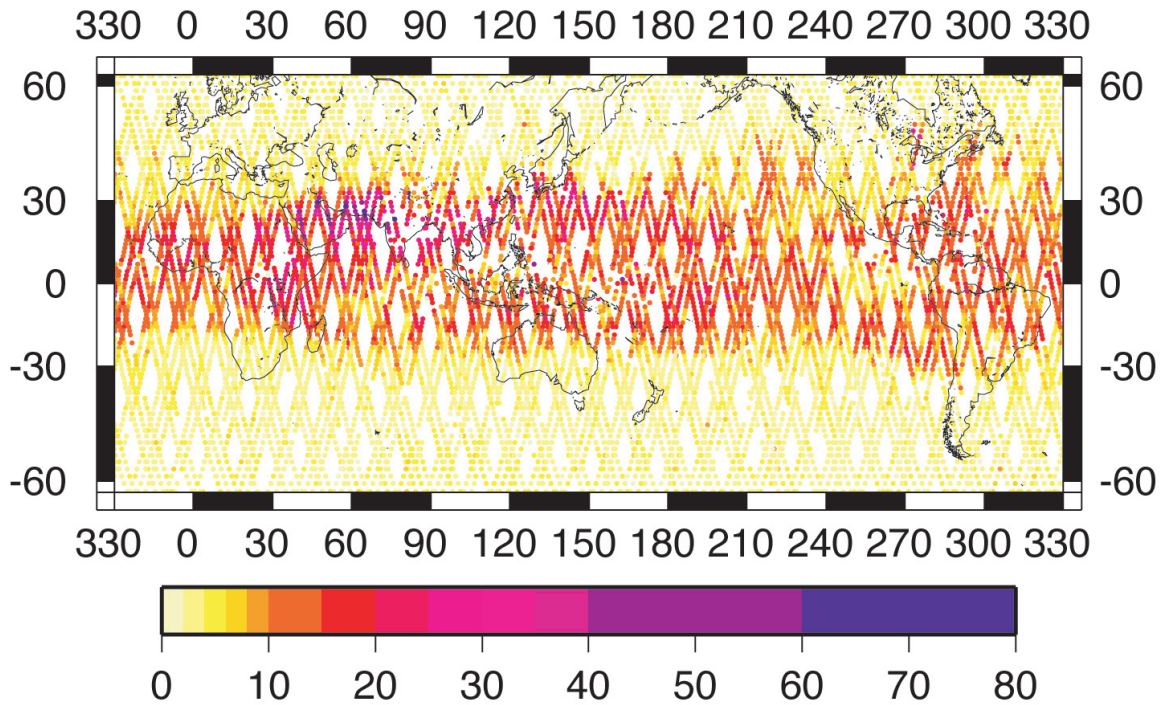


Figure 2: MLS ice water content (in mg/kg) 26-30 June 2005

Accessing the data

The MLS data are distributed via the Goddard Earth Sciences Data and Information Services Center (GES DISC, <http://disc.gsfc.nasa.gov>). At the time of writing, the data may not be obtained anonymously. To initiate data access, users should send an email to data@mls.jpl.nasa.gov. Any change in this policy will be announced on the GES DISC website. The data will be provided with a detailed data quality document: this is required reading for anyone intending to make use of the MLS data.

References

- Waters, J.W. et al., The Earth Observing System Microwave Limb Sounder (EOS MLS) on the Aura satellite, IEEE Trans. Geoscience and Remote Sensing, in review, 2005.
- Livesey, N.J., W. Van. Snyder, W.G. Read and P.A. Wagner. Retrieval algorithms for the EOS Microwave Limb Sounder (MLS) instrument, IEEE Trans. Geosciences and Remote Sensing, in review, 2005
- Froidevaux, L. et al., Early validation analyses of atmospheric profiles from EOS MLS on the Aura satellite, IEEE Trans. Geosci. Remote Sensing, in review, 2005.
- Filipiak, M.J., R.S. Harwood, J.H. Jiang, Q. Li, N.J. Livesey, G.L. Manney, W.G. Read, M.J. Schwartz, J.W. Waters and D.L. Wu, Carbon monoxide measured by the EOS Microwave Limb Sounder on Aura: First results, Geophys. Res. Lett., in press, 2005.

The Lower Stratospheric Water Vapour Trend, 1950s to 1970s, Revisited

H.K. Roscoe

British Antarctic Survey/NERC, Cambridge, England

Introduction

The SPARC Assessment Report of Water Vapour in the Stratosphere (WAVAS, SPARC 2000), and a companion paper [Rosenlof et al., 2001], showed that the mixing ratio of stratospheric water vapour has been increasing at about 1% per year since the 1950s. The rate of increase was particularly consistent in the middle stratosphere, from frost point hygrometers on balloons in USA. The rate of increase was observed in the lower and middle stratosphere by most available sensors, each with a different time span. But temperatures in the tropical upper troposphere and lower stratosphere, where air enters the stratosphere and where water vapour is removed by freezing, have decreased rather than increased, so we must be suspicious of this trend over the full period.

Furthermore, the WAVAS report stated that the earliest instrument, the frost point hygrometer on UK's Met Research Flight, was unchanged between the 1950s and the 1970s, but this is only partly true. The measurements were listed and analysed by Cluley & Oliver [1978], and the WAVAS report followed them by saying the two instruments were "the same design". However, a careful reading of Cluley & Oliver showed that there were in fact important differences, which are examined below. Finally, an important scaling error in the WAVAS report concerning these UK measurements is corrected and the implications discussed.

Differences between UK Met Research Flight's frost point hygrometer in the 1950s and the 1970s

The earlier instrument had a much larger hysteresis between frost forming and frost disappearing

Hysteresis is important because of the large non-linearity of saturation vapour pressure with temperature, so that the mean temperature is not the mean vapour pressure. Early analyses of 1950s data quoted mean frost point, and because the hysteresis of the earlier instrument was 6 K, this would lead to a systematic error that would be much larger than for the later instrument whose hysteresis was only 2.5 K. This would then bias the trend. However, all results were recomputed by Cluley & Oliver [1978] using mean vapour pressure, so it is hard to see how the change in hysteresis could create a bias. However, 6 K is more than a factor two in vapour pressure, so we would expect the earlier data to have more noise.

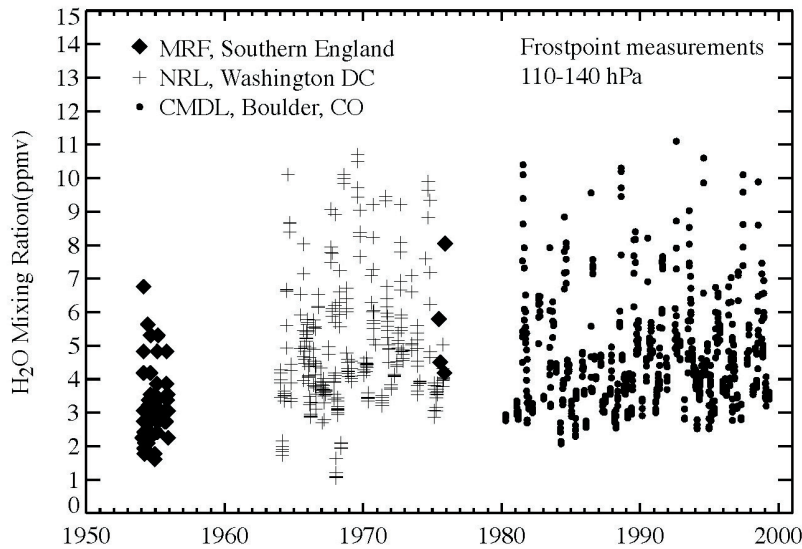


Figure 1: Northern midlatitude measurements at 110-140 hPa, by frost-point hygrometers [from Rosenlof & Roscoe, submitted as a correction to Geophys. Res. Lett.]

The earlier instrument had a much smaller flow rate and poorer visibility of the cooled mirror

These factors were no doubt responsible for the larger hysteresis above. But again it is difficult to see how they could create a bias, although again they should give rise to more noise in the earlier data.

The earlier instrument had a much smaller temperature gradient between the temperature sensor and the cooled mirror

The later instrument's large gradient of 2 ± 0.1 K was, fortunately, carefully measured in work associated to Cluley and Oliver [1978]. Unfortunately the smaller gradient in the earlier instrument had to be estimated at 0.6 ± 0.3 K, leaving significant scope for error which would bias all 1950s data, and so bias the trend. However, the error can equally well be of either sign, so any bias is can be of either sign. Hence we should treat this possible error by assigning a larger error bar to the trend between 1950s and 1970s than that from the straight-line fit alone.

Scaling error in data from UK Met Research Flight's frost point hygrometer

Most MRF data points, given by Cluley & Oliver [1978] in the ppm that was then the fashion for water vapour, were wrongly plotted in WAVAS [SPARC, 2000] as ppmv [Rosenlof & Roscoe, submitted to GRL], without rescaling by the ratio of the molecular weights of water and air (about 1.6). WAVAS and Rosenlof et al. [2001] were careful to deduce trends only from each individual data set because of possible errors in inter-calibration, so rescaling does not affect the trends. But data from frost point hygrometers alone, which should be less susceptible to inter-calibration errors than other sensors, are much more consistent after rescaling MRF data. This pleasing result is illustrated in Figure 1.

This easily-made mistake went un-noticed by the very large number of co-authors of the WAVAS report (Table 1). It also went un-noticed until now by the large numbers of referees, including myself.

Table 1. WAVAS co-authors and contributors (columns 1,2,3 and 4), and WAVAS referees (right-hand column).

J. Anderson	Michael R. Gunson	Larry Miloshevich	Ulrich Schumann	Jens Boesenberg
John J. Bates	John E. Harries	Philip W. Mote	Vanessa Sherlock	Bruno Carli
R. M. Bevilacqua	Paul Hartogh	Gerald E. Nedoluha	Steven C. Sherwood	Herbert Fischer
Ed Browell	Manfred Helten	Hermann Oelhaf	Herman Smit	Lesley Gray
Marie-Lise Chanin	Robert Herman	Samuel Oltmans	D. C. Smith	James R. Holton
Alain Chedin	Eric J. Hints	Joëlle Ovarlez	E. M. Stone	Dale Hurst
Er-Woon Chiou	F. W. Irion	Liwen Pan	Geoffrey Toon	Richard H. Johnson
William P. Chu	Syed Ismail	Leonhard Pfister	Ralph Toumi	Rod Jones
Andrew E. Dessler	E. J. Jensen	Hugh Pumphrey	Holger Vömel	Danny McKenna
Dieter H. Ehhalt	David G. Johnson	Patrick N. Purcell	Joe W. Waters	Gérard Mégie
Gerhard Ehret	Niklaus Kämpfer	William G. Read	Elliot M. Weinstock	Reginald E. Newell
Dietrich Feist	Hiroshi Kanzawa	Ellis E. Remsberg	Dave Whiteman	John Pyle
Herbert Fischer	Ken Kelly	Karen H. Rosenlof	Vladimir Yushkov	William J. Randel
R. Fu	Dieter Kley	James M. Russell III	Stephanie A. Vay	Howard Roscoe
Diane Gaffen	Randy May	Glenn Sachse	Xuelong Zhou	Ulrich Schmidt
Andrew Gettelman	Marty McHugh	E. P. Salathe		Darin Toohey
Larry Gordley	Hope A. Michelsen	Cornelius Schiller		Adrian Tuck
				Geraint Vaughan

References

- Cluley and Oliver, Aircraft measurement of humidity in the low stratosphere over southern England 1972-1976, Quart. J. Roy. Met. Soc. 104, 511-526, 1978.
- Rosenlof, K.H., S.J. Oltmans, D. Kley, J.M. Russell III, E-W. Chiou, W.P. Chu, D.G. Johnson, K.K. Kelly, H.A. Michelsen, G.E. Nedoluha, E.E. Remsberg, G.C. Toon and M.P. McCormick, Stratospheric water vapor increases over the past half-century, Geophys. Res. Lett. 28, 1195-1198, 2001.
- SPARC, Assessment of upper tropospheric and stratospheric water vapour, WMO/TD No 1043 (SPARC Report No 2), ed. D. Kley, J.M. Russell III, C. Phillips, 2000.

Session on Variability and Trends

Rapporteur: T. Gardiner, Analytical Science Group, National Physical Laboratory, England

The session started with an overview talk from Karen Rosenlof from the NOAA Aeronomy Laboratory, Boulder on 'Changes in Stratospheric Water Vapour: Observations, Uncertainties and Possible Mechanisms'. The talk reviewed the long term changes in stratospheric water vapour and the possible driving mechanisms for these. This information is needed due to the effect of water vapour on both the radiative and chemical balance in the stratosphere. However, there are significant problems in combining different data sets to get a long-term trend due to systematic uncertainties. Even the latest in-situ sensors show discrepancies of up to 2 ppmv. This level of uncertainty is acceptable for variability and radiative transfer studies, but not for trend analysis or investigation of stratospheric water entry mechanisms. From the data that is available between 1980 and 2000 the estimated change in stratospheric water is an increase of ~1 ppmv. This change is not explained by the corresponding change in tropical tropopause temperatures, which should have lead to a decrease of -1.5 ppmv, or the rise in methane levels, which would only explain 0.25 ppmv of the rise. Another interesting feature is the drop in stratospheric water vapour that has persisted since 2000, concurrent with a fall in tropical tropopause temperatures. This is probably due to enhanced uplift in the tropics, although the reasons for this are not fully understood.

The second paper was given by Mike McCarthy from the Hadley Centre on 'Variability and trends in tropical upper tropospheric relative humidity (UTRH)'. The results from the HadAM3 model were compared to satellite measurements from the High resolution InfraRed Sounder, and radiosonde temperature and relative humidity results from CARDS. The general conclusion was that a direct comparison of data showed reasonable agreement given the known uncertainties. However, this was not the case when looking at the long term trends, and it is not currently possible to comprehensively validate simulations of recent climate change in the upper troposphere. There is a requirement for a better estimate of the measurement uncertainties, as part of ongoing (re-)analyses of radiosonde and satellite data. There is also a requirement for improved water vapour observations, but these need to be linked to the existing record. Any future observing network needs to provide multi-variate measurements with well-characterised uncertainties over a wide geographic area.

Elizabeth Kennett from Imperial College then spoke on the 'Temperature dependence of atmospheric moisture lifetime'. This described a study of the lifetime of water vapour in different regions of the upper troposphere and lower stratosphere, where the lifetime was controlled by the difference between the rates of injection (eg. large scale transport, convection, evaporation) and removal (eg. transport, precipitation) of water vapour in a particular region. The results showed a strong temperature dependence, with a minimum lifetime occurring at around -40°C. Similar temperature dependences are seen in water vapour scale heights and observations of the vertical rate of change of ice water content in Cirrus clouds. The reason for the minimum is thought to be due to the micro-physical properties of water and in particular, the lack of super-cooled liquid water below -40°C.

Piero Cau described his work at Reading University using a trajectory model to look at the origin of 'Low Humidity in the Tropical and Subtropical Atmosphere'. Daily back trajectories were released using the January 1993 ERA-40 dataset. These covered a regular grid from 38°N to 38°S, every 4° longitude, and from 14 vertical levels between 950 hPa and 200 hPa. The saturation humidity was calculated along the back trajectory, and the time and location of the minimum saturation level (dry event) was recorded. In general, there was good agreement between the time to the dry event and to the minimum pressure observed along the trajectory. The spatial behaviour showed that dry air in the lower/mid troposphere originated mainly from the extra-tropical upper troposphere, while dry air in the upper troposphere originated mainly from the tropical upper troposphere.

The next talk was by A. Stenke from the DLR Institut für Physik der Atmosphäre on 'Simulated trends of water vapour in the UTLS between 1960 and 1999'. The main objective was to see if a coupled Chemistry-Climate model could reproduce the observed variations in water vapour between 1960 and 2000. The model used was CCM E39/C, combining the ECHAM dynamics and CHEM chemical models with additional external forcings including chemical emissions, Quasi Biennial Oscillation, volcanoes, and the 11-year solar cycle. The results showed a positive trend of 0.06 ppmv/yr since 1975 in the tropical water vapour content at 200 hPa. This was closely correlated with the concurrent increase in tropical upper troposphere temperatures (0.06 K/yr) which accounted for two thirds of the observed trend, with the remaining third coming from enhanced methane oxidation.

In a change to the planned programme the next talk was given by Hugh Pumphrey from the University of Edinburgh on 'Upper Troposphere and Lower Stratosphere data from the EOS MLS instrument on AURA'. The objectives of the Microwave Limb Sounder (MLS) are to track the recovery of the ozone layer through studies of Cl, Br and H chemistry, to study pollution in the upper troposphere through O₃ and CO measurements, and investigate the relationship between composition and climate through measurements of H₂O in the upper troposphere. A summary of the MLS products was presented, together with preliminary results for H₂O, CO, O₃ and Ice Water Content measurements. The data products are currently being validated, and a detailed data quality document will be released in the next few months. Questions following the talk confirmed that the planned lifetime for the satellite was 5 years, and that there is currently no funding for a successor instrument.

The final paper in the session was presented by Howard Roscoe from British Antarctic Survey on 'The lower stratospheric water vapour trend, 1950s to 1970s, revisited'. The SPARC Assessment Report of Water Vapour in the Stratosphere (WAVAS) showed that the mixing ratio of stratospheric water vapour has been increasing at about 1%/yr since the 1950s. Over the same period temperatures at the entry point have decreased, not increased, so the water vapour trend remains unexplained. The WAVAS assessment was based on the trends observed within each dataset, not between datasets. However, investigation has shown that a number of previously unconsidered changes were made to the earliest frost point hygrometers on the Met Research Flight (MRF). Study of these changes indicates that they may lead to a change in the trend for this data set, but the bias could be of either sign, therefore the uncertainty on the trend for this dataset should be increased. In addition, the original WAVAS plots have incorrect units for the early MRF data (ppmm not ppmv). This does not affect the trend results, but correcting this error brings the MRF results into line with the later measurements.

The main issue discussed at the end of the session was the validity of using the ice saturation pressure corresponding to the minimum temperature observed by an air parcel during its transport into the lower stratosphere (the 'entry point temperature') to define the water vapour content of that air parcel. It was recognised that large scale averages of the temperature field were generally not suitable for this purpose, and that a consideration of local temperature variations and the time of transit through the temperature minimum needed to be included. In addition, issues such as supersaturation and deposition rates would affect the water vapour content. It was noted that the trend results for stratospheric water vapour presented by Karen Rosenlof do not show a correlation with the tropopause temperature trend, however the intra-annual variability of the two parameters shows strong positive correlation. A successful model for stratospheric water vapour content should be able to explain this change in the correlation over the different timescales.

Ice Supersaturation

Introduction

Ice supersaturated regions (ISSRs) are cold dynamic regions of ice-supersaturated air in the upper troposphere (and sometimes extending into the lower stratosphere). The temperature is lower than the supercooling limit of micrometer sized droplets of pure water, at about -38°C , i.e. liquid water drops cannot be found in Ice supersaturated regions. Ice formation takes place within Ice supersaturated regions via homogeneous freezing of aqueous solution droplets or via heterogeneous nucleation, probably mainly immersion freezing. Homogeneous nucleation seems to be the main pathway to cirrus clouds. These form in updraughts when certain supersaturation thresholds of the order 40% and more are surpassed. Often these thresholds are not reached in an ISSR, then the air mass is supersaturated but cloud free. Hence ISSRs are large regions where cirrus clouds are embedded at some locations whereas at other locations there is clear air.

Historical notes

Nearly 300 years ago people began to think about and experiment with metastable thermodynamic states (i.e. supercooling and supersaturation). D. Fahrenheit, in 1721, could keep water droplets contained in an evacuated glass bulb liquid at -9°C ($=15.8^{\circ}\text{F}$) for several hours. Almost 100 years ago, A. Wegener (1912/13) found on an expedition in NE Greenland that during winter the clear air was on the average ice supersaturated. Around 1940 there was a scientific discussion about the formation of the ice phase in the atmosphere. While Wegener and W. Findeisen thought that ice would usually form by direct deposition onto appropriate solid particles, L. Krastanow and E. Wall gave arguments and presented thermodynamic calculations showing that the ice phase in the atmosphere usually forms via the liquid phase, i.e. by freezing of supercooled droplets. E. Glückauf and H. Weickmann were probably the first who measured ice supersaturation in the tropopause region. In 1945, Glückauf reported from hair hygrometer measurements over southern England that (very high) ice supersaturation occurs frequently in the upper troposphere, and Weickmann, who took microphotographs of ice crystals on research flights, concluded that cirrus clouds form mainly via the water phase and not as soon as ice saturation is reached. He characterised the upper troposphere as a region of high ice supersaturation, albeit a region of low absolute humidity. Only a few years later, 1946-48, B.M. Cwilong and V.J. Schaefer succeeded to supercool small water drops down to the supercooling limit for pure water.

Unfortunately, in spite of the long standing agreement within the cloud physics community that ice supersaturation often occurs in the upper troposphere and lower stratosphere, most large scale models still ignore this. They treat the ice phase analogously to the water phase, which is, admittedly, much more convenient, but wrong.

Ice supersaturation, cirrus clouds, and climate - a problematic relationship

When we compare cirrus clouds with water clouds, we can emphasise the peculiar problems involved in cirrus modelling that renders their physical treatment in large-scale models so inconvenient. First, cirrus clouds may heat or cool the Earth-Atmosphere system depending on their micro-macro-physical properties, on their temperature (i.e. altitude), and perhaps on their generation mechanism (this implies dependencies on synoptic situations and geographic location). In contrast, water clouds always cool the system. Second, there is a myriad of crystal shapes, often crystals are complex aggregates of regular (rosettes) or irregular (or stochastic) assembly, and apart from temperature and supersaturation there seem to be still other factors that determine which crystal habit in a certain cloud is predominant. These complex habits inhibit a straightforward method to compute their radiation scattering phase functions which renders radiation transfer in cirrus clouds a tough problem. In contrast, water droplets are (nearly) spherical and their scattering properties can be computed with the Mie theory. Third, while water clouds form by condensation on pre-existing solid aerosol particles at water saturation or very small degrees of supersaturation (of the order one percent), ice crystals in Ice supersaturated regions can form by a multitude of processes, predominantly by homogeneous freezing of aqueous solution droplets, but also by heterogeneous freezing involving solid particles. Of the latter, immersion freezing seems to be the most important in the cold upper troposphere and lower stratosphere, but deposition freezing and other pathways may also occur. There are still many unsolved problems with heterogeneous nucleation, as well on the microphysics of the processes themselves, but also on the potential role these processes play for cirrus clouds.

As we have seen, cirrus clouds have a loose relation to ice saturation, first, because they do not form at saturation, and second, once they are formed, the crystal growth process is not so strong that supersaturation within the clouds is quickly relaxed to saturation. Consequently, there is plenty of ice-supersaturated but clear air in the upper troposphere (sometimes marked by persistent contrails), the cirrus clouds are embedded within Ice supersaturated regions, but the boundaries of the cloud and the boundaries of its parental Ice supersaturated region are not congruent (again in contrast to water clouds), and their can be highly supersaturated air even within the clouds.

All these peculiarities make it extremely difficult to describe cirrus clouds and Ice supersaturated regions in a physically consistent manner in large scale models. But even if that would work satisfyingly it is not clear whether it would be possible at all to predict cirrus occurrence in a future climate. The reason is, that the high humidity threshold for homogeneous nucleation is an extremal state in the humidity field, and extremal states react much more sensitively to changes of background conditions than do averages. Let us consider as an example two exponential probability density functions (pdfs) of supersaturation S_i that are typical for ISSRs, i.e. $f(S_i) = \exp(-S_i/m)/m$ with mean value m . Let one pdf have $m=10\%$, the other $m=11\%$; we would think, a minor change. However, now look at the part with supersaturation in excess of an assumed nucleation threshold of 40% supersaturation. In spite of the minor change in the mean values, the probability that S_i exceeds the threshold, $\exp(-40\%/m)$, changes by about one third! If nothing else would change in a future climate this small change of the pdf of S_i would have a dramatic effect on the frequency of occurrence and fractional coverage of cirrus clouds. This makes me sceptical as to whether cirrus clouds in a future climate can be predicted at all.

Observations

Figure 1 shows the global distribution of ISSRs obtained from Microwave Limb Sounder (MLS) data on two pressure levels, 147 hPa and 215 hPa [Spichtinger et al., 2003]. The vertical resolution of the data is about 3 km, thus probably only very thick specimen can be detected by Microwave Limb Sounder. On the other hand, in spite of the cloud clearing applied to the Microwave Limb Sounder data, it is not possible to clear the data from signals from ice crystals smaller than $100\ \mu$ in diameter, since such small crystals do not scatter microwave radiation. Hence cirrus clouds containing only small crystals (e.g. sub-visible cirrus) contribute to the Microwave Limb Sounder retrieved humidity (fortunately, 1 kg of ice produces only half the signal as 1 kg of water vapour).

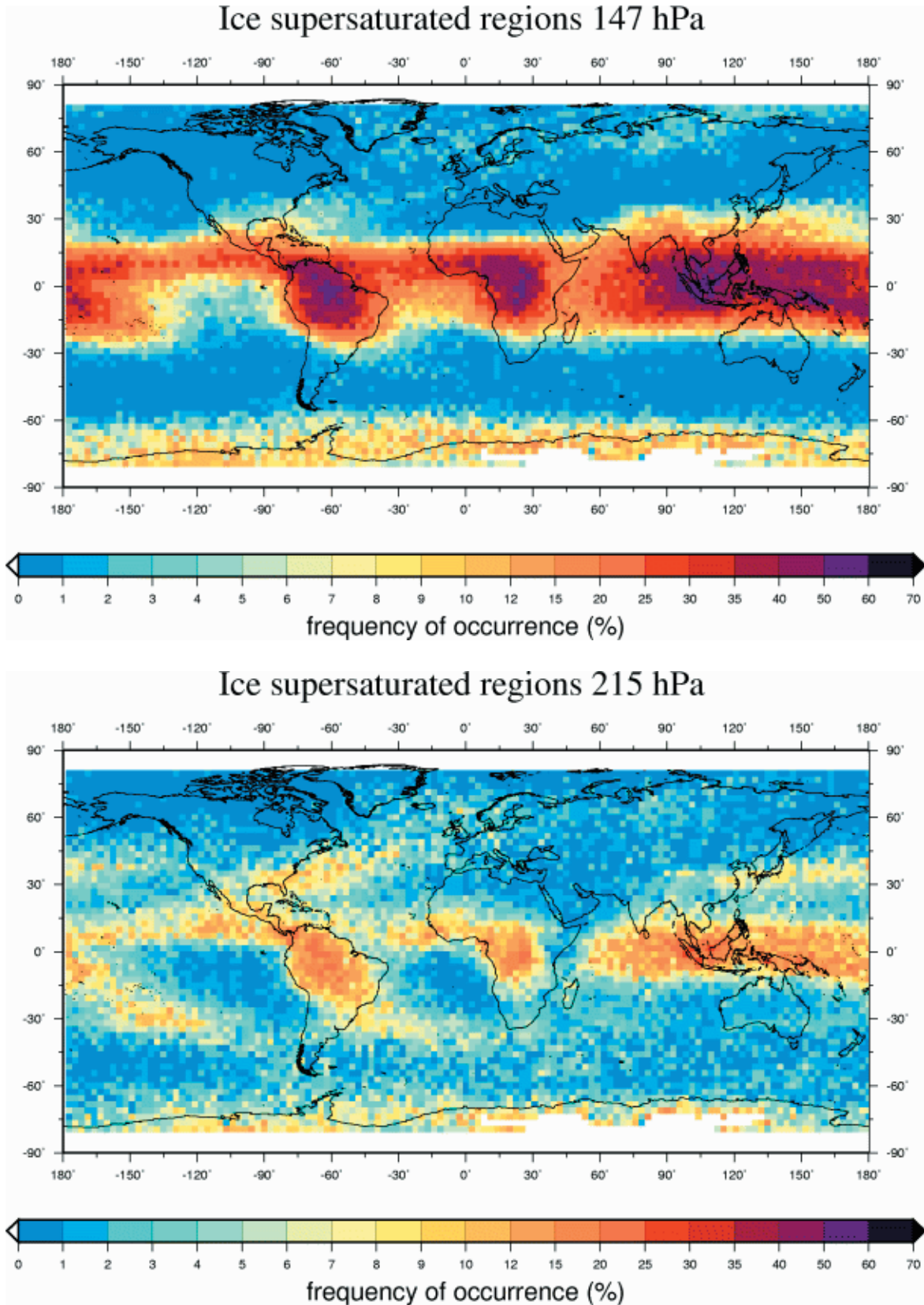


Figure 1: Frequency of occurrence of ice supersaturated regions, as detected by the Microwave Limb Sounder on two pressure levels, 147 and 215 hPa [colour version of the corresponding figure in Spichtinger et al., 2003].

On the 147 hPa level there are strong maxima with more than 40-50% frequency of occurrence over the tropical parts of the continents, over Amazonia, central Africa, and over the Indonesian archipelago. These maxima are bridged by a band of high values of frequency of occurrence along the intertropical convergence zone. Note also the high values over Antarctica that are caused by radiative cooling in the polar winter when the air is confined by the polar vortex. High values of frequency of occurrence also occur in the Arctic, but weaker than their southern counterparts, because of the weaker and more perturbed northern polar vortex. 147 hPa is at the lower boundary of the tropical tropopause layer, and it can be expected that the frequency of ice supersaturation is not considerably less in the tropical tropopause layer than at its lower boundary. This should be kept in mind in considerations about freeze drying of air that enters the tropical lower stratosphere.

On the 215 hPa level there are the same maxima of ISSR occurrence as on the 147 hPa level, but with considerably reduced values of frequency of occurrence (20-30%). Additionally, the middle latitude storm tracks become prominent features, and again high values over Antarctica show up. For more details, see Spichtinger et al. [2003].

When these spatial distributions of ISSR occurrence are compared to distributions of high clouds (e.g. from ISCCP or HIRS data), of sub-visible cirrus [SAGE II data, Wang et al., 1996] or with climatologies of the so-called potential contrail coverage [Sausen et al., 1998] we find always a great degree of similarity in the features of the maps, which sounds plausible since ISSRs are cloud formation regions. However, the prominent cirrus occurrence in the tropics is mostly due to deep convection (anvil cirrus), which I would not count as ISSR related. But of course, deep convection is in the tropics also the ultimate source of water vapour in the upper troposphere and lower stratosphere and tropical tropopause layer, hence the similarity of the spatial distributions is no surprise.

Statistical analyses of temperature and moisture contrasts between ISSRs and their subsaturated environment show that ISSRs are always (in a statistical sense) colder and moister than their environment. The magnitude and physical significance of the contrasts differ from region to region. These contrasts point to the main formation pathways of ISSRs, namely adiabatic and diabatic (radiation) cooling and moisture transport from below. Case studies [Spichtinger et al., 2005a,b] have been performed to investigate formation of ISSRs in more detail.

Ice supersaturation within clouds has been measured in various recent campaigns. This can happen when the crystal growth time scale is longer than other relevant time scales in a cloud, in particular the cooling (or updraught) time scale and sedimentation time scales. Cloud resolving simulations [Spichtinger and Gierens, in prep.] reveal in-cloud supersaturation a rather common phenomenon. Additionally, effects from physical-chemistry, mainly at $T < 200\text{K}$, can lead to in-cloud supersaturation, in particular when ice forms in the cubic crystal lattice [Murphy, 2003], or when the ice surface is covered by nitric acid trihydrate [Gao et al., 2004].

Physics

The physics of homogeneous nucleation of aqueous solution droplets is the ultimate reason for the widespread existence of ISSRs. In short: Pure water cannot exist below the maximum supercooling temperature of about -38°C , only solution droplets remain liquid in colder layers, because the foreign molecules impede the formation of the ice crystal lattice. At increasing supersaturation the solution droplets grow by uptake of water molecules from the gas phase, thereby rarefying the foreign molecules. When the foreign molecules are rarefied enough then the ice lattice can be formed and the droplet freezes. This generally needs supersaturations of more than 40%, increasing with decreasing temperature. The Koop et al. [2000] theory of water activity controlled homogeneous nucleation implies that the freezing threshold supersaturation is independent of the composition of the droplets; freezing is a thermodynamically driven process (however, droplets containing ammoniated species have been observed to behave differently for so far unknown reasons).

Heterogeneous ice formation can proceed at lower supersaturations. However, ice nuclei that are appropriate to form ice below the humidity threshold for homogeneous nucleation seem to be rare, and even if they are present and if they form ice crystals, they may not hinder the later production of much more ice crystals via the homogeneous pathway.

Whereas the fractional cover of cirrus clouds is at least 20-30% (much larger if we include sub-visible cirrus), the probability to surpass the homogeneous nucleation threshold is only of the order one percent \approx seemingly a contradiction. This may be resolved partly by considering that a large fraction of cirrus is produced by tropical deep convection. The remaining gap may be explained by consideration of the time scales. The time span an air parcel is above the nucleation threshold is certainly much smaller than the life time of a cirrus cloud. Hence it is much more probable to find a cirrus cloud than an air mass with humidity exceeding the nucleation threshold, which may resolve the contradiction.

Concluding remarks

It is overdue that large scale models treat cirrus clouds and ISSRs in an appropriate way, for example to allow forecast of persistent contrails. This is also a minimum prerequisite for the prediction of cirrus in a warmer climate. Additionally, we need better data on vertical wind speeds in the upper troposphere and lower stratosphere, ideally with a few cm/s resolution.

Unfortunately, our data of relative humidity (RH) in the upper troposphere and lower stratosphere are not good. A source of much data noise is the practice of reporting relative humidity with respect to liquid water, RH_w. Since bulk liquid water does not exist below -38°C , its vapour pressure cannot be measured, and, to translate RH_w into something useful, we all use a wide variety of mathematical extrapolations that differ by more than 10% at -60°C , even more at still colder temperatures. If WMO would report radiosonde and other measurements of relative humidity in the cold layers of the atmosphere as relative humidity with respect to ice, RH_i, much of the uncertainties would be overcome, because vapour pressure over ice can be measured, and existing formulations differ only by 2% or so.

References

- Gao, et al., Evidence that nitric acid increases relative humidity in low-temperature cirrus clouds, *Science*, 303, 516-520, 2004.
- Koop, T., B. Luo, A. Tsias and T. Peter, Water activity as the determinant for homogeneous ice nucleation in aqueous solutions, *Nature*, 406, 611-614, 2000
- Murphy, D.M., Dehydration in cold clouds is enhanced by a transition from cubic to hexagonal ice, *Geophys. Res. Lett.*, 30, 2230, doi:10.1029/2003GL018566, 2003.
- Sausen, R., K. Gierens, M. Ponater and U. Schumann, A diagnostic study of the global distribution of contrails, Part I. Present day climate. *Theor. Appl. Climatol.* 61, 127-141. Schaefer, V.J., 1946: *Science*, 104, 457, 1998.
- Spichtinger, P., K. Gierens and W. Read, The global distribution of ice-supersaturated regions as seen by the Microwave Limb Sounder. *Q.J.R. Meteorol. Soc.*, 129, 3391-3410, 2003.
- Spichtinger, P., K. Gierens, and H. Wernli, A case study on the formation and evolution of ice supersaturation in the vicinity of a warm conveyor belt's outflow region, *Atmos. Chem. Phys.*, 5, 973-987, 2005a.
- Spichtinger, P., K. Gierens, and A. Dörnbrack, Formation of ice supersaturation by mesoscale gravity waves, *Atmos. Chem. Phys.*, 5, 1243, 2005b.
- Wang, P.-H., et al., A 6-year climatology of cloud occurrence frequency from Stratospheric Aerosol and Gas Experiment II observations (1985-1990), *J. Geophys. Res.*, 101, 29407, 1996.

Further References

- Cwilong, B.M., *Proc. R. Soc. Lond. A*, 190, 137, 1947.
- Findeisen, W., *Meteor. Z.*, 55, 121, 1938.
- Krastanow, L., *Meteorol. Z.*, 57, 357, 1940.
- Wall, E., *Meteorol. Z.*, 59, 177, 1942.
- Wegener, A.: cited from E. Wall, *Meteorol. Z.*, 59, 109, 1942.
- Fahrenheit, D.G., *Philos. Trans. R. Soc. London*, 33, 78, 1724.
- Glückauf, E., *Q.J.R. Meteorol. Soc.*, 71, 110, 1945.
- Schaefer, V.J., *Bull. Am. Meteorol. Soc.*, 29, 175, 1948.
- Wall, E., *Meteorol. Z.*, 60, 94, 1943.
- Weickmann, H.K., *Beitr. Phys. fr. Atm.*, 28, 12, 1945.

Tropical Cirrus Clouds Modelling and Tests in Field Campaigns

C. Ren, and A.R. MacKenzie

Department of Environmental Sciences, Lancaster University, England

Following the Dobson-Brewer circulation, water enters the stratosphere through the tropical tropopause layer (TTL), just like many other trace species. But unlike other species, the water content of an air parcel entering the stratosphere is controlled by microphysical processes.

To account for the freezing-dry processes, a cirrus parametrisation has been developed which includes the most important microphysical processes in cirrus clouds, and captures the principal features of the behaviour of detailed particle-size-resolved models [Ren & MacKenzie, 2005]. When the parametrization is run with domain-filling trajectories, the results can be used to reconstruct a kind of field of cirrus clouds.

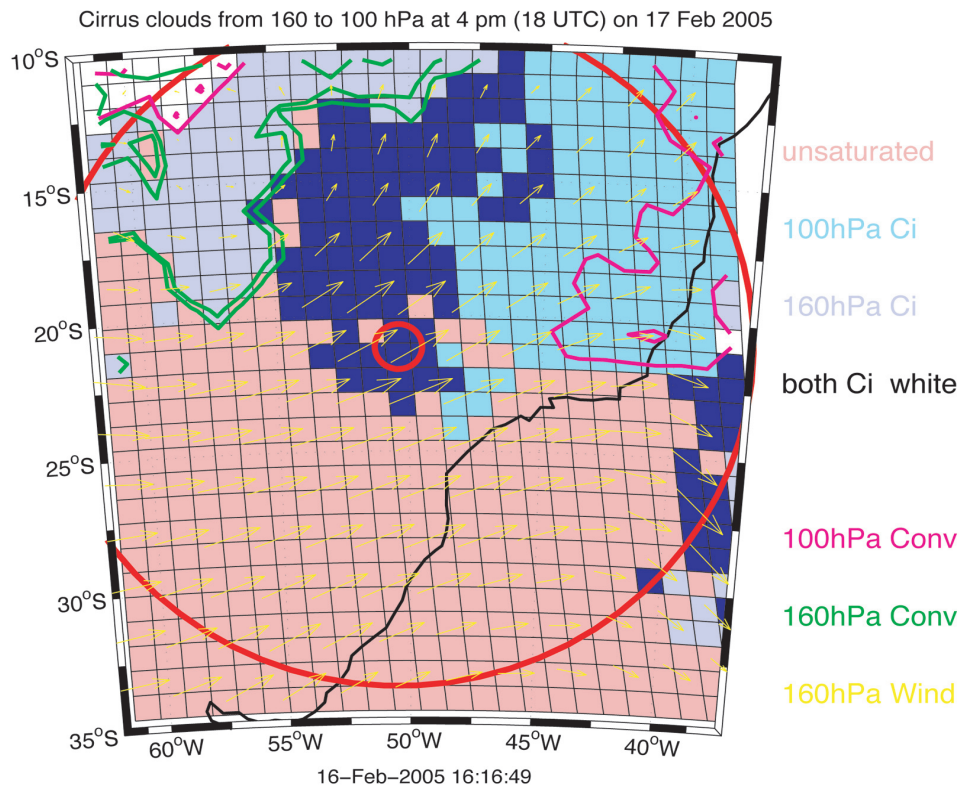


Figure 1: An example of cirrus cloud forecast. The smaller red circle shows the aircraft base, the bigger red circle is the reach of Geophysica. Pink shows where air is unsaturated at both levels; cyan shows cirrus at 100 hPa, grey shows cirrus at 160 hPa, white shows cirrus at both levels, and blue shows saturation at either level. Magenta contours encompass cirrus at 100 hPa that might be influenced by convection. Green contours show the same but for 160 hPa. Yellow vectors show the displacements of air parcels in the previous three hours.

During the 2nd field campaign of TROCCINOX project carried out in January/February 2005 in Brazil, the occurrence of cirrus clouds was built (forecasted) using trajectories generated from ECMWF forecast data. Such products were provided to the flight-planning group for their information (<http://campion.lancs.ac.uk/public/troccinox>). While our products were in line with other forecasts, they were presented in an intuitive way (Figure 1).

The TROCCINOX field campaigns provided a unique opportunity to elaborate the processes determining the entry-level of stratospheric water. The FISH instrument onboard Geophysica made measurements of total water in the tropical tropopause layer and lower stratosphere. These measurements were used to check our modelled results. To enable this, water vapour mixing ratios along a flight track were first reconstructed by applying the microphysical parametrization to trajectories, which were 10-day backward trajectories using ECMWF analysis data and initialised from the flight track every 10 seconds. Figure 2 shows the reconstructed water

mixing ratios (blue line). Also shown in the figure are ECMWF analysis water vapour mixing ratios interpolated to the flight track (red line). On the left is reconstructed water on 15th February. This is the case we got the best agreement among the three values, because this ENVISAT validation was undertaken in a rather simple weather condition. However, several downward spikes of reconstructed water hint the processes having not been taken into account, i.e., mixing and rehydration. On the right of the figure is reconstructed water mixing ratios on 8th February. In this case, connection of maxima of the reconstructed water vapour gives the best match to the observation. This means dehydration has been treated well, except the peak just before 15.5 UTC. As homogeneous nucleation of ice particles is assumed in the parametrization, existing ice particles or ice nuclei could be responsible for the exceptions. On the other hand, as rehydration is not included in the parametrization, many low values of water vapour mixing ratios are achieved along the flight track, even lower than the analysis values. The analysis water vapour is systematically lower than the observation, because no supersaturation is allowed in the ECMWF model. Also in this day, Geophysica caught micrometer particles (most possibly ice crystals) four times. For the four parts of flight track, our model got one cloud, two supersaturated regions, and one dry place that was at around a quarter before 14 UTC.

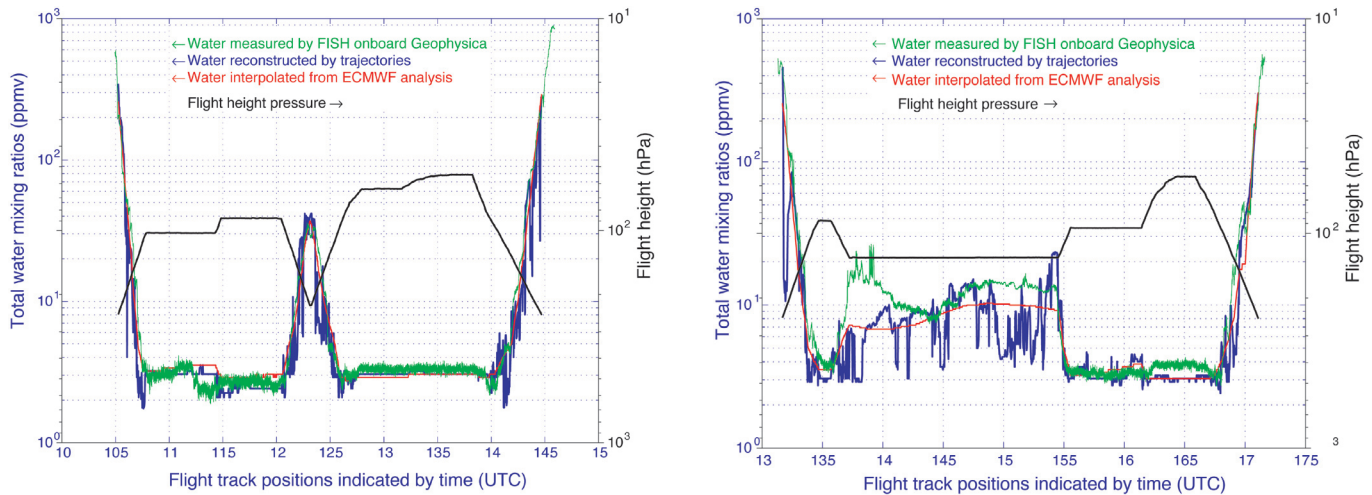


Figure 2: Water mixing ratios along the flight track of Geophysica on 15th February 2005 (left), and on 8th February 2005 (right). Blue line: reconstructed water vapour; red line: interpolation of analysis water vapour; green line: total water measured by FISH onboard Geophysica; black line: flight height in hectopascal.

This kind of cirrus clouds could be the clouds that make the final tweak of water content entering the stratosphere. Such results encourage us to validate the method and carry on forecast tests for the SCOUT-O3 field campaign.

Acknowledgements

The authors thank to TROCCINOX field campaign team for getting the valuable data, British Atmospheric Data Centre for providing forecast and analysis data, D. Brunner for providing trajectories. FLEXTRA code was used to generate trajectories from flight tracks. The study was funded by NERC CWVC project GST/02/2892, EC TroCCiNOx project EVK2-CT-2001-00122, and EC SCOUT-O3 project GOCE-CT-2004-505390.

References

Ren, C. and A.R. MacKenzie, Cirrus parametrization and the role of ice nuclei, Q.J.R. Meteorol. Soc. 131, 1585-1605, 2005.

Cirrus Clouds and Ice Supersaturated Regions Observed by Raman Lidar and Radiosondes

F. Immler¹, K. Krüger¹, O. Schrems¹, D. Engelbart², P. Fortuin³, G. Verver³

¹Alfred Wegener Institute for Polar and Marine Research, Germany; ²Meteorological Observatory Lindenberg, Germany;

³Royal Netherlands Meteorological Institute, Netherlands

With our mobile Aerosol Raman Lidar (MARL) we have performed field campaigns in the mid latitudes in 2003 (Lindenberg/Germany, 53°N, 15°E) and in the tropics in 2004/05 (Paramaribo/Suriname, 6°N, 55°W). The lidar system detects aerosols and clouds in the UTLS region. It is capable of detecting thin cirrus including extremely thin clouds with optical depth below 10^{-3} . The system measures cloud altitudes with high vertical and temporal resolution and determines the depolarisation and optical depth. It operates day and night. During daytime cloud types including contrails are classified with the help of a video camera. During the campaigns, water vapour was measured by means of balloon borne sondes (Vaisala RS80/RS90, 'Snow white' frost point hygrometer) and by the LIDAR using the Raman technique. We investigated the occurrence of ice supersaturated regions and their relation to the occurrence of clouds. The accuracy of the water vapour measurements needs to be critically evaluated for this purpose. The cloudiness in the upper troposphere was found to be very high in the tropics where in about 90% of all measured profiles cirrus was present. In the middle latitudes cirrus were found in 55% of the measurements.

Middle latitudes

According to the radiosonde data, ice supersaturated regions (ISSRs) occur most often between 6 and 9 km altitude. In about 25% of all radiosoundings ISSRs were detected. However these were most often very thin layers, so in total only 4% of the upper troposphere ($h > 6$ km) was supersaturated with respect to ice. The lidar detected only in a few cases ice particles in these layers. On the other hand, cirrus clouds were frequently detected in the upper troposphere above 9 km. About 35% of these clouds were subvisible. They occurred regularly during stable high pressure regimes, which were predominant during the exceptionally hot and sunny

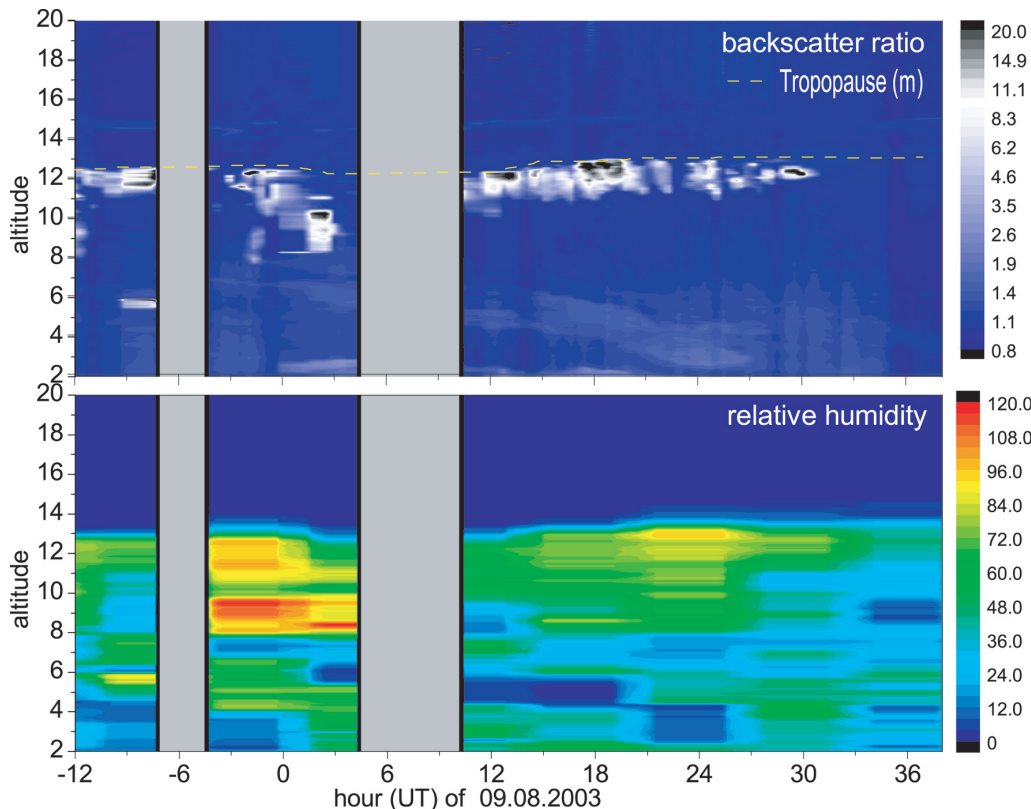


Figure 1: Measurement of cirrus clouds by a lidar (upper panel) and water vapour by radiosondes (lower panel) from 8th August 2003 12:00 UT to 10th August 2003, 14:00 UT at Lindenberg.

midlatitudes, the frequency of subvisible cirrus is enhanced in the tropics. Often subvisible cirrus occur at the cold point tropopause (CPT). We define the tropical tropopause layer (TTL) as the region between the CPT and an upper tropospheric inversion (UTI) which frequently occurs about 2-3 km below the CPT. We investigated the occurrence of cirrus in the TTL with a trajectory model which was recently developed at the AWI [Tegtmeier et al., 2004]. This model derives vertical transport from diabatic heating rates which were calculated with a radiative transfer model. Further, we derive the relative humidity from the backward trajectories by assuming that the air is dehydrated to saturation vapour pressure when supersaturation occurs upon adiabatic cooling. The cirrus occurrence determined with the lidar as well as the relative humidity measured by the Snow White frost point hygrometer agree amazingly well with the model output. We conclude that vertical transport in the TTL is determined mainly by diabatic heating. Also, the cirrus in the TTL dehydrate the air efficiently. The humidity of air entering the stratosphere is therefore determined by the saturation vapour pressure at the coldest point of the trajectory of an air parcel. This result is in good agreement with the results obtained by Fueglistaler et al. [2005]. However it remains an open question, why cirrus can form so easily and does not seem to require high supersaturations. The results are discussed in detail by Immler et al. [2005].

summer 2003. More than 60% of the contrails that were identified with a CCD camera, were embedded in thin or subvisual cirrus. Cirrus occurrence is correlated to high humidity as shown in Figure 1. However, according to the radiosonde data, saturation is generally not reached. This is most likely due to a dry bias of the radiosonde data. This bias is found when comparing humidity measured by the radiosonde with the results from the Raman lidar. Accordingly, there is a significant dry bias of the RS80 at temperatures below 230 K. A precise determination of the conditions at which subvisible cirrus and contrails form, require more precise water vapour measurements than currently available.

Tropics

During the STAR pilot study from 20th September to 15th November 2004 numerous measurements were made by the same lidar in Paramaribo. Cirrus were present in almost 90% of all cases. Compared to the

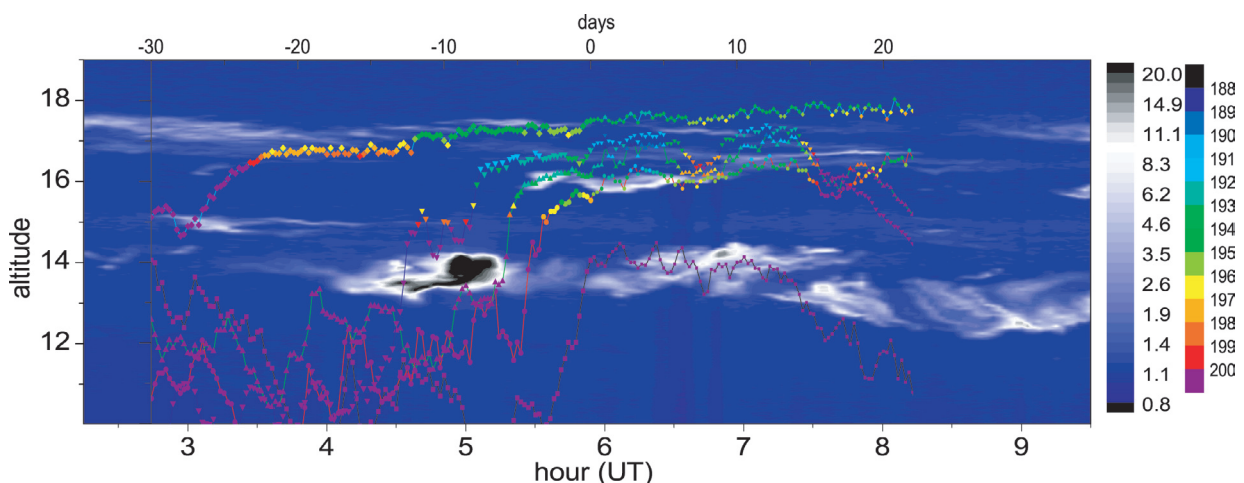


Figure 2: Cirrus measurement by lidar in Paramaribo from 2nd October 2004 and trajectories calculated for 06:00 UT by the AWI trajectory model. Colour coded is the Temperature in K.

References

- Immler F., K. Krüger, G. Verver, P. Fortuin O. Schrems, Cirrus clouds, humidity, and dehydration at the tropical tropopause observed in Paramaribo/Suriname (5.8° N, 55.2° W), submitted to J. Geophys. Res., 2005.
- Fueglistaler, S., M. Bonazzola, P. H. Haynes and T. Peter, Stratospheric water vapor predicted from the Lagrangian temperature history of air entering the stratosphere in the tropics, J. Geophys. Res., 110, D08107, doi:10.1029/2004JD005516, 2005.
- Tegtmeier, S., K. Schoellhammer, M. Rex, I. Wohltmann and J.J. Morcrette, Variations of the residual circulation in northern hemispheric winter and the impact on Arctic ozone, Poster presentation at 3rd SPARC General Assembly, 16 August 2004, Victoria, British Columbia, Canada, 2004.

Ice supersaturation and persistent contrail occurrence over Reading, UK

G. Rädcl and K.P. Shine

Department of Meteorology, University of Reading, England

Persistent contrails that spread and form extended cirrus clouds may perturb the radiation budget of the Earth. In order to be able to quantify this radiative forcing, the frequency of occurrence of persistent contrails has to be known; this depends on the air traffic density and on the presence of favourable atmospheric conditions, which is most importantly the presence of cold atmospheric regions supersaturated with respect to ice. We studied the occurrence of supersaturation for the UK using measured atmospheric temperature and humidity profiles from five different UK radiosonde stations, covering different latitudes and longitudes and delivering data regularly since 2000. The radiosondes are of type RS80-H and were corrected for known biases at low temperatures according to Wang et al, 2002. The criteria we impose are: the layer, in a pressure interval of 150 to 400 hPa, must be supersaturated with respect to ice, i.e. RH_{ice} must be larger than 100% and the temperature must be lower than -40°C [e.g. Schumann, 1996].

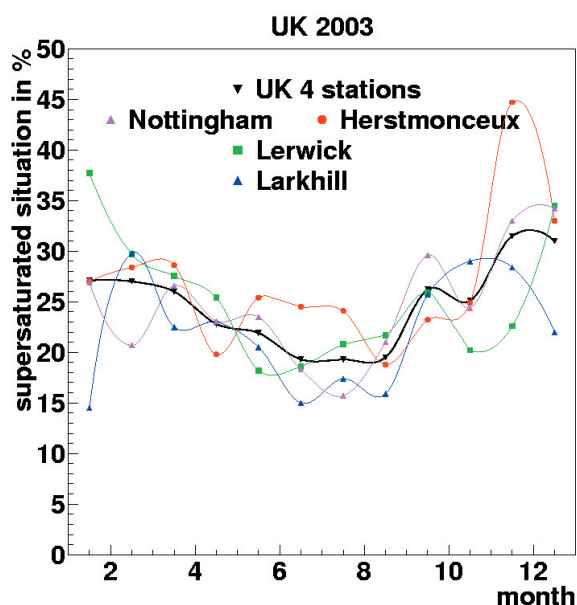


Figure 1: Seasonal variation of the percentage of cases when an atmospheric layer is supersaturated w.r.t. ice and the temperature is lower than -40°C for four different radiosonde stations in the UK in 2003.

Figure 1 shows the percentage of supersaturated conditions with respect to all radiosonde measurements as a function of the month separately for four different stations in 2003. All curves show qualitatively the same behaviour, in summer the probability that a permanent contrail may form is smallest and in winter it is largest.

Analysing the vertical profiles of these corrected relative humidity measurements for all data from 2000-2003, it was found that atmospheric layers susceptible to persistent contrails are on average about 55 hPa thick in winter and 39 hPa thick in summer (median values); 25% of the times these layers are thinner than 20 hPa for winter; the value is 30% in summer; maximum values go up to about 200 hPa in winter but only about 130 hPa in summer.

In order to confirm the assumption that the presence of a cold supersaturated atmospheric layer gives rise to the occurrence of persistent contrails we compared the radiosonde measurements to actual observations of persistent contrails over Reading. Since July 2004 we tried to check routinely at least four times a day, i.e. at 0900, 1200, 1500, and 1800, whether persistent contrails formed over Reading. One full year of observations (July 2004 - June 2005) have been collected now.

We compared the times of our observations with radiosonde launches from the five different stations Larkhill, Herstmonceux, Nottingham, Camborne and Lerwick. The distances to Reading for these stations are, respectively, 63 km, 111 km, 170 km, 330 km and 970 km.

A statistical analysis of all observations was performed creating 2x2 contingency tables, as defined in Table 1, for each of the stations. They are shown in Table 2. A possible method to compute the statistical significance of these results is the 'Odds ratio' which has been proposed by Stephenson [2000] for the use in a meteorological application. The Odds ratio is defined

Contrails:		observed	
predicted	yes	a	b
	no	c	d

	Larkhill	Herstmonceux	Nottingham	Camborne	Lerwick
yes	23	24	10	19	10
no	1	3	6	8	10
total	24	27	16	27	20

Table 1: 2x2 contingency table

Table 2: 2x2 contingency tables for the 5 radiosonde stations:

as $R=(a*d)/(b*c)$. It is 1 for the null hypothesis, i.e. no correlation between observation and prediction, larger 1 in case of a positive correlation, and smaller 1 for a negative correlation. The natural logarithm of R is asymptotically Gaussian distributed, with a standard deviation of $\frac{1}{\sqrt{a + 1/b + 1/c + 1/d}}$. Results for the Odds ratios, hit- and false alarm-ratios, the ratio of correct predictions, i.e. $(a+d)/(a+b+c+d)$ and the significance computed from $\ln R$ and $\frac{1}{\sqrt{a + 1/b + 1/c + 1/d}}$, that is the probability to observe a configuration that is more extreme than the observed one, are given in Table 3, along with the Peirce skill score [Peirce, 1984] which is just the hit-rate - false alarm rate and its significance. This score gives a measure of the accuracy both for 'yes' and 'no' events. It ranges from -1 to 1, and is 0 for a random forecast. It is -1 if neither 'yes' nor 'no' events are predicted correctly.

For the two stations Larkhill and Herstmonceux, which are 63 km and 111 km away from Reading respectively, there is a clear match between the observations and the predictions. Nottingham, at 168km distance, suffers from the fact that the radiosondes could for the moment not be fully corrected. Camborne gives surprisingly good results. A possible reason could be pre-dominant dynamical conditions due to the location of Camborne to the west of Reading. This still has to be studied. As expected, Lerwick which is almost 1000km away shows no correlation at all between observations and predictions.

Table 3: Results of statistical analyses of radiosonde versus visual observation comparisons

distance to Reading	Odds ratio (a*d)/(b*c)	hit rate a/(a+c)	false alarm rate b/(b+d)	ratio of correct predictions	significance log Odds ratio	significance Peirce score
63 km	46	0.58	0.03	0.76	3.8±1.1 <0.05%	0.55 <0.05%
111 km	16	0.57	0.08	0.74	2.8±0.7 <0.05%	0.49 <0.05%
168 km	1.6	0.32	0.23	0.53	0.5±0.6 23%	0.09 43%
332 km	3.5	0.50	0.21	0.64	1.3±0.5 1.7%	0.28 1%
969 km	0.7	0.40	0.47	0.46	-0.4±0.6 55%	-0.08 59%

Acknowledgement

GR is funded by Airbus and the Department of Trade and Industry. The radiosonde data was obtained from the NERC British Atmospheric Data Centre.

References

- Peirce, C.S., The numerical measure of the success of predictions, *Science*, 4, 453-454, 1884.
 Schumann, U., On conditions for contrail formation from aircraft exhausts. *Meteorol. Zeitschrift*, 5, 4-25, 1996.
 Stephenson, D.B., Use of the "Odds Ratio" for Diagnosing Forecast Skill, *Weather and Forecasting*, 15, 221-232, 2000.
 Wang, J., H.L. Cole, D.J. Carlson, E.R. Miller, and K. Beierle, Corrections of Humidity Measurement Errors from the Vaisala RS80 Radiosonde - Application to TOGA COARE Data, *J. Atmos. Ocean. Techn.*, 19, 981-1002, 2000.

World War II Bomber Contrails: A Study of Aviation Effects on Climate

A. Faux¹, A.R. MacKenzie¹ and Roger Timmis²

¹Environmental Science Department, Lancaster University, England; ²Environment Agency, England

Over the last few years, studies on the condensation trails formed by aircraft have shown that there may be a significant link between the total amount of aviation produced cloud cover over a region and a change in the diurnal temperature range of the same region [Marquart et al., 2003; Travis et al., 2004, 2002; Meerkotter et al., 1999; Schumann et al., 1998]. Condensation trails, or contrails, form when the hot, humid air from aircraft jet engines mixes with the cold air of the troposphere. Recent assessments by the International Panel on Climate Change (IPCC) and the Royal Commission on Environmental Pollution have investigated both the direct radiative forcing of narrow contrails as well as the indirect effect caused by the induction of a cirrus cloud deck. Both the IPCC and the Royal Commission on Environmental Pollution have stressed the need to examine the effects of these aircraft induced cirrus cloud, on the climate.

In general, the climate forcing influence of contrails is difficult to distinguish from other climatic effects as the changes can be masked by simple weather variations. However, during times when all aircraft activity is suddenly changed, the influence of contrails may become more apparent. A unique example of this occurred when all commercial aircraft activity was banned over the United States of America for a period of 72 hours following the terrorist attacks in September 2001. A study carried out during this three day grounding found there was on average a 1.8°C increase in the diurnal temperature range when compared to the adjacent three day periods of normal aircraft activity and approximately a 1°C increase when compared to the long term, yearly normals. Furthermore, the greatest increases in daily temperature range, over twice the national average, were reported to have occurred in those regions of the United States where contrail coverage was usually most abundant such as the Midwest [Travis et al., 2002]. The most plausible explanation for this deviation from normal was the lack of substantial contrail coverage due to the grounding of aircraft.

In considering World War II bombing raids from England to Europe, we are studying an opposite situation to that which occurred between 11th to 14th September 2001. During 1943 - 45 there were many intense and well-defined bombing raids that left England, which may be used for an analysis of the effects from intensively increased aviation as compared to the intensively decreased aviation of 11th to 14th September 2001. Using these raids it may be possible to identify a suppression of the diurnal temperature range, an increase in total cloud cover and a decrease in total sunshine reaching the Earth's surface. The raids were carried out in a period of history when general air travel was not commonplace and therefore had a predominantly contrail free background sky from which to quantify any results. The location of the bomber and fighter bases and the organisation of the raids themselves would allow temporal comparison of periods with very high frequency and spatial extent of contrails with periods when there were none as well as geographic comparison of overflown and non-overflown regions. There were also significant numbers of meteorological observations. Together, these factors provide the best possible opportunity of finding aviation induced climatic signals, as

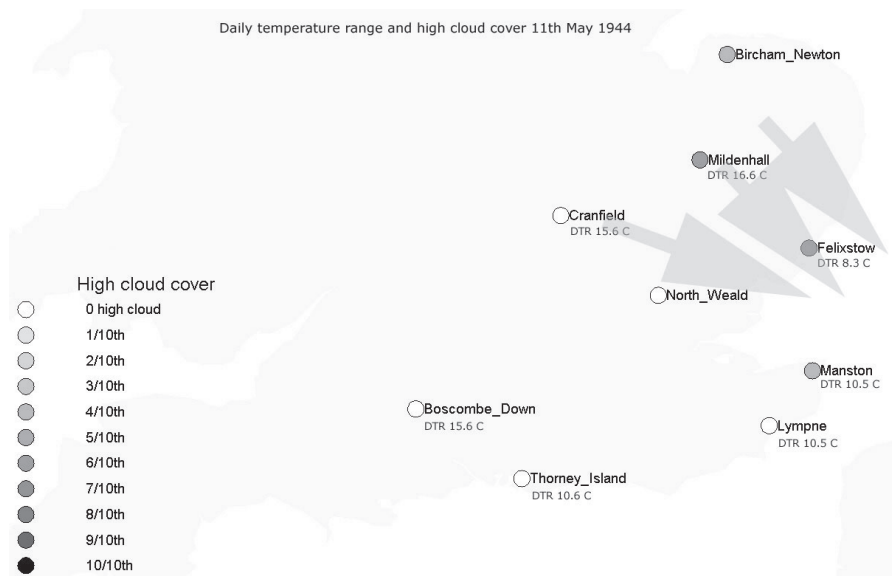


Figure 1: Daily temperature ranges (DTR) for each station that reported a max and min temperature at 0700 and 1800 GMT. High cloud cover amounts are for 1400 GMT on the 11th May 1944, the approximate time at which the aircraft from the morning raid were returning, and those participating in the afternoon raid were taking off. The grey arrows indicate the outward flight path of the aircraft in the second raid.

well as potentially mimicking the effect of the increase in air traffic expected to occur over the next fifty years. To this end, the raids carried out by the United States Army Air Force Eighth Bomber Command, later renamed the Eighth Air Force were selected. By examining tactical mission reports and archived meteorological data, suitable raid dates were selected and the relevant meteorological information extracted from the archives. By comparing data from raid days with the adjacent non-raid days, and same day overflow and non-overflow regions, both temporal and geographic comparisons can be made. If found these will strengthen the argument for the direct effect of contrails on the climate.

Bombing raids were selected for further study if:

- they were adjacent to days that were raid-free,
- the aircraft gathered into formation and flew at an altitude suitable for contrail formation over England (approximately 20,000ft or 6 km altitude)
- there were photographic or first-hand accounts of the raids producing persistent contrails
- they had over 1000 aircraft participating.

From an initial number of approximately 1000 raids carried out between May 1943 and May 1945 by the Eighth and Ninth Air Force, and after examining all the archived meteorological and military information, we found no raids that precisely met our criteria. Given the time limitations, rather than widen the criteria and search again, it was decided that one of the raid periods, the 10th to 14th May 1944, which had come close to fulfilling the original parameters, would be studied. The only failing of this raid period was the weather on the 10th to 14th May, the non-raid days, was poor and so no temporal comparison could be made. Therefore, this study focused on the geographical comparisons of overflow and non-overflow regions on these particular raid days.

Initial results from the 11th and 12th May 1944 indicate an increase in high cirrus and cirrostratus reported at both the directly overflow stations and those immediately adjacent to the flight path when compared to the non-overflow meteorological stations, see figure 1. In addition, the directly overflow meteorological stations appear to show a suppression of their daily reported temperature range of up to 8.3 degrees Celsius. However, although these initial results look promising, further analysis as to the influence of sea breezes at the coastal meteorological stations for example, must be taken into account before any firm conclusions can be drawn as the climate forcing effect of World War II bomber and fighter contrails.

References

- Intergovernmental Panel on Climate Change (IPCC), Aviation and the global atmosphere, special report, summary for policymakers, Editors: J.E. Penner, D.H. Lister, D.J. Griggs, D.J. Dokken, and M. McFarland, Cambridge University Press, 1999.
- Marquart, S., M. Ponater, F. Mager, R. Sausen, Future development of contrail cover, optical depth and radiative forcing: Impacts of increasing air traffic and climate change, *J. Climate*, 16, 2890-2904, 2003.
- Meerkotter R., U. Schumann, D.R. Doelling, P. Minnis, T. Nakajima, Y. Tsushima, Radiative forcing by contrails, *Ann Geophys*, 17, 1080-1094, 1999.
- Schumann U., On conditions for contrail formation from aircraft exhausts, *Meteorol.Z.*, 5, 4-23, 1996.
- Travis D.J., A.M. Carleton and R. G. Lauritsen, Contrails reduce daily temperature range, *Nature*, 418, 601, 2002.
- Travis D.J., A.M. Carleton, R.G. Lauritsen, Regional variations in U. S diurnal temperature range for the 11-14 September 2001 aircraft groundings, Evidence of jet contrail influence on climate, *Amer. Meteor. Soc.* 17, 1123-1134, 2004.

Thin Cirrus and Upper Tropospheric Humidity from TOVS Path-B: Natural Variability and Impact of Air Traffic on Cirrus Coverage

C.J. Stubenrauch¹, A. Chédin¹, U. Schumann² and K. Gierens²

¹CNRS - IPSL Laboratoire de Météorologie Dynamique (LMD), Ecole Polytechnique, Palaiseau, France

²DLR-Institut für Physik der Atmosphäre Oberpfaffenhofen, Germany

Data

The TOVS Path-B data set [Scott et al., 1999] provides atmospheric temperature and water vapor profiles as well as cloud properties over the globe, from 1987 to 1995. The relatively high spectral resolution of this instrument yields reliable cirrus properties, day and night [Stubenrauch et al., 1999a].

After a multi-spectral cloud detection [Stubenrauch et al., 2004], the HIRS radiances are averaged separately over clear pixels and over cloudy pixels within 100 km x 100 km regions. The average cloud-top pressure (p_{cl}) and the average effective cloud emissivity (e_{cl}) over cloudy pixels are obtained from five radiances along the 15 mm CO₂-absorption band, with peak responses from 400 hPa levels to the surface [Stubenrauch et al., 1999b]. Cloud height of the revised TOVS Path-B data set has been evaluated [Stubenrauch et al., 2005] by using quasi-simultaneous vertical profiles of backscattered radiation from the Lidar In Space Technology Experiment (LITE). The cloud height determined by TOVS corresponds in general well to the height of the 'apparent middle' of the cloud system.

In the case of clear sky and thin clouds, the vertical distribution of specific humidity is obtained by using a neural network approach on channels most sensible to water vapour absorption combined with those sensitive to tropospheric temperature [Chaboureaud et al., 1998]. Due to the relatively coarse resolution of the channels sensitive to water vapour, the TOVS instruments only provide water vapour integrated over relatively thick layers. Upper tropospheric relative humidity with respect to ice, U_{ice}, is therefore computed from the specific humidity integrated over atmospheric layers between 300 and 100 hPa (or between 500 and 300 hPa), W, and using the retrieved temperature in pressure steps of about 25 hPa, T(p):

$$U_{ice}(\Delta p) = \frac{g \rho W}{0.622 \int_{100-300 \text{ hPa}} dp e_{sat}^{ice}(T(p)) [p - (1 - 0.622)e^{ice}(T(p))]}$$

with gravity g, water density ρ and saturated partial water vapour pressure e_{sat} with respect to ice (Sonntag 1990), which is determined from the temperature profile within the height interval.

Frequency distributions of upper tropospheric relative humidity integrated over an atmospheric layer between 300 and 100 hPa, are slightly narrower for situations with clear sky than for those with thin cirrus [Figure 1 of Stubenrauch & Schumann, 2005], but few clear sky scenes are also ice saturated in agreement with other observations [Gierens et al., 1999]. It is interesting to note that most of these ice saturated regions are situated near the subtropical jet streams.

An analysis combining information on upper tropospheric relative humidity and cirrus coverage has been carried out for investigating the impact of air traffic on cirrus formation. Contrails form when the hot and humid exhaust gases from the combustion of fuels by an aircraft mix with the ambient, cold atmosphere [Schumann, 1996]. Their persistence depends on upper tropospheric humidity and temperature [Sausen et al., 1998]. Upper tropospheric relative humidity from TOVS is used to distinguish situations favorable for persistent contrails. Trends of seasonal mean effective high cloud amount (e_{cl} weighted by cloud cover over a 1° latitude x 1° longitude grid) have been analysed in regions with high and low air traffic density. The difference in trends of effective high cloud amount between potential contrail situations and cirrus or between potential contrail situations and all situations could be used as an indicator of cirrus increase due to air traffic increase. Over Europe, a region with especially high air traffic density, this difference amounts to 2.8% or 3.5% per decade, respectively.

However, situations of potential contrails only occur in about 5 to 10% of all situations. Weighted by frequency of potential contrail occurrence, the overall increase amounts to at least 0.20% - 0.25% per decade over Europe. On average over all situations, the increase amounts to at least 0.3% per decade in these regions. A detailed analysis and results are published in [Stubenrauch and Schumann, 2005].

References

- Chaboureaud, J.-P., A. Chédin and N.A. Scott, Remote sensing of the vertical distribution of atmospheric water vapor from the TOVS observations: Method and validation, *J. Geophys. Res.*, 103, 8743-8752, 1998.
- Gierens, K., U. Schumann, M. Helten, H. Smit and A. Marengo, A distribution law for relative humidity in the upper troposphere and lower stratosphere derived from three years of MOZAIC measurements. *Ann. Geophysicae*, 17, 1218-1226, 1999.
- Sausen, R., K. Gierens, M. Ponater and U. Schumann, A diagnostic study of the global distribution of contrails. Part I: Present day climate, *Theor. Appl. Climatol.*, 61, 127-141, 1998.
- Schumann, U., On conditions for contrail formation from aircraft exhausts, *Meteorol. Z.*, 5, 2-23, 1996.
- Scott, N.A., A. Chédin, R. Armante, J. Francis, C.J. Stubenrauch, J.-P. Chaboureaud, F. Chevallier, C. Claud and F. Chéruy, Characteristics of the TOVS Pathfinder Path-B data set, *Bull. Amer. Meteor. Soc.*, 80, 2679-2701, 1999.
- Sonntag, D., Important new values of the physical constants of 1986, vapor pressure formulation based on the ITS-90 and psychrometer formulae, *Z. Meteorol.*, 70, 340-344, 1990.
- Stubenrauch, C.J., W.B. Rossow, N.A. Scott and A. Chédin, Clouds as seen by Infrared Sounders (3I) and Imagers (ISCCP): Part III) Spatial Heterogeneity and Radiative Effects, *J. Climate*, 12, 3419-3442, 1999a.
- Stubenrauch, C.J., A. Chédin, R. Armante and N.A. Scott, Clouds as seen by Infrared Sounders (3I) and Imagers (ISCCP): Part II) A New Approach for Cloud Parameter Determination in the 3I Algorithms, *J. Climate*, 12, 2214-2223, 1999b.
- Stubenrauch, C.J., and the CIRAMOSA team 2004. Final report on the European Environmental project EVK2-CT-2000-00063, 99 pp., available at: <http://www.lmd.polytechnique.fr/CIRAMOSA/Welcome.html>.
- Stubenrauch, C.J., F. Eddouinia and L. Sauvage, Cloud heights from TOVS Path-B: Evaluation using LITE observations and distributions of highest cloud layers, *J. Geophys. Res.*, in press, 2005.
- Stubenrauch, C.J. and U. Schumann, Impact of air traffic on cirrus coverage, *Geophys. Res. Lett.*, 32, L14813, doi:10.1029/2005GL022707, 2005.

The topic of this session was ice supersaturation and its relationship to clouds. At the beginning of the session a summary of the current knowledge about ice supersaturated regions was given by K. Gierens. Ice supersaturated regions are large, cold ($T < -38^\circ\text{C}$) dynamic regions where air is supersaturated with respect to ice. Maximum occurrence of ice supersaturated regions is observed over tropical continents, mid-latitude storm-track regions, Antarctica, and, to a smaller extent, over northern polar regions. Temperature and humidity measurements show that ice supersaturated regions are significantly colder and moister than their environment. Generally, the temperature contrast between ice supersaturated regions and their environmental air masses is smaller in the tropics than in mid-latitudes, but the humidity contrast is more pronounced in the tropics. These geographical differences indicate two different formation mechanisms: ice supersaturated regions, which are colder than their environment, are mainly caused by adiabatic or diabatic cooling (e.g., radiative cooling during polar night). In the case of ice supersaturated regions, which are moister than their subsaturated environment, moisture transport from lower altitudes (e.g., in tropical convection) dominates the formation process.

A major topic of this session was the relation of ice supersaturated regions to clouds and contrails. While water clouds start to form at 100% relative humidity (with respect to water), cirrus clouds do not form at saturation (with respect to ice), but need large values of ice supersaturation. For example, the threshold humidity for homogeneous nucleation at $T = -38^\circ\text{C}$ amounts to $\text{RH}_i \approx 140\%$. Heterogeneous nucleation requires less supersaturation, but appropriate condensation nuclei. The relative importance of heterogeneous nucleation for the formation of cirrus clouds is still an open question.

During this session various observational data sets of humidity and cirrus clouds were presented. Ice supersaturated regions are frequently observed in connection with cirrus clouds and contrails, but they can also exist in clear air. Satellite observations of water vapour (MLS, TOVS Path-B) and clouds (HIRS, SAGE) show a very similar geographical distribution of ice supersaturated regions and (sub-visible) cirrus clouds. However, tropical cirrus may also form from convective anvils. Generally, satellite data suffer from a coarse vertical resolution. Since only a few ice supersaturated regions reach an equivalent vertical extent, it is expected that satellite observations underestimate the occurrence of ice supersaturated regions. F. Immler presented a Mobil Aerosol Raman Lidar (MARL), which is capable of detecting very thin cirrus clouds and provides vertical profiles in high resolution. Therefore, simultaneous LIDAR and radiosonde measurements might provide useful information about the relation of ice supersaturated regions to cloudiness. However, for this purpose humidity measurements of high accuracy are required. Furthermore, G. Rädcl presented observations of ice supersaturated regions and persistent contrails over Reading. In fact, persistent contrails have been observed on days when radiosonde profiles show ice supersaturation over Reading. J. Whiteway presented observations in mid-latitude and tropical cirrus from the EMERALD campaigns. In a thick anvil of tropical convection remarkably high values of relative humidity with respect to ice up to 200% were observed. One point of discussion was the role of turbulence in the formation of cirrus clouds: High ice crystal concentrations are related to strong turbulence and vice versa. The question was whether turbulence and associated temperature variations are essential for cirrus cloud formation or whether turbulence is caused by the release of latent heat related to the formation of ice crystals. Generally, the role of fluctuations of temperature and vertical wind speed for cirrus cloud formation is not yet understood. Measurements in high temporal resolution would be necessary to answer this open question.

Cirrus clouds as well as persistent contrails that spread and form extended cirrus clouds have an impact on the radiation budget of the Earth. Depending on their macro- and microphysical properties like altitude, geographical location and ice crystal shape, cirrus clouds can have either a cooling or a heating effect on the earth-atmosphere system. Therefore, changes in the occurrence of ice supersaturated regions, cirrus clouds and contrails, respectively, might be a crucial issue to climate change. High values of ice supersaturation as required for the formation of cirrus particles constitute extreme states in the distribution of relative humidity. Generally, extreme values are much more sensitive to changes of background conditions than average values. Thus, it is very difficult to estimate how the frequency of ice supersaturated regions, the probability of cirrus cloud formation and, therefore, the radiation budget will change in a changing climate.

Reliable predictions of contrail formation, cirrus cloudiness as well as possible changes in a changing climate are hampered by the lack of parameterisations of cirrus clouds and ice supersaturation in most of the common weather forecast and climate models. Most models cut relative humidity at 100% or allow for only small values of ice supersaturation. Currently, various attempts are made to develop cirrus parameterisations for large scale models, which capture the principal features of detailed particle-size-resolving models. C. Ren presented a cirrus parameterisation which was successfully applied for cirrus clouds forecasts during the TROCCINOX field campaign. The development of cirrus cloud parameterisations including ice supersaturation for large-scale models is an important outstanding issue.

As mentioned above, the occurrence of persistent contrails is strongly related to ice supersaturated regions. Furthermore, contrails might spread and form cirrus clouds. C. Stubenrauch analysed the air traffic effect on cirrus clouds using TOVS Path-B data from 1987 to 1995. The comparison of cirrus trends for situations favourable for contrails to those in general and to those favourable for cirrus leads to an indicator of the air traffic effect on cirrus clouds. However, the overall air traffic effect on cirrus clouds is rather small, e.g., over Europe the increase of cirrus is approximately 0.20 - 0.25%/decade.

Aviation and contrail effects on climate are difficult to measure, but in times of increasing air traffic a topic of gaining scientific interest. A. Faux presented a new approach using historic events to detect the climate forcing from contrail formation. During World War II well defined periods of intense air traffic occurred, while commercial air traffic was not yet common. Meteorological data for raid and non-raid days were compared in order to determine the contrail effect on temperatures and cloud cover. Despite more than 1000 raids from England to Europe between 1943 and 1945, the available data do not seem to be sufficient for finding a significant climate forcing signal from contrails, because the selection criteria leave only one single event to analyse.

Another important point of discussion was the role of ice supersaturation in the dehydration of air masses entering the stratosphere. The observed decrease of tropical tropopause temperatures seems to disagree with the observed increase of lower

stratospheric water vapour. K. Gierens mentioned that microphysical processes become slower with decreasing temperatures and higher ice supersaturations are required for nucleation, possibly resulting in higher water vapour entry-values. This process might explain the observed water vapour increase despite decreasing tropopause temperatures. Therefore, model studies concerning possible dehydration mechanisms which do not represent ice supersaturation might fail.

Several problems concerning observations of ice supersaturated regions were discussed. Besides the coarse vertical resolution of satellite data, measurements of ice supersaturation are often regarded as errors and the resulting satellite data products like UTH are constrained to values below saturation. Furthermore, WMO still holds to the practice to report relative humidity with respect to liquid water at low temperatures, although bulk liquid water does not exist below $T=-40^{\circ}\text{C}$. Hence, a lot of widely varying extrapolation formulae of saturation pressure for supercooled water are used which leads to unnecessary uncertainties about the true meaning of the humidity measurements. Perhaps one should convince WMO to abandon this practice.

Observations

Introduction

This article will be mainly concerned with humidity measurements in the upper troposphere. This is a region of the atmosphere crucial for climate change, where the humidity field is highly variable in space and time and where marked vertical gradients in absolute humidity are the norm. This contrasts with the lower stratosphere (more than 3 km above the tropopause) where water vapour concentrations, although very low, are much less variable. The challenge for the measurement community in the upper troposphere is to make accurate measurements at high horizontal and vertical resolution - a challenge, as this article will show, that is some way from being met.

A comprehensive summary of current measurement techniques at the end of the twentieth century was provided by the SPARC water vapour assessment 2000:

- a) Specialist research instruments - frost-point hygrometers, Lyman- α fluorescence instruments and tuneable diode lasers. These are flown on research balloons or aircraft platforms with accuracy 5-10% in concentration in the upper troposphere.
- b) Routine *in situ* instruments - radiosondes and the MOZAIC sensor. The latter is similar to a Vaisala Humicap and is carefully calibrated before and after flight, yielding an accuracy 5-7% relative humidity. There are many radiosonde sensors with differing performance and the SPARC report did not venture to quote an overall accuracy (see below).
- c) Ground-based remote sensing - IR and FIR spectrometry, Raman lidar. Passive techniques suffer from poor vertical resolution in the tropopause region (because of the sharp vertical gradients in humidity); the accuracy of IR remote sensing was quoted as 5-13%. Raman lidar potentially has excellent vertical resolution (< 50 m) and accuracy 5-10%; precision is a problem for this technique in the UT where long averaging times are usually required.
- d) Space-borne remote sensing - the SAGE-2, ATMOS and ILAS instruments (all limb scanners) were identified in the SPARC report as measuring below 100 mb, with systematic errors 27%, 6% and 10%; and random errors 14%, 10% and 5% respectively. The Microwave Limb Sounder offered an accuracy in relative humidity of several 10s % relative humidity, while the nadir-sounding HIRS sounder on the operational weather satellites provides a measure of upper tropospheric water vapour whose accuracy was not evaluated.

It is clear that even the best research instruments can only claim an accuracy of 5%, and indeed in intercomparison exercises differences of more than 10% are found between research grade instruments, both in the field and (somewhat more worryingly) the laboratory. For the more routine instruments, the accuracy is considerably worse than 10%. This matters, since the ability of atmospheric models to represent clouds correctly is very sensitive to the relative humidity - an error of 10% in RH at ice saturation and above will lead to serious errors in the calculated cloud cover, and therefore the radiation field.

Developments in the past five years, since SPARC 2000, have been incremental rather than revolutionary, and the basic picture outlined there remains valid. This article will concentrate on three areas of progress: fundamental thermodynamics, radiosonde measurements and lidar. It should be read in conjunction with other articles in this volume on advances in satellite and *in situ* sensing to gain a wider perspective on recent advances in water vapour measurement.

Thermodynamic considerations

Murphy & Koop [2005] have reviewed data available in the literature on the thermodynamic properties of water vapour. Their review highlights a number of areas of confusion. Most measurement techniques measure either absolute molecular concentration or mixing ratio of water vapour, yet instruments such as radiosondes quote their result as relative humidity. This introduces two sources of error: the temperature measurement (a surprisingly difficult parameter to measure accurately, especially from an aircraft) and the assumed variation of saturated vapour pressure with temperature for ice and liquid.

The SVP of water vapour is traditionally calculated using parameterisation formulae based on laboratory work. There are a number of these in the literature, differing by up to 1% at atmospheric temperatures. To compound the problem, the so-called Goff-Gratch formula [actually based on Goff, 1965] is erroneously quoted in WMO publications. Furthermore, the WMO parameterisation of the SVP of liquid water is based on measurements above the freezing point and is extrapolated to temperatures < -38°C where liquid water does not exist beyond the nanoscale. WMO's practice of quoting water vapour measurements in the upper troposphere as relative humidity with respect to something that does not exist may at best be described as perverse, and leads to differences up to 10% at 200 K between different parameterisations.

A further thermodynamic consideration is the formation in the atmosphere of cubic ice (with a larger vapour pressure than hexagonal ice) below 200 K. This has a number of implications for models of cold cirrus and polar stratospheric clouds.

Radiosonde humidity measurements

A considerable effort has been spent over the past five years improving our understanding of radiosonde humidity measurements in the upper troposphere. Radiosondes have the advantage of a regular network of soundings distributed across the globe, and are compiled into meteorological databases by weather services. There are studies in the literature comparing radiosonde climatologies with climate model representations - but in the upper troposphere the quality of a radiosonde measurement depends critically on the type of sonde launched and its ground preparation, information which is not included in the databases.

The different kinds of radiosonde humidity sensors were reviewed in SPARC, 2000, which concluded that the only type capable of measuring in the upper troposphere is that based on thin film capacitors. These sensors have been available on Vaisala sondes for the past 20 years but unfortunately there are a number of Vaisala sensors, each with particular systematic errors:

- a) RS80A Humicap. This sensor was manufactured from the mid 1980s to the present (although production of RS80 sondes is scheduled to cease in 2005). The sensor has a slow response (~1 minute, corresponding to ~250 m) in the upper troposphere and suffers from a calibration error which can be corrected retrospectively using the formula of Miloshevich et al. [2000]. However, the correction is not applied to routine radiosonde ascents. The RS80A was also susceptible to contamination in storage (up to 2% dry bias after a year) prior to 2001 so the measurement error depends on the age of the sonde. (Sondes after 2001 were packaged differently).
- b) RS80H Humicap. This sensor uses a different polymer with a faster response but is consequently more sensitive to contamination (up to 10% dry bias after 1 year's storage prior to 2001). It does not suffer from the calibration error of the A type. This sonde type became available in the mid 1990s but only superseded the A type in some radiosonde stations.
- c) RS92 Humicap. The RS92 is the current version of Vaisala radiosonde with a similar humidity sensor to the H type. The main innovation with the RS90 (the RS92's predecessor) was the use of a dual humidity sensor, one of which measured while the other was heated. This was to combat the problem of icing up of the sensor when the sonde ascended through a supercooled water layer.

A number of intercomparison exercises have been conducted to try to evaluate the accuracy and precision of these sondes. One example is shown in Figure 1 from Vaughan et al. [2005], comparing an RS80A profile (with Miloshevich correction applied) with that from a Snow White chilled mirror instrument. From a set of 23 such profiles the authors concluded that there was no net bias between the two techniques in the upper troposphere, to an accuracy of 2% relative humidity. The issue is far from resolved however, and work continues to understand the different behaviour of the different kinds of radiosonde sensors [e.g. Wang et al. 2002; Soden et al. 2004 and other articles in this volume]. There is a need in particular to establish the accuracy of the newer (RS90/92) sensors in the upper troposphere although so far the results are encouraging.

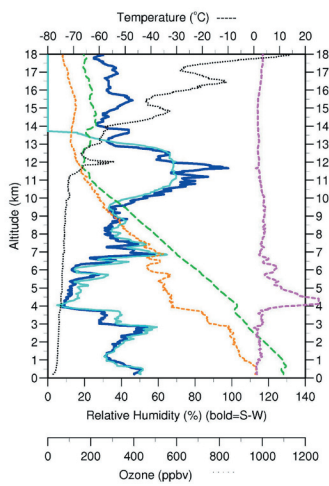


Figure 1: Profile measured on 11 Dec 2001 from Aberystwyth, Wales. Dark blue: Snow white; light blue: RS80A, shown as relative humidity with respect to ice. Green denotes temperature, °C; orange: Snow White dew point, °C; black: ozone, ppbv and magenta: phototransistor output, with 0-5V is scaled to 0 - 20 °C.

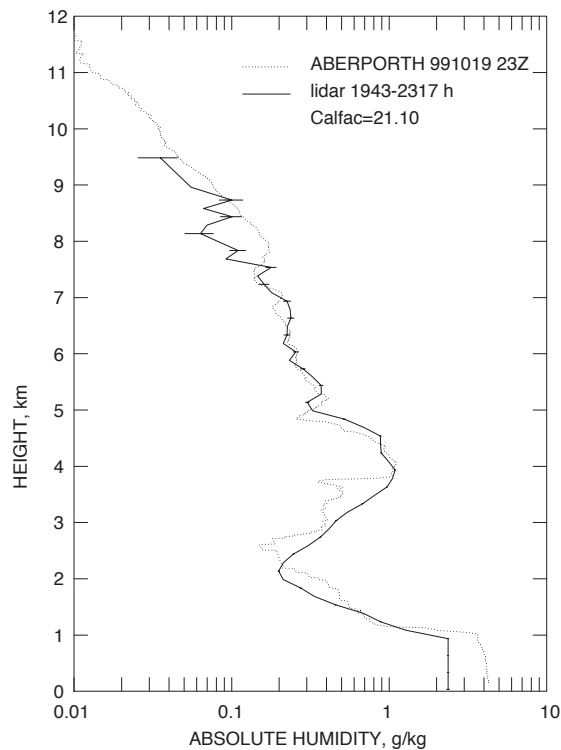


Figure 2: Humidity profile measured by RS80H radiosonde from Aberporth compared with a 4-hour lidar profile from Aberystwyth, 40 km away.

Lidar

The technique of measuring water vapour by Raman lidar is well-established [e.g. Melfi, 1972] and is potentially capable of providing an accuracy standard in the upper troposphere. The main systematic errors with Raman lidar are height-independent, so if the lidar can be accurately calibrated at low levels the calibration should transfer to the upper troposphere. The main drawback of the Raman technique is the very low backscatter signal, necessitating powerful lasers and large telescopes and (for the upper troposphere) restricting observations to night-time. Nevertheless there has been a resurgence of interest in this technique in the past 5 years. The US Atmospheric Radiation Monitoring (ARM) programme compared lidar profiles with RS90H radiosondes and with GOES 6.7 µm radiances [Soden et al., 2004], and found very good agreement between the satellite radiometer and radiances synthesised from the lidar profile; agreement with the radiosondes was markedly worse. An example of an intercomparison between the Raman lidar at Aberystwyth and an RS90 radiosonde is shown in Figure 2; here, the lidar was calibrated spectroscopically rather than relying on the usual method of fitting to a radiosonde at the lowest altitudes.

Although Raman lidar is well suited for use in a ground-based lidar, its bulk and the need for long averaging times makes it unsuitable for airborne use. Recently, differential absorption lidars have begun to be used for this purpose. These are technically much more challenging than a Raman lidar, particularly in the laser technology where very stable narrow-line lasers in the near infra-red (920-950 nm) are needed. From the ground, differential absorption is not appropriate since the water vapour concentration falls sharply with height. This however becomes an advantage when sensing from above, where the greater sensitivity from the increased concentration offsets the decrease in signal precision with distance. An example of such a lidar is flown on the DLR Falcon, data from which were presented by Flentje et al. [2005]. Such a lidar is being developed for the BAe146 FAAM aircraft.

Concluding remarks

Considerable progress is being made in better characterising Vaisala radiosonde humidity sensors in the upper troposphere. The aim is to enable the climatology of upper troposphere water vapour to be determined from past measurements, and to constrain

atmospheric models with accurate data. At the present time great care must be exercised in using radiosonde humidity data above about 5 km from the standard meteorological archives because of the many different kinds of sonde with different characteristics. Raman lidar seems to be emerging as a technique of choice for a reference measurement in the upper troposphere but suffers from the faint Raman backscatter which limits observations in the upper troposphere to night-time (this limitation can be overcome with narrow-band lasers and receivers but at considerable cost). Satellite instruments such as POAM [Nedoluha et al., 2002] and AURA MLS are improvements on the previous generation of space-borne instruments but the accuracy of these instruments is difficult to establish in the upper troposphere because of the lack of an agreed reference measurement.

References

- Flentje, H., A.D. Dornbrack, G. Ehret et al., Water vapor heterogeneity related to tropopause folds over the North Atlantic revealed by airborne water vapor differential absorption lidar, *J. Geophys. Res.* 110, art. no. D03115, 2005.
- Goff, J.A., Saturation pressure of water on the new Kelvin scale, in *Humidity and Moisture: Measurement and control in science and industry*, vol.3, ed. A. Wexler, Reinhold publishing, New York, 1965.
- Melfi, S., Remote measurements of the atmosphere using Raman scattering, *Appl. Opt.*, 11, 1605-1610, 1972.
- Miloshevich, L. M., H. Vömel, A. Paukkunen, A.J. Heymsfield and S.J. Oltmans, Characterization and correction of relative humidity measurements from Vaisala RS80-A radiosondes at cold temperatures, *J. Atmos. Ocean Tech.*, 18, 135-156, 2001.
- Murphy, D.M. and T. Koop, Review of the vapour pressure of ice and supercooled water for atmospheric applications, *Q.J. Roy Met Soc.*, in press, 2005.
- Nedoluha, G.E., R.M. Bevilacqua, K.W. Hoppel, et al., Polar Ozone and Aerosol Measurement III measurements of water vapor in the upper troposphere and lowermost stratosphere, *J. Geophys. Res.*, 107 (D10): Art. No. 4103 2002.
- Soden, B.J., D.D. Turner, B.M. Lesht and L.M. Miloshevich, An analysis of satellite, radiosonde and lidar observations of upper tropospheric water vapour from the Atmospheric Radiation Measurement Program, *J. Geophys. Res.* 109, art. No. D0401, 2004.
- Vaughan, G., C. Cambridge, L. Dean and A.W. Phillips, Water vapour and ozone profiles in the midlatitude upper troposphere, *Atmos. Chem. Phys.*, 5, 963-71, 2005.
- Wang, J.H., H.L. Cole, D.J. Carlson, E.R. Miller, K. Beierle, A. Pakkunen and T.K. Laine, Corrections of humidity measurement errors from the Vaisala RS80 radiosonde - Application to TOGA COARE data, *J. Atmos. Ocean. Technol.*, 19, 981-1002, 2002.

Cloud and Aerosol Detection by Balloon-borne Lidar and Laser Backscattersonde in the UTLS during the HIBISCUS Campaign: Optical and Dynamical Properties

G. Di Donfrancesco¹, F. Fierli², F. Cairo³, C. Buontempo³, L. Liberti³, M. Snels³, F. Cardillo³ and M. Viterbini³

¹ENEA- Climate department, Frascati, Italy; ²Institute for Atmospheric Sciences and Climate, CNR, Bologna, Italy; ³Institute for Atmospheric Sciences and Climate, CNR, Rome, Italy

A case study based on upper troposphere lower stratosphere *in situ* observations of aerosol show that cirrus can show great meso-scale variability in height, thickness and optical properties. The light-weight microlidar measurements were taken on-board the MIR (Infrared Montgolfier) at one wavelength (532 nm) and double polarization (parallel and perpendicular) during the HIBISCUS 2004 campaign held in Bauru dedicated to tropical upper troposphere and lower stratosphere survey. Measurement started at 23 UT on 24th January 2004 and ending at 2 UT the following day. The instrumental configuration allows to retrieve aerosol backscatter ratio (BSR) and aerosol depolarization. The time versus height evolution of BSR and aerosol depolarization are reported in Figure 1 (left and right panel, respectively). Three distinct layers can be easily identified: a thick cirrus characterized by high BSR (up to 30) and average depolarization values (< 20 %) at 13 km height during the first half of the flight; a low BSR (< 20) and high depolarization (> 30 %) cirrus between 13 and 15 km height during the second part of the flight above a third cirrus at 12 km height characterized by the same BSR and depolarization values than the first layer. Joint BSR and depolarization analysis show clearly that optical properties of layer 1 and 3 are similar while layer 2 is definitely characterized by different optical characteristics. Layer 3 seems also to be subject to wave perturbation, visible in BSR maxima wavy structure.

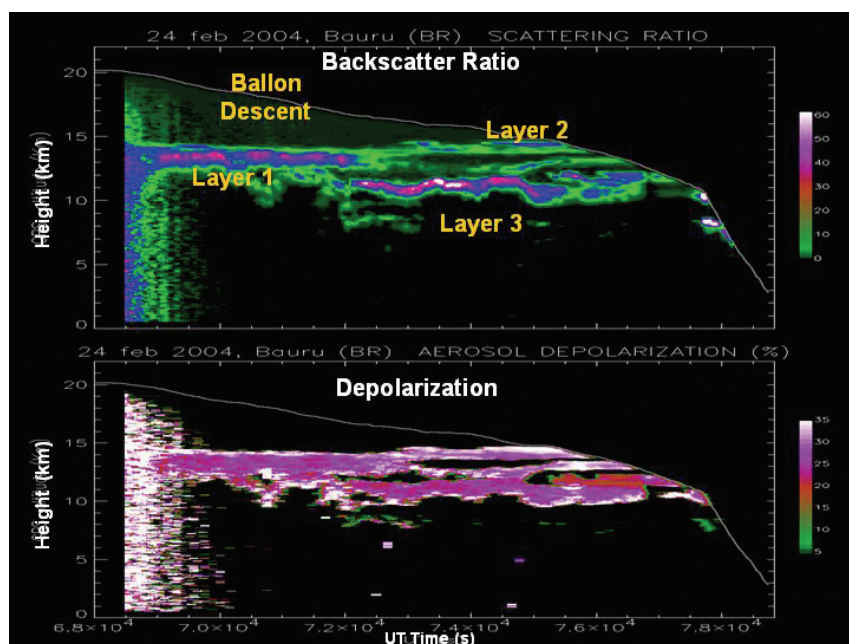


Figure 1: Left, aerosol backscatter ratio at 532 nm (BSR) function of the flight time and of the height. Right, same as left but for aerosol depolarization. The layers 1-3 are indicated in the figure and described in the text.

MODIS instrument onboard the TERRA satellite provided Cloud Top pressure (CTP) for the Brazilian area 11 hours before lidar measurement; data are reported in Figure 2 (only pixels with CTP < 300 hPa are plotted). Large convective region is visible NE of the balloon measurement site with several convective towers reaching a CTP lower than 150 hPa (red areas). Aerosol optical thickness (AOT, not reported) shows also that the higher part of the cloud is optically thick (up to 1), while the large cirrus outflow (55°W, 15°S to 44°W, 28°S) is characterised by higher CTP and low optical thickness (< 0.2). Clearly, the observed cirrus layers (the blue cross in Figure 2 indicates the average position of the balloon) originates from the convective outflow. ECMWF T312 analyses show to be accurate enough to reproduce the convective system and the associated dynamical fields. The "High cloud product", plotted as a black line in Figure 2, is in reasonably good agreement with the MODIS observation. Moreover, analyses indicates the presence of a strong jet in the outflow region and of a strong wind shear corresponding to layer 3.

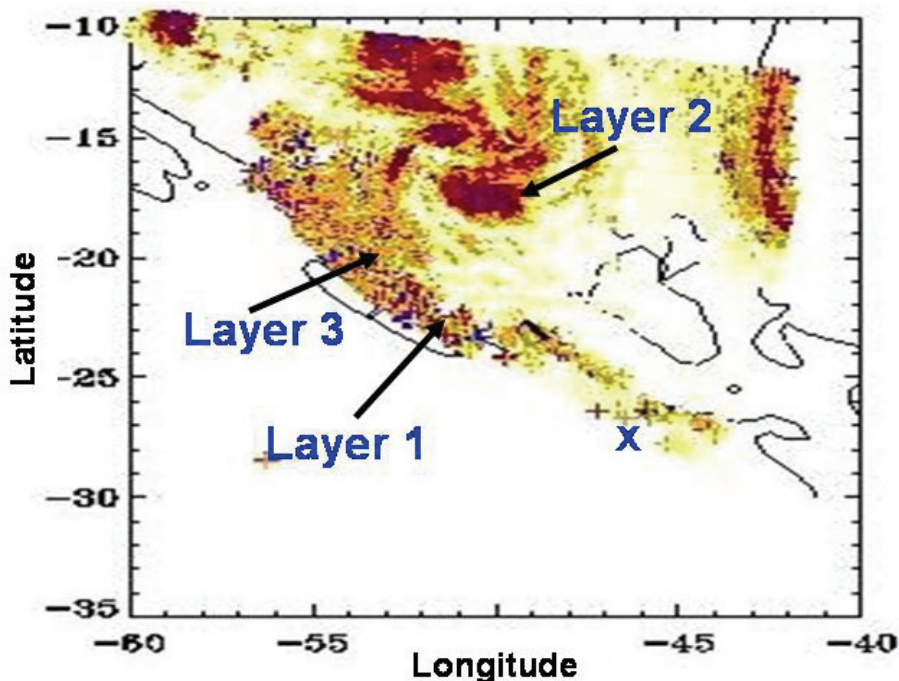


Figure 2: Cloud top height (in hPa) estimated from MODIS imager onboard the TERRA satellite at 13 UT, 24th January. The color scale ranges from 250 hPa (light yellow) to 100 hPa (dark red). The balloon position is indicated by the blue cross and the average position of the back-trajectories clusters ending in correspondance with layers 1-3 are indicated with black arrows

ECMWF analyses also show strong (-20hPa/hr) upward velocities in the convective region. The origin of the sampled airmasses is identified using back-trajectories cluster analysis based on ECMWF analysis and FLEXTRA model [Stohl et al., 1999]. The clusters are composed by 24 hours back-trajectories originated in the surroundings of each layer (as identified in Figure 1) leading to a total number of 15000 trajectories. We have estimated the water vapor content and the saturation ratio with respect to ice for each trajectory following the simplified approach from Pierrhumbert & Roca [1998] in order to correct the water vapor estimate of the ECMWF analyses.

The average position of the clusters ending in layer 1, 2 and 3 at the time of the MODIS measurement are reported in Figure 2, superposed to the satellite image. It becomes clear that layer 1 and 3 originates from the outflow, while layer 2 seems to be originated in the region characterised by active convection; moreover significant fraction of air-masses composing layer 2 are uplifted from an height of 3500 m up to the measurement height (15000 m). Relative humidity with respect to ice exceed 100% only for 30% of air-masses composing layer 2.

Despite its simplicity, this analysis provides some hints on the cirrus formation mechanisms and their influence on the observed optical parameters. In fact, the observations show the evidence for high variability in optical properties of tropical cirrus; it also appear that high depolarization - lower BSR cirrus could be composed by larger and sparser particles. Trajectory cluster analysis indicates that larger aerosols could be generated under rapid and recent uplift while cirrus composed by smaller and more dense particles seems to be generated at earlier stages, experiencing a slow uplift in the upper troposphere after having encountered convectively active region.

References

- Pierrhumbert, R. T., R. Roca, Evidence for control of Atlantic subtropical humidity by large scale advection, *Geophys. Res. Lett.*, 25(24), 4537-4540, 10.1029/1998GL900203, 1998.
- Stohl, A., L. Haimberger, M.P. Scheele, and H. Wernli, An intercomparison of results from three trajectory models, *Meteorol. Applications*, 127-135, 1999.

Trace Water Vapour Measurements and Calibration

T. Gardiner, N. Swann, G. Leggett, A. Woolley*, B. Goody and P. Woods
Analytical Science Group, National Physical Laboratory, Teddington, England
*now at Facility for Airborne Atmospheric Measurement, Cranfield, England

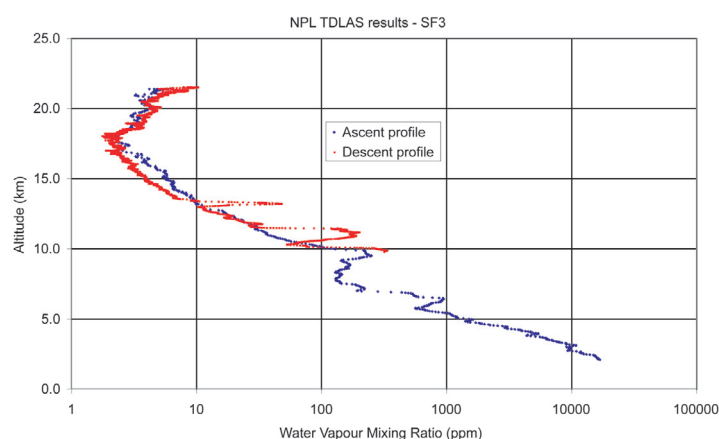


Figure 1: Water vapour profile measured with the new TDLAS instrument above Bauru, Brazil in February 2004.

This paper focuses on two aspects of trace water vapour measurements. The first part concerns a new instrument for high-resolution, in-situ sensing of water vapour in the upper troposphere and lower stratosphere. The second part describes a facility for absolute calibration of trace water vapour sensors that has been developed at the National Physical Laboratory.

The new water vapour instrument is based upon a proven tunable diode laser absorption spectrometer (TDLAS) design for balloon borne measurements of methane [van Aalst et al., 2004]. This instrument uses a near-infrared tunable diode laser and an astigmatic Herriott cell to measure absorption over a pathlength of up to 101 m. The conversion to water vapour measurements required major design changes to be made to the tunable diode laser absorption spectrometer instrument, principally a change in operating wavelength and detection scheme, and an all-metal open-cell design to minimise outgassing.

Water vapour measurements are made over three main absorption lines between 7339.2 cm^{-1} and 7341.3 cm^{-1} . These lines have different line strengths of 1.7×10^{-20} , 5.8×10^{-21} and 2.2×10^{-23} $\text{cm}/\text{molecule}$ to give the wide dynamic range required for water vapour profile measurements. Figure 1 shows an example of the water vapour profile measured by the tunable diode laser absorption spectrometer instrument during a short duration balloon flight from Bauru, Brazil in the recent Hibiscus campaign. This shows the ascent profile through the free troposphere and into the lower stratosphere, and the profile measured during the slow balloon descent through the tropical tropopause layer. The descent data ends when the optics froze up - the temperature of the optics at this point gives an effective measurement of the frost point at this altitude. The data analysis was carried out using the Hitran, 2004 spectroscopic parameters [Rothman et al., 2004]. The estimated uncertainty for measurements is 10% with a detection limit of 0.5 ppm. The effective frost-point measurement on descent agrees with the tunable diode laser absorption spectrometer data to within the uncertainties, giving a reasonable degree of confidence in the absolute levels. These results demonstrate the capability of the new instrument to provide high resolution measurements of water vapour throughout the troposphere and lower stratosphere. The scientific interpretation of the Hibiscus data is now underway.

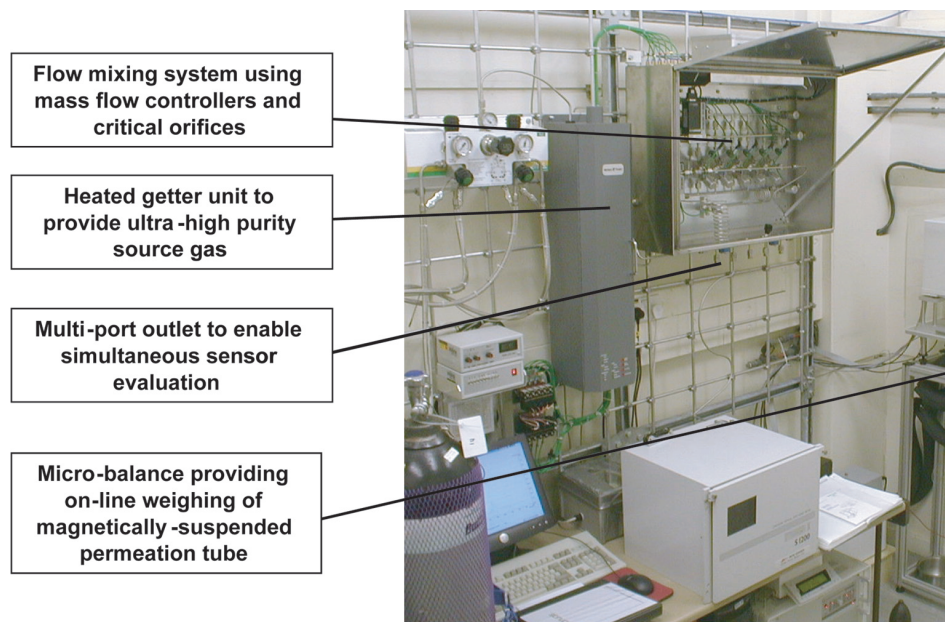


Figure 2: NPL trace water vapour calibration facility.

Figure 2 shows the trace water vapour calibration facility at the National Physical Laboratory. Absolute calibration is achieved through gravimetric traceability by adding a known mass of water vapour to a diluent gas with verified purity. The source of water vapour is a permeation system with on-line weighing and magnetic load suspension, while control of the output concentration is achieved by flow switching and dynamic dilution. The system is carefully designed to minimise dead volumes, all pipework is clean-room welded electro-polished stainless steel, and all gas-wetted surfaces are metal. As a result, the zero-offset level is less than 2 ppbv, limited by the spectroscopic technique used to measure it. An evaluation of the facility using a calibrated frost point hygrometer have demonstrated good agreement between frost points of -67°C and -90°C (4 ppmv to 30 ppbv) [Stevens et al., 2004].

An example of the work carried out with the facility was the simultaneous evaluation of a group of 12 trace moisture instruments in order to provide general information on the performance of different sensor types [Bell et al., 2004]. A key capability of the facility is its ability to make fast response changes to the water vapour concentration. Figure 3 shows the 10% and 90% response times for each of the 12 sensors when exposed to a rapid step change in water vapour concentration from 0.3 ppmv to 0.85 ppmv. This highlights the difference in performance of the different sensor types, and the potentially long response times for trace water sensors. This work demonstrated that, in addition to evaluating measurement accuracy, the facility can be used to assess other important aspects of trace water sensor performance, such as linearity, response time, hysteresis and long term stability.

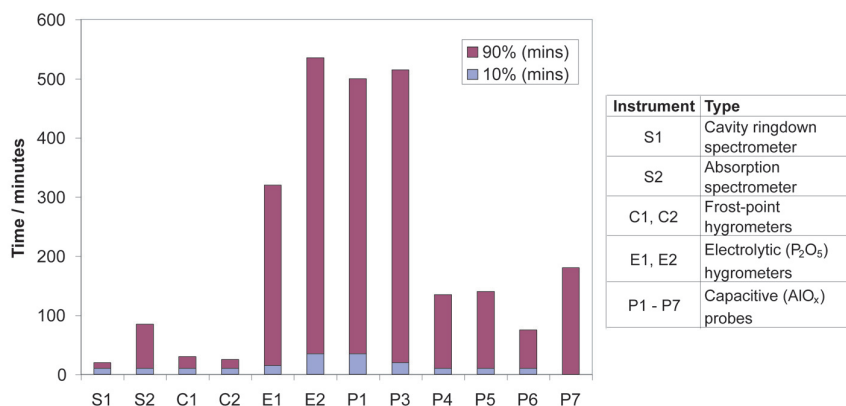


Figure 3: Trace water vapour sensor response times.

References

- van Aalst, M.K. et al., Trace gas transport in the 1999/2000 Arctic winter: comparison of nudged GCM runs with observations, *Atmos. Chem. Phys.*, 4, 81-93, 2004.
- Rothman, L. et al., The Hitran 2004 Molecular Spectroscopic Database, *Journal of Quantitative Spectroscopy and Radiative Transfer*, vol. 96, No.2, 1 December (2005) in press.
- Stevens, M., S.A. Bell, R.M. Gee, T. Gardiner and A. Woolley, Preliminary Investigation of the Agreement Between the Temperature-Related and Mass-Related Trace Moisture Standards Held at NPL, *Proceeding of the 9th International Symposium on Temperature and Thermal Measurements in Industry and Science*, June 2004.
- Bell, S.A., T. Gardiner, R.M. Gee, M. Stevens, K. Waterfield, and A. Woolley, An Evaluation of Performance of Trace Moisture Measurement Methods, *Proceeding of the 9th International Symposium on Temperature and Thermal Measurements in Industry and Science*, June 2004.

FLASH-B Lyman-Alpha Hygrosonde for Upper Troposphere Lower Stratosphere: Instrument Design, Observations and Comparison

V. Yushkov¹, L. Korshunov¹, S. Khaykin¹, A. Lukyanov¹, N. Sitnikov¹, M. Müller², H. Vömel³ and E. Kyro⁴
¹Central Aerological Observatory, Dolgoprudny, Russia; ²Alfred Wegener Institute for Polar and Marine Research, Potsdam, Germany; ³Cooperative Institute for Environmental Science, University of Colorado, Boulder, USA; ⁴Arctic Research Centre of the Finnish Meteorological Institute, Sodankylä, Finland

Lyman- α FLASH-B (FLUorescent Advanced Stratospheric Hygrometer) is an open cell balloon-borne instrument developed at Central Aerological Observatory, Russia for in-situ water vapour observations in the upper troposphere and lower stratosphere. The instrument applies a fluorescent method [Kley & Stone, 1978] which is based on H₂O molecule photodissociation when exposed to radiation at a wavelength $\lambda=121.6$ nm (Lyman- α - hydrogen emission) here provided by a hydrogen discharge lamp. The generated electronically excited OH radical relaxes to ground state by fluorescence as well as by collision with air molecules.

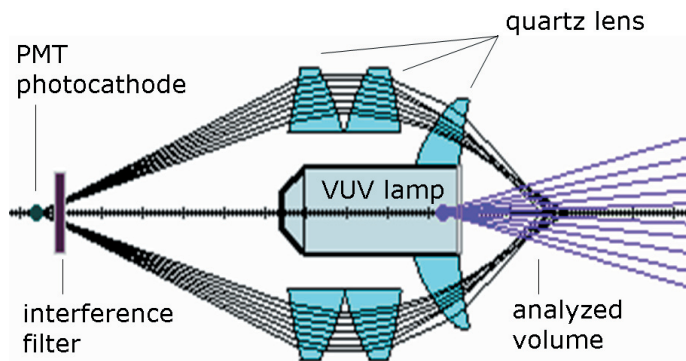


Figure 1: Schematics of the optical arrangement of the FLASH-B instrument.

The detector of OH fluorescence within 308 - 316 nm wavelength range is a Hamamatsu photomultiplier run in photon counting mode with the narrowband interference filter. The intensity of fluorescent light as well as the instrument readings is directly proportional to the water vapour mixing ratio under stratospheric conditions. The co-axial optical layout (Figure 1) allows reducing the size of the instrument to a single cylinder of 120 mm x 220 mm with a total weight of about 0.5 kg. However this arrangement is suitable for night-time measurements only at SZA > 980.

The calibration of FLASH-B is performed for every single instrument using the vacuum chamber and the commercial reference frost point hygrometer MBW-373L. The calibration factor is generally very stable, however a brief pre-flight test is required. Long-term stability and calibration tests performed in the laboratory have demonstrated that total uncertainty of the instrument is less than 9% under stratospheric conditions. Details of the hygrometer design are given in [Yushkov et al., 1998].

During LAUTLOS-WAVVAP field campaign (January-February 2004, Sodankylä, Finland) FLASH-B was flown together with NOAA/CMDL frostpoint hygrometer. A number of simultaneous water vapour measurements allowed a direct comparison of these two sensors in the stratosphere and upper troposphere. The comparison reveals excellent agreement between the two hygrometers; with the exception of instrumental artifacts the mean difference obtained for the 7 soundings is $2.6 \pm 3.1\%$ (1σ) in the stratosphere (Figure 2). Larger disagreement in the tropopause region is caused by the feedback gain change in the NOAA hygrometer [H. Vömel, personal communication]. Fine structures in the water vapour profile at the edge of polar vortex are captured well by both instruments.

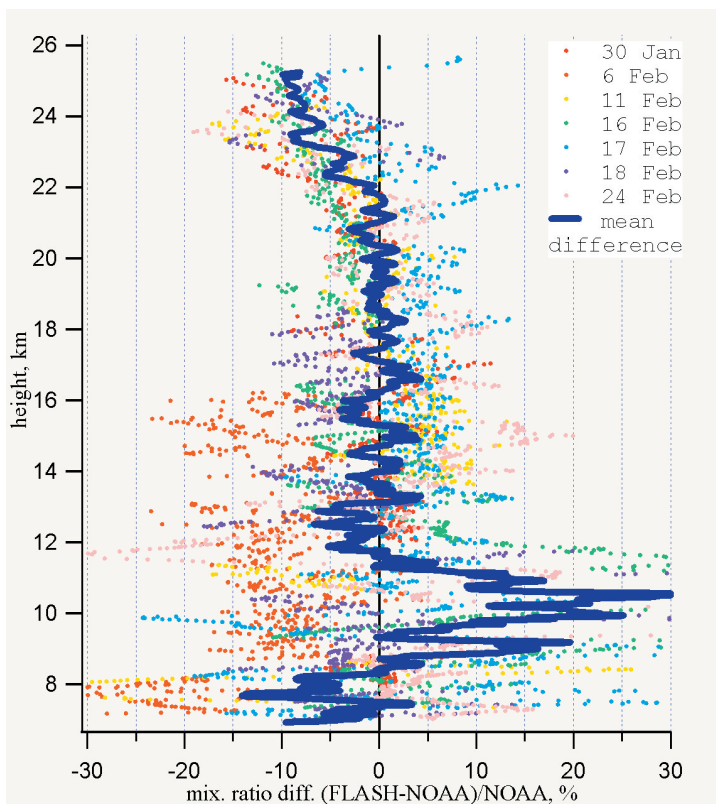


Figure 2: Comparison of the FLASH-B and NOAA/CMDL water vapour observations during descent.

In addition to balloon instruments the microwave 22 GHz radiometer MIAWARA was operated during the LAUTLOS campaign. The stratospheric water vapor profiles of FLASH-B and the NOAA hygrometers in the range of 20-26 kilometers were compared with the lowermost retrieval points of MIAWARA. The agreement between the balloon instruments and MIAWARA was better than 2% for a total number of 10 comparable flights [Deuber et al., 2005].

Apart of the instrument intercomparison the water vapour profiles obtained inside, outside and at the edge of polar vortex during LAUTLOS campaign reveal a detailed view on the Arctic upper troposphere and lower stratosphere water vapour distribution. The measurements clearly demonstrate typical differences of water vapour vertical distribution in the stratosphere inside and outside the vortex; at 20 hPa the difference reaches 1.4 ppmv (Figure 3). Also it has been pointed out that water vapour profiles obtained at the edge or close to the edge of vortex have generally some laminae structure in it. The results of RDF-analysis showed that this structure can be explained by differential advection of air masses originating from inside and outside the vortex.

The reliable and reproducible results acquired using FLASH-B instrument provide a valuable dataset for the validation of model and satellite data. The comparison of retrieved H₂O profiles with the results of model simulations made by applying trajectory model to ECMWF hu-

midity fields shows model dry bias of about 1 ppmv in the lower stratosphere above 400 K [Müller et al., manuscript in preparation].

During winter 2004/05 FLASH-B has been flown from Ny-Ålesund (79°N, 120°E). The water vapour profiles obtained in the presence of ice PSCs show the dehydration layers.

Airborne version of FLASH hygrometer was operated during APE-GAIA, EUPLEX and TROCCINOX field campaigns for upper troposphere lower stratosphere water vapour observations onboard high altitude M55 "Geophysica" aircraft. Aircraft and balloon versions of FLASH will be used in SCOUT-O3 project.

References

- Kley, D. and E.J. Stone, Measurements of water vapor in the stratosphere by photodissociation with Ly-alpha (1216A) light, *Rev. Sci. Instrum.*, 49, 661-697, 1978.
- Yushkov V., S. Merkulov and Astakhov, Optical balloon hygrometer for upper stratosphere and stratosphere water vapour measurements, in *Optical remote sensing of the atmosphere and clouds* ed. by J. Wang, B. Wu, T. Ogawa, Z-h. Guans, *Proc. SPIE*, 3501, 439-445, 1998.
- Deuber, B., A. Haefele, D.G. Feist, L. Martin, N. Kämpfer, G.E. Nedoluha, V. Yushkov, S. Khaykin, R. Kivi and H. Vömel, Middle Atmospheric Water Vapour Radiometer (MIAWARA): Validation and first results of the LAPBIAT Upper Tropospheric Lower Stratospheric Water Vapour Validation Project (LAUTLOS-WAVVAP) campaign, *J. Geophys. Res.*, 110, D13306, doi:10.1029/2004JD005543, 2005.

FL AS H-B
Sodankylä (67.4N, 26.6E)

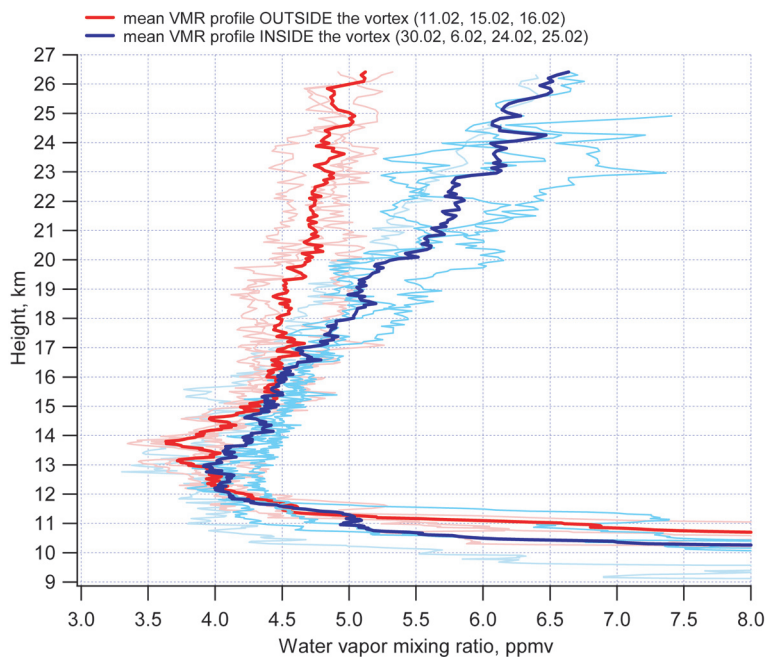


Figure 3: Mean water vapour profiles inside (thick blue) and outside (thick black) the vortex calculated using the measurements made by the FLASH-B hygrometer during the LAUTLOS campaign (January 29 - February 27, 2004, Sodankylä). Thin blue and black lines on the plot indicate the profiles obtained inside the vortex (flights on 30.01, 6.02, 24.02, 25.02.2004) and outside the vortex (flights on 11.02, 15.02, 16.02.2004).

The Homogeneity of the Vaisala Radiosonde Humidity Records (Preliminary Results)

T. Suortti

Arctic Research Centre, Finnish Meteorological Institute, Finland

The longest continuing water vapor profile information is in radiosounding archives. Radiosonde records start from 1950s, long before the time of satellite missions or ground based profiling instruments. The complication is that the radiosonde records are plagued by inhomogeneities caused by the instrument development. The aforementioned facts set challenges for the development of water vapor measurement technology and especially for the accurate homogenization of the historical records. This study aims to assess the homogeneity and trends of relative humidity measurements from Finnish radiosounding records. This long timeseries, beginning from 1965, generates a challenge as a result of the rapid sensor development. The most remarkable changes happened when hairhygrometers were replaced by Humicap technology in 1981, and RS80-A by RS90 in 1999. There is also a remarkable change during the hairhygrometer era when RS18 was brought into use in the 1970s.

Finnish observation sites Sodankylä (67°N), Tikkakoski (62°N), and Jokioinen (61°N) each have long and continuous radiosonde measurement records with reported histories on changes of instruments and measuring practices. This gives an opportunity for a study with an aim on shedding light to the radiosonde timeseries homogeneity issue, by recommendations for homogenisation efforts, and assessment of the recent correction algorithms for the Vaisala RS80-A radiosonde. The study includes also a radiosonde comparison for assessing the RS80, RS90 and RS92 generation gaps. The aforementioned comparison is a part of the international hygrometer intercomparison (LAUTLOS-WAVAP), which was held on February 2004 at Sodankylä.

In this work it has been assumed, and eventually shown, that it is inevitable that the changes in instrument performance will affect the homogeneity of the radiosonde record, and eventually to the calculated RH-trends. The effects of developing measurement technology are demonstrated best in the comparison of radiosonde data and ERA-40 time-series. Based on an ERA-40 comparison, climatological trends and means for the whole record, and its sub-periods, i.e. technical eras, have been compared and the effects of changes in sonde generations estimated. In the beginning of the trend comparison study, it was shown that it is not possible to derive a robust climatological trend for RH -time series unless the effect of the developing measurement technology has been taken account. The previous findings obligate this study to seek for the opportunities for RH -record homogenisation, which is the first task of this report.

As a second task, the differences between various Humicap applications, namely RS80-A, RS90, RS92, and FN-sonde, are assessed with the help of a representative set of parallel measurements during LAUTLOS-WAVAP -campaign. The performance of RS80-A in the upper troposphere have been debated for some years, and several correction algorithms have been presented for correction of these errors [Wang et al., 2002; Leiterer et al., 2000; Miloshevich et al., 2001]. The main problems with Humicap measurement technology are related to the temperature dependent dry bias and time lag, and in addition, the chemical contamination (in RS80). The third task of this study has been to evaluate these reported corrections and their impact on tropospheric RH along with the first and second tasks. The final aim would be to deduce climatological trends from homogenised measurements, but this work does not go that far.

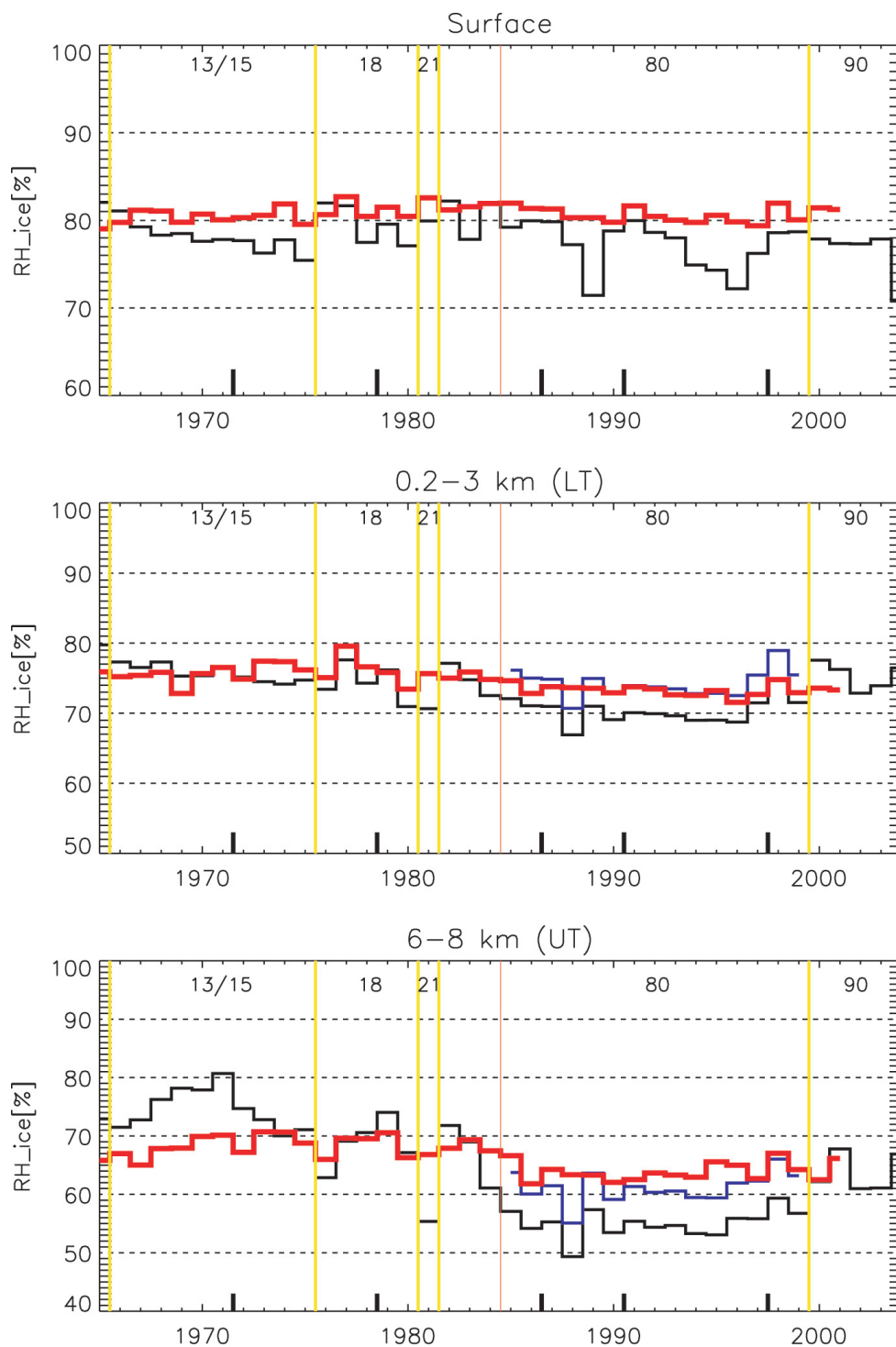


Figure 1: Annual averages of radiosonde time-series of RH with respect to ice at three different altitudes above Sodankylä (troposphere). ERA-40 data are shown in red, radiosonde data from Sodankylä (black). Corrected RS80-A data are shown as a blue line. In this example, the worst cases of iced RS80-A soundings are filtered out. Sub-periods of ERA-40 are shown with black markers above the x-axis. (ERA-40 data have been downloaded from the ECMWF data server (http://data.ecmwf.int/data/d/era40_modal/)).

According to LAUTLOS-WAVAP radiosonde inter-comparison it was seen that RS92 and FN -sonde had best mutual agreement. FN disagreed from RS92 by some RH% in cold temperatures, by underestimating in humid conditions and over-estimating in dry layers. The disagreement was temperature dependent. In comparison to RS92, RS90 had a semi-linearly growing wet bias with decreasing temperature being approximately 10 RH% at -60 Celcius. In the comparison, RS80-A had a dry-bias over 30 RH% in the proximity of ice clouds and approximately 5 RH% near 0 Celcius. The RS80-A dry bias was observed to grow exponentially with the decreasing temperature. It was shown that the RS80-A dry-bias could be partly removed with the correction algorithm by Leiterer et al. [2000].

The homogeneity assessment of Finnish radiosonde records showed that the hairhygrometer and Humicap measurements should be separated for trend calculations. In addition, all hairhygrometer generations (RS13, RS15 and RS18) may be united for trend calculations in the lower troposphere (below approximately 3 km), but above that, RS18 should be separated from the others due to smaller thermal lag. Also RS80-A and RS90 with Humicap sensors are suggested to be separated for trend calculations at all heights. This generation gap can be narrowed with the help of the Leiterer's correction algorithm for RS80-A. With the corrected RS80-A humidity, all compared sonde generations may be united for the lower tropospheric trend calculations. The unifying of the hairhygrometer and Humicap data in the upper troposphere is not possible with correcting only RS80-A data. According to the LAUTLOS-comparisons, it seems that the introduction of a new Vaisala radiosonde (RS92) will result to the need for developing of a correction for RS90 also.

The humidity climatology derived from the Finnish radiosonde record showed that by applying corrections for RS80-A, the tropospheric trend diminished close to zero, and even changed its sign to positive in the mid- and upper troposphere if compared to the earlier reported trend in IPCC 2001 [Ross & Elliot, 2001].

References

- Leiterer, U., H. Dier and T. Naebert, Method for Correction of RS80 A-Humicap Humidity Profiles, 2000, Available at: <http://www.met-office.gov.uk/research/interproj/radiosonde/reports/leiterer.pdf>
- Miloshevich, L., H. Vömel, A. Paukkunen, A. J. Heymsfield and S. Oltmans, Characterization and correction of relative humidity measurements from Vaisala RS80-A radiosondes at cold temperatures, J. Atm. Oc. Tech., 18, 135-156, 2001.
- Oltmans, S., H. Vömel, D. Hofmann, K. Rosenlof and D. Kley, The Increase in Stratospheric Water Vapor from Balloonborne Frostpoint Hygrometer measurements at Washington, D.C., and Boulder, Colorado, Geoph. Res. Lett., 27(21), 3453-2456, 2000.
- Ross, R. and W. Elliott, Radiosonde-based Northern Hemisphere Tropospheric Water Vapor Trends, J. Climate, 16(7), 1602-1612, 2001.
- Wang, J., H. Cole, D. Carlson, E. Miller, K. Beierle, A. Paukkunen and T. Laine, Corrections for Humidity Measurement Errors from the Vaisala RS80 Radiosonde Application to TOGA COARE Data, J. Atm. Oc. Tech., 19, 981-1001, 2002.

Tropical Tropopause Layer Water Vapour and Clouds Observed by the MIPAS Instrument

H. Sembhi, J.J. Remedios and J. Greenhough

Earth Observation Science, SRC, Department of Physics and Astronomy, University of Leicester, England

Introduction

The tropical upper troposphere and lower stratosphere is a key region where the variability and concentrations of the natural greenhouse gases, water vapour (H_2O) and ozone (O_3), are influenced by intricate radiative, chemical and dynamical processes. Of particular interest is the Tropical Tropopause Layer (TTL), a 'transition' layer between 150 and 50 mb that connects the moist, convection-dominated upper troposphere to the dry, radiatively-active, stable lower stratosphere. Overshooting convection [Sherwood & Dessler, 2002], horizontal transport through the cold trap regions [Holton & Gettleman, 2002] and interactions with cirrus clouds, either formed *in situ* or from convective anvil outflow [Jensen & Pfister, 2004] are some of the factors that can explain the decreased moistness of stratosphere-bound air as it is transported through the tropical tropopause layer.

Satellite instruments can potentially a) provide a wealth of long-term, global data down to the mid-troposphere, b) overcome the spatial and temporal limitations of using ground and air-based instruments and c) act as a valuable comparative source for *in situ* and model measurements of the tropical upper troposphere and lower stratosphere. Previous satellite instruments for example the Microwave Limb Sounder (MLS) and the Halogen Occultation experiment (HALOE) on the Upper Atmosphere Research Satellite (UARS) provide upper troposphere and lower stratosphere water vapour distributions but are limited by cirrus cloud contamination and in distinguishing clear-sky from sub-visible cirrus. In this extended abstract, we present results from the Michelson Interferometer for Passive Atmospheric Sounding (MIPAS) showing "clear-sky" water vapour following application of a cloud detection methodology for sub-visible and thicker cirrus.

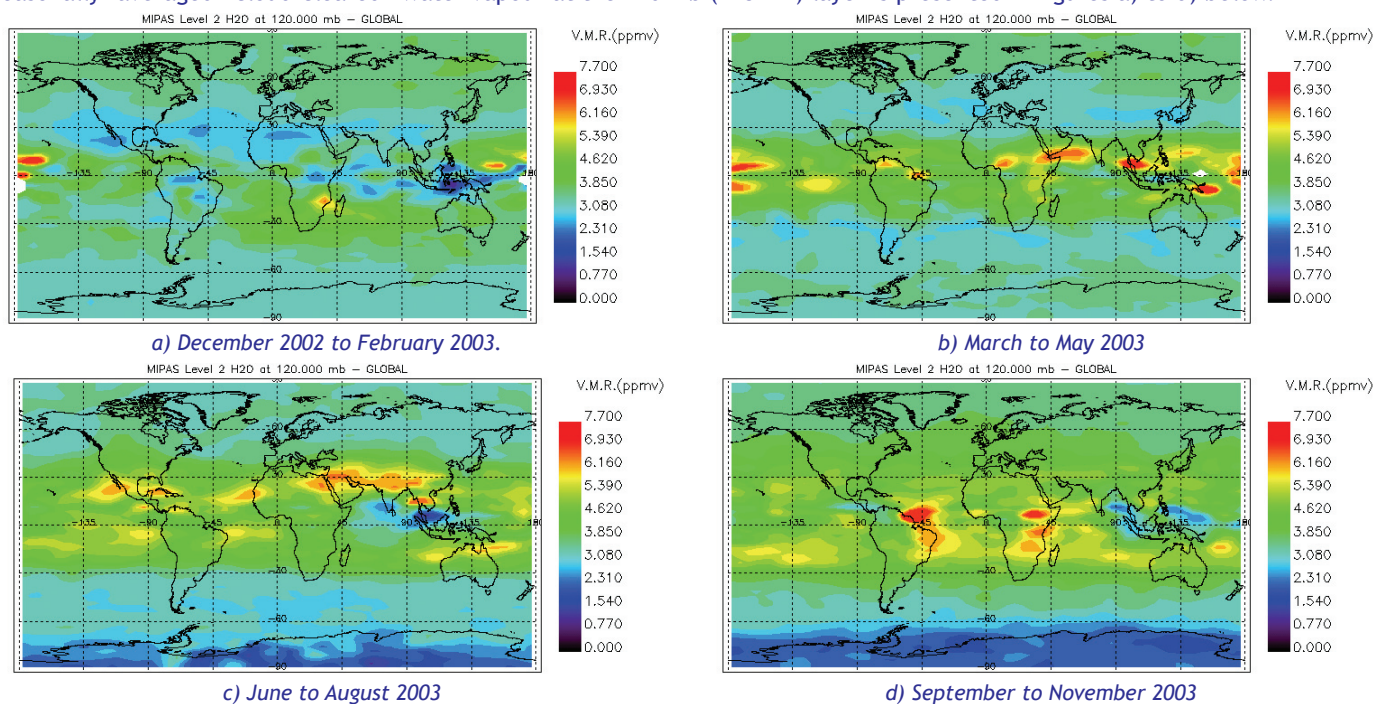
The MIPAS instrument and cloud detection

The MIPAS is a high-resolution limb-viewing Fourier transform spectrometer onboard the polar sun-synchronous orbiting ENVISAT mission. The instrument observes the Earth's radiance in the near to mid-infrared region with a spectral range of 4.16 to 14.5 mm (685 to 2410 cm^{-1}), a high spectral resolution of 0.025 cm^{-1} unapodised and a 3×30 km instantaneous field of view. It makes 14 orbits per day and collects radiance spectra (Level 1b data) that contain information on at least 25 atmospheric constituents including clouds and aerosols, from 68 to 6 km with a vertical resolution of 3 km in the lower atmosphere. These Level 1b spectra are then used to obtain Level 2 vertical profiles for pressure, temperature and six trace gases including H_2O and O_3 .

Limb emission spectra are highly influenced by clouds that emit, absorb and scatter radiation over a broad range of wavelengths hence resulting in inaccurate trace gas concentrations. A Leicester cloud detection algorithm is incorporated into the MIPAS operational processor to allow identification of "cloud-free" vertical profiles. A cloud index (CI) is a simple method for distinguishing regions of the spectra that are enhanced by clouds and aerosols and is calculated by taking the ratio between the CO_2 -dominated microwindow (MW1: $788.2 - 796.25$ cm^{-1}) and the aerosol-dominated microwindow (MW2: $832.3 - 834.4$ cm^{-1}). These microwindows have been selected for their low sensitivity to trace gases and together they minimise the dependence of the CI on temperature [Spang et al., 2002]. The ESA operational processor uses a CI threshold of 1.8; values below this indicate thick cloud (an extinction of >10 - 3 km^{-1}) in the instantaneous field of view. However, preliminary investigation at the University of Leicester suggests that this threshold may be insufficient to thoroughly decontaminate MIPAS water vapour and ozone profiles. In this analysis, the CI threshold value is increased to 2.2 to remove possible corruption caused by optically thinner clouds and is applied to reprocessed offline MIPAS level 2 profiles for December 2002 to November 2003 (versions 4.61/4.62). For additional information on the CI and MIPAS cloud distribution and frequencies, see Greenhough et al. [2005].

MIPAS "cloud-free" water vapour

Seasonally- averaged "cloud-cleared" water vapour at the 120 mb (~15 km) layer is presented in figures a) to d) below.



Figures a) to d) show three month averaged H_2O on a $64^{\circ} \times 72^{\circ}$ latitude/longitude grid. There are an average of 9500 profiles per season between 30° North and 30° South and the features observed are summarised in table 1 below.

Table 1: Observed H₂O features in MIPAS 2002/2003 at 120 mb.

Region	Features observed by MIPAS
West Pacific	Enhanced H ₂ O concentrations (> 6.5 ppmv) from December to May 2003 Enhanced features appear further eastwards from June to November
Central and South America	Enhancement over this region in July to August and the east coast of Brazil from September to November (> 6.2 ppmv)
Africa	Increased H ₂ O over Equatorial Africa from May onwards. A prominent feature of increased H ₂ O over Northeast Africa, India and Thailand (> 5.3 ppmv and < 7 ppmv) - could be a signature of the Asian monsoon season.
Indonesia and Darwin	Low H ₂ O concentrations between 1 and 3 ppmv for most of the year but less intense in March to May. Dehydrated features persist in December to February and June to August and extend over the Indian Ocean.

Some of these water vapour features are consistent with those observed by the UARS MLS [Jiang et al., 2004] but the possibility of residual cloud effects and is the focus of ongoing work. To summarise, the MIPAS instrument provides cloud and cloud-free water vapour information down to 12 km, which may shed light on convection and dehydration processes in the tropical tropopause layer.

References

- Greenhough, J., J.J. Remedios, H. Sembhi and L.J. Kramer, Towards cloud detection and cloud frequency distributions from MIPAS infra-red observations, *Adv Space Res*, in press, 2005.
- Holton, J.R. and A. Gettelman, Horizontal transport and the dehydration of the stratosphere, *Geophys. Res. Letts.*, 28, 2799-2802, 2001.
- Jiang, J.H., B. Wang, K. Goya, K. Hocke, S.D. Eckerman, J. Ma, D.L. Wu and W.G. Read, Geographical distribution and interseasonal variability of tropical deep convection: UARS MLS observations and analysis, *J. Geophys. Res.*, 109, D03111, doi:10.1029/2003_JD003756.
- Jensen, E. and L. Pfister, Transport and freeze-drying in the tropical tropopause layer, *J. Geophys. Res.*, 109, D02207, 10.1029/2003JD004022, 2004.
- Sherwood, S.C. and A.E. Dessler, On the control of stratospheric humidity, *Geophys. Res. Letts.*, Vol. 27, No. 16, pp. 2513-2516, 2000.
- Spang, R., G. Eidmann, M. Reise, D. Offerman, P. Preusse, L. Pfister and P. Wang., CRISTA observations of cirrus clouds around the tropopause, *J. Geophys. Res.*, 107(D23), 8174, doi:10.1029/2002_JD000698, 2002.

Analysis of Upper Tropospheric Humidity Measurements by Microwave Sounders and Radiosondes

V.O. John and S.A. Buehler

Institute of Environmental Physics / Remote Sensing, University of Bremen, Germany

This short abstract summarises some of the results of several studies of humidity measurements by microwave humidity sounders and radiosondes, discussions mostly focused on the upper troposphere, roughly between 500 - 200 hPa, due to the importance of this region in the climate system.

The microwave humidity data used in the analyses are from the Advanced Microwave Sounding Unit-B (AMSU-B) instruments on-board the NOAA-15, 16, and 17 satellites. AMSU-B is a five channel microwave radiometer which is designed for measurements of tropospheric humidity. The radiative transfer model (Atmospheric Radiative Transfer Simulator) ARTS was used extensively as a tool for the analysis of these data. ARTS was configured and validated for AMSU-B.

It was demonstrated that the weak ozone lines present in the AMSU-B frequency range have an impact on the measured brightness temperatures. Accurate line-by-line radiative transfer calculations were performed using climatological and re-analysis data to check this impact. The results indicated that AMSU-B Channel 18 is the most affected, with brightness temperature differences of about 0.5 K. The difference was not just an offset, but shows a dependence on the channel brightness temperature, the differences being smaller for colder brightness temperatures and larger for warmer brightness temperatures. Therefore bias correction schemes used in NWP will not be able to successfully eliminate the ozone effect by a constant. Channels 17 and 20 are also marginally affected by the ozone lines. One recommendation of this study was that the ozone lines should be used in radiative transfer calculations, thus improving the use of AMSU-B radiances for NWP or climate applications.

A simple method to transform AMSU-B Channel 18 brightness temperatures to Upper Tropospheric Humidity (UTH) was developed. This method is referred to as a brightness temperature transformation method. The method can be used to retrieve Jacobian weighted upper tropospheric humidity (UTH) in a broad layer centered roughly between 6 and 8 km altitude. Retrieval results are sensitive to the type of Jacobian used to define upper tropospheric humidity. It was found that the retrieval of UTH based on the fractional water vapor VMR Jacobian works better than the more traditional retrieval of UTH based on the relative humidity Jacobian, and that the new upper tropospheric humidity definition does not need a reference pressure in the regression relation. A comparison of AMSU upper tropospheric humidity and radiosonde UTH for the radiosonde station Lindenberg was used to validate the retrieval method. The agreement is reasonable if known systematic differences between AMSU and radiosonde are taken into account. A qualitative comparison of upper tropospheric humidity climatologies from AMSU data and HIRS also showed a good agreement.

A robust method to compare radiosonde humidity data to AMSU data was developed, which is planned to be used for future global studies. The new method has some unique features: Firstly, the comparison is done for a target area, allowing an estimation of the atmospheric variability. Secondly, displacement and cloud filters are applied. Thirdly, a complete and consistent error model is used. The method was validated by a detailed case study, using the high quality Lindenberg radiosonde data and the NOAA-15 and 16 satellite data for the time period from 2001 to 2002. The study confirmed that low vertical resolution data, as found in operational archives, is sufficient to accurately predict AMSU radiances. It also demonstrated that corrections applied in Lindenberg to the standard Vaisala data processing make a significant difference, particularly in the upper troposphere. Overall, the AMSU

data are in very good agreement with the radiosonde data, with the notable exception of a slope in Channel 18. By re-processing with perturbed radiative transfer model parameters, radiative transfer model error was ruled out as a possible explanation for the slope, leaving only AMSU data and radiosonde data. Of these two, the latter seem the more likely explanation, which would mean that the corrected Lindenberg radiosonde data has a small residual dry bias at low humidities, giving 0% relative humidity when the true humidity is still approximately 2 - 4% relative humidity.

The method was applied to all European radiosonde stations for which data were readily available. The method seems to be useful for monitoring upper tropospheric humidity data from radiosonde stations using microwave satellite data as reference. The stations used in this study launch Vaisala radiosondes which suffer a known dry bias. The results of this study also confirm this dry bias in the Vaisala radiosonde data. There is a large variability in the dry bias among stations and years. There are believed to be several reasons for this such as radiosonde age, difference in calibration and launch procedures. A systematic difference in bias of about 1 K between NOAA-15 and NOAA-16 was also found, which was found to be due to time dependent errors in the radiosonde data such as radiation error.

The details of this work are presented in several articles and in a PhD thesis. These can be downloaded from: <http://www.sat.uni-bremen.de/members/viju/publication.php>

Observations

Rapporteur: G. Rädcl, Department of Meteorology, University of Reading, England

This session consisted of seven contributions on observations of water vapour content in the upper troposphere and lower stratosphere (UTLS). Progress in observational techniques as well as measurement results were presented and compared.

The introductory talk by Geraint Vaughan (University of Manchester) gave an overview of recent developments in observational techniques, in particular he addressed the question what progress had been achieved concerning accuracies of the different techniques since the SPARC water vapour assessment, 2000. He pointed out that one of the important questions to ask at this workshop is what accuracy for humidity as well as temperature measurements is really needed for atmospheric applications and should be aimed for. It was felt that for references at least a precision of 1% is needed for humidity measurements.

He concluded that recent improvements are not dramatic but progress has been made for instance in better understanding Vaisala radiosonde data, in the use of Raman lidars for reference measurements in the upper troposphere and global measurements will profit from a new generation of satellite instruments, whose accuracy however still has to be established.

Concerning the Vaisala humicap radiosondes he stressed the fact that humidity measurements above about 5 km absolutely need to be corrected for temperature dependent dry biases, time-lag, calibration biases, chemical contamination errors, etc., where the relative importance of the different corrections depend on the type of the radio sonde.

The performance of Vaisala radiosondes was also topic of the talks by Tuomo Suortti (Finish Meteorological Institute) and Viju John (University of Bremen). The first talk described a study of the homogeneity of Vaisala radiosonde humidity records in Finland covering a time period from 1965 until today, thus many different radio sonde types from the early hairhygrometers to several generations of humicap sondes. It concluded that inhomogeneities of the record are inevitably linked to the change of sonde types and need specific corrections, the temperature dependent dry bias time-lag corrections being probably the most important for humicap measurements in the upper troposphere. To establish long-term trends by combining information from the different sonde types is therefore difficult.

V. John presented a method comparing radiosonde humidity data to data from the Advanced Microwave Sounding Unit-B (AMSU-B) on the polar orbiting NOAA/NASA operational weather satellites, showing that corrections applied to the Lindenberg Vaisala RS80-A data improved the comparison. The method was then applied to all European radiosonde stations and it was found that there is a large variability in the dry bias depending on the station and the year. Probable reasons being the age of the sondes, different launching procedures and calibrations.

In this talk also the method to obtain the upper tropospheric humidity (UTH) from brightness temperatures measured using the AMSU-B channel 18 (183.31 GHz) which is based on fractional water vapour VMR Jacobians was detailed.

Results of water vapour measurements using balloon-borne *in situ* instruments or remote sensing techniques from satellites were topic of the four remaining talks of this session by Tom Gardiner (National Physical Laboratory), Serguey Khaykin (Central Aerological Observatory) and Federico Fierli (ISAC-CNR) for the *in situ* measurements and Harjinder Sembhi (University of Leicester) for the remote-sensing part. In addition Tom Gardiner presented as well the new trace water calibration facility at the National Physical Laboratory (NPL). This new facility is capable to deliver controlled amounts of water vapour from about 4 ppmv to about 30 ppbv. Absolute calibration is achieved by gravimetric traceability. But also other important aspects of trace water sensor performance can be studied, such as linearity, response time, hysteresis and long term stability.

Concerning the *in situ* water vapour measurements T. Gardiner presented a new tunable diode laser absorption spectrometer for the near infrared (TDLAS) which was used on a short balloon flight during the HIBISCUS campaign, 2004, in Bauru, Brasil. Measured water vapour profiles for the troposphere and lower stratosphere were presented with an estimated uncertainty of about 10%.

Also F. Fierli showed first results from the HIBISCUS campaign on cirrus and aerosol detection in the UTLS and their optical and dynamical properties determined from lidar and laser backscattersonde data. He presented several example cases showing evidence of different aerosol optical properties, related to different air parcel origins.

S. Khaykin presented another new measuring device for the use on balloons in the upper troposphere and lower stratosphere: the Flash-B Lyman-Alpha hygrosone. With this instrument it is possible to measure mixing ratios from 0.5 to 500 ppmv with the minimum response time of 0.2s and an uncertainty of 9% under stratospheric conditions. It can be used for a temperature range of -95 °C to +40 °C and at altitudes of 7 to 35 km. The instrument was employed during the LAUTLOS-WAVVAP field campaign, 2004, in Sodankylä, Finland. The measurements provide a detailed view of the Arctic upper troposphere lower stratosphere water vapour distribution, giving clearly different results in the stratosphere inside and outside of the polar vortex. For validation comparisons of measured water vapour mixing ratios with results from a simultaneously flown frostpoint hygrometer showed good agreement with an average difference of $2.6\% \pm 3.1\%$. Measurements were also successfully compared to results from the MIAWARA microwave radiometer.

H. Sembhi showed global water vapour and cloud measurements from the MIPAS, high-resolution limb-viewing Fourier transform spectrometer, onboard the ENVISAT satellite. The horizontal and vertical resolutions of this instrument is $30^\circ \times 30^\circ$ and 3km in the lower atmosphere, respectively. The spectral range is 4.16 to 14.5mm. In order to obtain 'cloud-free' vertical profiles of the atmospheric water vapour a cloud detection algorithm has to be employed which was also presented in this talk.

Last but not least an important point was made already by G. Vaughan and later was stressed several times in the discussions was the fact that still relative humidities are usually quoted (e.g. by the WMO) with respect to liquid water, even at very cold temperatures. These values originate from extrapolations from above the freezing point to temperatures smaller than -40 °C where liquid water practically does not exist. This does not make sense and leads furthermore to large differences depending on which of the many existing parameterizations is used.

Radiation and Chemistry

and

Chemical Impacts

Observations and Analysis of Far IR Emission and Cooling in the Upper Troposphere: A Progress Report

J E Harries, J Murray, P Green, G Straine, C Cox and J Pickering
Space and Atmospheric Physics Group, Imperial College, London, England

Introduction and Background

We still have only a poor understanding of how the components of the ERB vary with space, and with time, especially in presence of cloud. Why should we be interested in knowing the spectral dependence of the cooling of the Earth to space? The reason is that, because of the low emission temperature of the Earth, the Planck function peaks in the far IR. Therefore, an accurate understanding of the far IR radiative properties of the atmosphere is important if we are to correctly simulate the present and future climate.

However, until recently, the far IR cooling to space, or more precisely the far IR fluxes in the atmosphere which give rise to this cooling, had never been measured. So, we have developed the Tropospheric Airborne Fourier Transform Spectrometer, TAFTS, to fly on experimental aircraft, to measure the cooling rates within the atmosphere for the first time. It is also intended to fly TAFTS whenever possible along with a mid-IR spectrometer developed by the UK Met Office, to eventually provide complete spectral coverage.

TAFTS is designed to measure up-welling and down-welling radiances in the troposphere. Allowing (see below) the derivation of the heating (or cooling) rates, throughout the far IR from about 50 to 800 cm⁻¹. Design, development and data analysis of TAFTS has been carried out at Imperial College, and funded by NERC.

Theory

A simple interpretation of the solution to Schwarzschild's equation of radiative transfer is as follows,

$$R(\nu) = R_s(\nu)\tau_s(\nu, z_s) + \int B(\nu, T(z)) \{ \partial\tau(\nu, z) / \partial z \} dz$$

where $R(\nu)$ is radiance, s represents surface, z is altitude, T is temperature, τ is transmittance and B is the Planck function (source function). The first term on the rhs represents surface emission, modified at each wavenumber, ν , by the transmittance of the whole atmosphere. The second term represents the emission to space of all the layers of the atmosphere. For now we will assume that the radiance field is isotropic so that a simple factor of π relates radiance to flux.

The energy loss of the atmosphere to space per unit volume and unit time is defined by the 'cooling rate', h (which depends on optical depth and temperature, and the transmittance from each level towards space):

$$h(z) = \frac{\partial T(z)}{\partial t} = \frac{1}{\rho(z)c_p} \frac{\partial \Phi(z)}{\partial z}$$

where

$$\Phi_{\nu}(z) = F_{\nu}^{\downarrow}(z) - F_{\nu}^{\uparrow}(z)$$

and

$$F_{\nu}^{\downarrow}(z) = \pi R_{\nu}^{\downarrow}$$

We may break down the cooling rate into spectral elements, h_n , where

$$h(z) = \sum_m h_{\nu}^{\downarrow}(z) \Delta \nu_m = \sum_m \frac{1}{\rho(z)c_p} \frac{\partial \Phi_{\nu}(z)}{\partial z} \Delta \nu_m$$

We can define Ψ : a TAFTS-measured parameter, the cooling rate for an increment of height, Δz , and wavenumber, $\Delta \nu$.

$$\Psi_{\Delta z \Delta \nu} = \frac{1}{\Delta z} \sum_n \sum_m \frac{\pi}{\rho(z)c_p} \frac{\partial \{ R_{\nu}^{\downarrow}(z) - R_{\nu}^{\uparrow}(z) \}}{\partial z} \Delta z_n \Delta \nu_m$$

where

$$\Delta z = \sum_n \Delta z_n$$

The net cooling to space is strongly controlled by thermal emission to space from the pure rotation band of H₂O in the far IR from the mid and upper troposphere. This modifies the flux to space, which depends on humidity, temperature and cloud amount. Measurements will be used to: determine FIR radiative properties of clear and cloudy atmosphere; evaluate radiative properties of the Hadley Centre climate model; and to determine the need for future monitoring from space.

TAFTS Instrument and Flights

A description of the Tropospheric Airborne Fourier Transform Spectrometer, TAFTS, may be found at the web site:

<http://www.imperial.ac.uk/research/spat/research/tafts/index.htm> , and will be featured in a forthcoming paper [Murray et al., in preparation]. The instrument is based on a polarizing Fourier transform spectrometer which uses wire grids to divide an input beam according to the usual principles of a FTS. TAFTS is able to make measurements of two inputs simultaneously, using two sets of helium-cooled output detectors, and can select between up-welling, down-welling, and internal calibration black-bodies. Full absolute calibration is achieved through using black bodies at different temperatures. Measurements are made from aircraft flying at several levels in the upper troposphere. The net flux is formed from the difference between the up- and down-welling radiances, assuming an isotropic field, and the heating rate is then calculated from the vertical divergence of the net flux (see equations earlier).

In this paper we report data measured for clear skies from the EMERALD project in November 2002 over N. Australia, using the Australian EGRETT aircraft; and the EAQUATE campaign over the North Sea during November 2004 from the UK BAe 146 aircraft. Measurements during cirrus cloud conditions were also made during these missions and also during a special series of flights over the North Sea in February 2005.

Preliminary Results: Clear Skies

We present preliminary results here. More detailed data analyses will be published in due course. We have measured the heating rates as described above for clear sky portions of the observations made during EMERALD on 19 November 2002, and these are presented in the top left panel of Figure 1. Data are shown from about 400 to 200 hPa in altitude, and spectrally from 50-300 cm^{-1} . We have estimated the uncertainty of these heating rates to be about $\pm 0.3 \text{ K day}^{-1}$. For initial comparison purposes we have simulated the heating rates quite independently in two ways. First, by taking measurements of the atmospheric state taken from a variety of aircraft and sondes at the time and location of the observations, and using these as input to a radiative transfer model (MODTRAN) to give the simulated heating rates shown at bottom left. Second, by using the tropical standard model atmosphere, giving the results at bottom right.

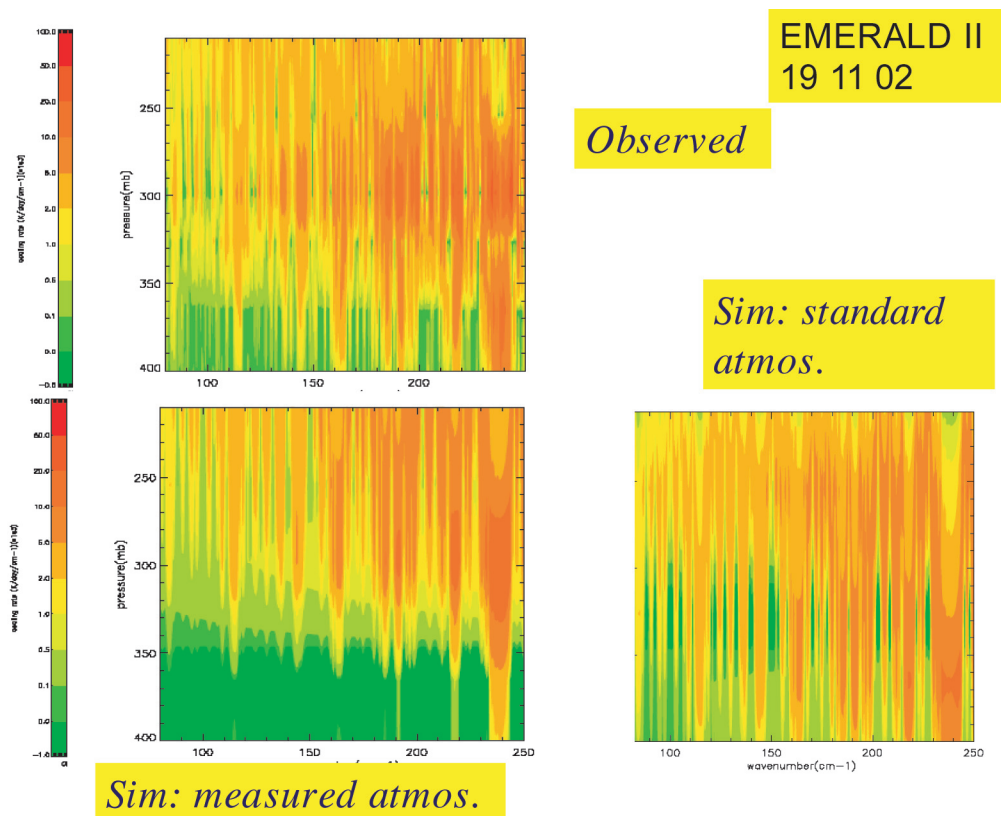


Figure 1: Heating rates measured on 19 November 2002 from the EMERALD campaign (Observed: top left). The other two frames show simulations using the atmospheric conditions as measured during the observations from both the EGRETT and other aircraft and sondes Bottom left); and simulated using a tropical standard atmosphere (right).

To make the comparison more quantitative, we have integrated the heating rates in the three cases between 325-254 hPa and 100-200 cm^{-1} . In the observations we find $1.34 \pm 0.30 \text{ K day}^{-1}$; the simulations using the measured atmosphere gives 0.83 K day^{-1} ; and the standard atmosphere gives 1.10 K day^{-1} . Thus it is clear, even on the basis of this preliminary analysis that the real heating rates in the far IR and upper troposphere would be significantly in error if deduced from a simulation. Direct measurement as we are making with TAFTS first need to be undertaken and analysed in detail to ensure that the simulations are correct. Much further work is planned.

Preliminary Results: Cloudy Skies

It is expected from the spectral properties of ice that cirrus clouds will significantly alter the up- and down-welling fluxes in the far IR. We show here some preliminary spectra from the EMERALD II campaign over North Australia which confirm this postulate. Figure 2 shows in the lower frame a flight profile (black) of aircraft altitude versus local time on 19 November 2002. The colours show LIDAR measurements of the presence of cloud. The four coloured vertical arrows just before 07.00 indicate the positions

where the four coloured coded downwelling spectra in the top curve were taken. It can be seen that the progression dark blue, red, green, light blue correspond to decreasing cirrus reflectivity in the LIDAR returns, and also to increasing transparency in the far IR spectrum between the strong water vapour absorption lines. This is to be expected since a thick cirrus cloud would emit a spectrum close to the black body at the local temperature, which is the case in the dark blue spectrum, for example. Thus these observations clearly point to the importance of characterising the emission properties of high cirrus cloud, and how this might be changing with time, in climate models. This is an extremely difficult problem, but the first step is to ensure that accurate measurements are available of the phenomenon.

This work continues on both clear and cloudy skies.

Downwelling LW cloudy spectra

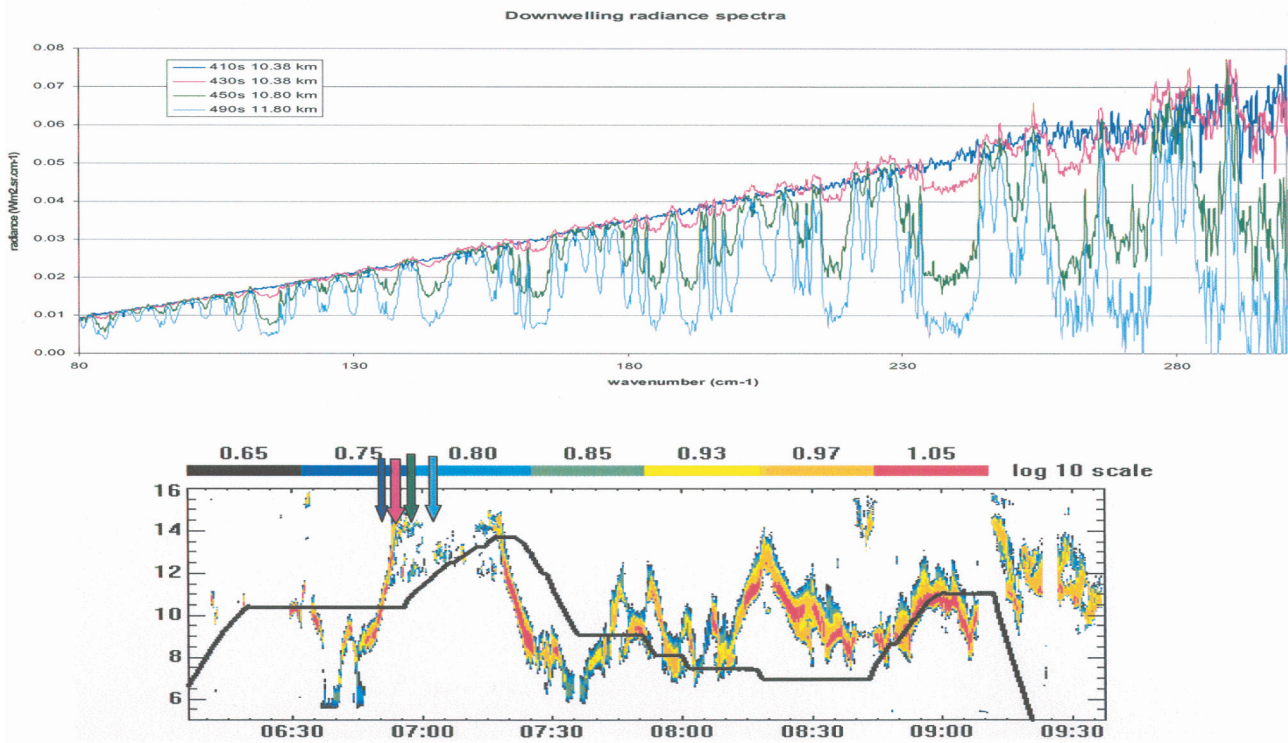


Figure 2: EMERALD II cirrus cloud spectra

Solar and Volcanic Influences on the Polar Annular Modes

J.D. Haigh¹, and H.K. Roscoe²

¹Imperial College London, England; ²British Antarctic Survey, Cambridge, England

At northern high latitudes the leading modes of variability in surface pressure are the North Atlantic Oscillation (NAO) and the Pacific-North America oscillation. Some authors regard these as part of a hemispheric-scale variation, the Northern Annular Mode (NAM), which has been found by statistical analysis of geopotential heights to be present throughout the lower atmosphere, although to what extent they represent different aspects of the same physical process is not well established. At southern high latitudes the equivalent Southern Annular Mode (SAM) has also been detected throughout the troposphere and lower stratosphere. Over the past few decades the NAO, NAM and SAM have all shown biases towards more positive values (representing greater latitudinal pressure gradients and stronger polar vortices) which have led to speculation that they are responding to climate change. Studies of the NAM and SAM have also suggested that changes in the stratosphere may propagate downwards and influence surface climate. Perturbations to the state of the stratosphere may indeed be induced by changes in the concentrations of greenhouse gases, and ozone, but may also be influenced by natural factors such as volcanic eruptions or solar variability. Here we present results of multiple regression analyses of monthly, de-seasonalised NAO, NAM and SAM time series in which we seek to extract signals of possible influences.

Figure 1 shows the indices implemented in the regression. The linear trend is used in the northern hemisphere while the stratospheric chlorine index (representing ozone loss) is used in the southern hemisphere to better represent the major climate forcings in these regions. Also incorporated in the analysis is an auto-regressive noise model whose parameters are determined iteratively with those of the regression until the residuals of the fit satisfy a red noise signal. The solar index is the F10.7 radio flux, the Quasi-Biennial Oscillation (QBO) index Singapore winds at 40 hPa and the volcanic index global stratospheric aerosol.

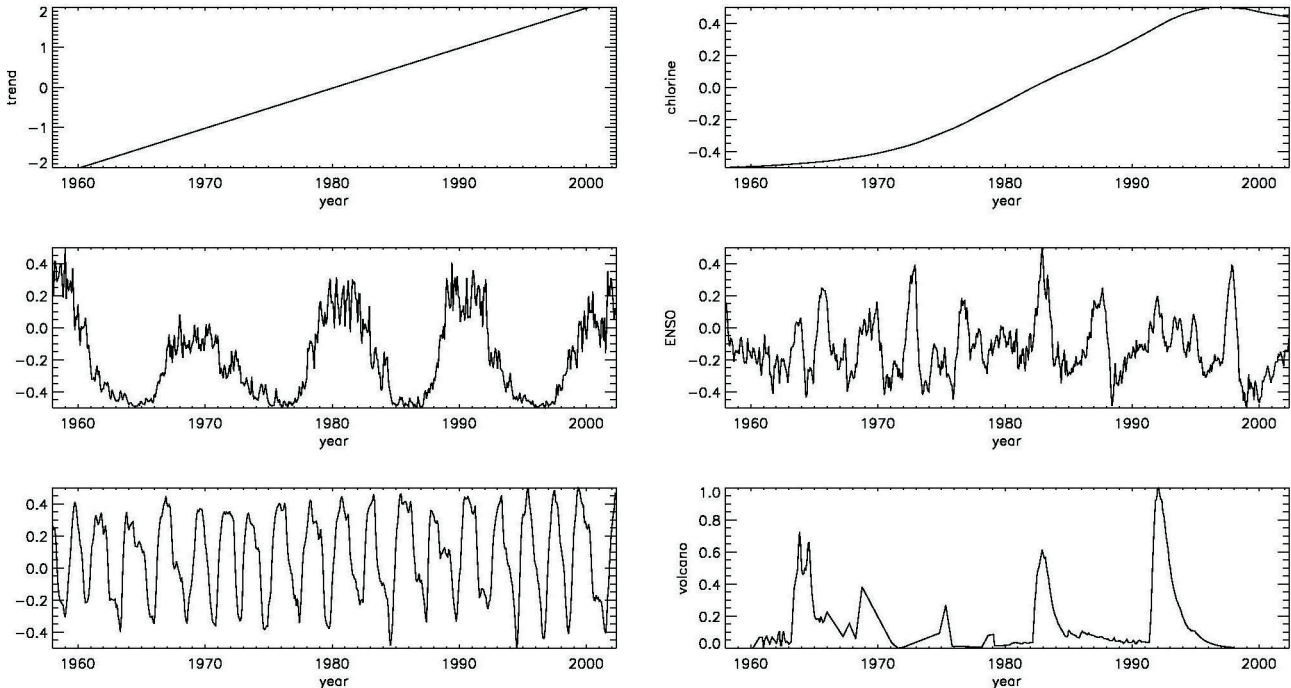


Figure 1: Indices used in the regression analysis - see labels on vertical axes.

Table 1 presents the regression coefficients derived using these indices; the values represent the maximum range of the mode due to the given index over the time period of the data (1958-2002) except in the case of the linear trend where the change over one decade is given. For the NAO only a small linear trend is found but there are clear signals of both volcanic and solar influence. Other authors have suggested that this might be the case but we believe this to be the first study to detect them in a statistically robust framework. The volcanic influence is felt throughout the atmosphere in both the NAM and SAM, but with different signs in the two hemispheres. No statistically significant solar influence is found in any mode apart from the NAO and little QBO effect is detected except in stratospheric NAO.

Table 1: Regression coefficients for the five standard indices. Colours indicate the statistical significance levels of values, derived using the Student-t test, as follows: 99%, 95%, 90%, 80%, <80%.

	pressure (hPa)	Trend	Cl	ENSO	Vol	Sol	QBO
NAO		0.02		-0.09	0.89	0.63	0.24
NAM	30	0.09		-0.37	0.30	-0.03	0.32
	250	0.02		-0.49	0.46	-0.02	0.05
	1000	0.13		-0.53	0.53	0.09	0.20
SAM	30		-0.30	-0.14	-0.44	-0.17	0.24
	250		0.61	-0.26	-0.65	-0.09	-0.14
	1000		1.01	-0.82	-0.65	-0.04	0.13

Labitzke and van Loon have suggested, using data composites, that northern hemisphere winter polar stratospheric temperatures vary in phase with solar activity (implying that solar activity is anti-correlated with the NAO) when the QBO is westerly, but in anti-phase (solar activity correlated with the NAO) when the QBO is easterly. However, their composites do not allow for the influence of other factors, nor produce an estimate of the statistical significance of the correlation. To test these factors we have repeated our regression analysis using a new index, composed of the product of the original solar and the QBO indices as shown in Figure 2, in place of the these two used independently.

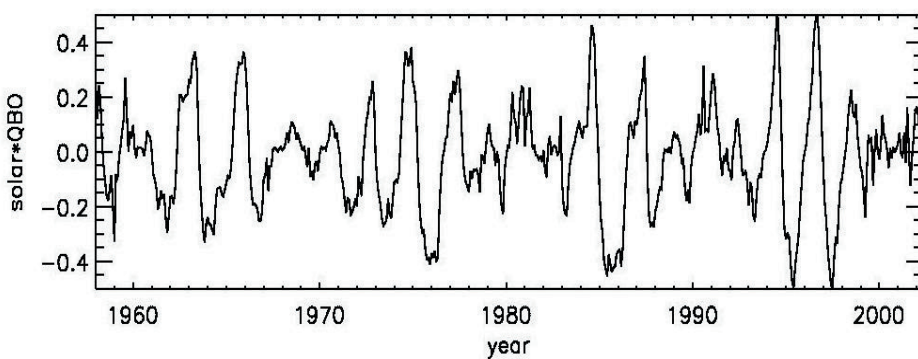


Figure 2: Composite index; this is the product of the independent solar and QBO indices shown in Figure 1, scaled to lie within unit range.

The derived regression coefficients are shown in Table 2 and it is immediately apparent, from the coloured elements in the final column, that a significant amount of the variance can be attributed to this index. This is particularly the case with SAM for which a strong signal emerges at all levels where very little was shown for the solar and QBO individually. As an example the time series of the derived components of SAM at 1000hPa for the two analyses are shown in Figure 3. For NAM the magnitudes are larger than seen in the former case but not statistically significant unless the analysis is applied only to winter data when again the compound index produces a strong signal.

Table 2: As Table 1 but for values derived using the compound solar*QBO index in place of the two indices independently.

	pressure (hPa)	Trend	CI	ENSO	Vol	Sol*QBO
NAO		0.03		-0.13	0.85	0.11
NAM	30	0.09		-0.35	0.27	-0.37
	250	0.02		-0.47	0.45	-0.16
	1000	0.13		-0.52	0.50	-0.27
NAM (DJFM)	30	0.12		-1.23	0.62	-2.04
	250	0.07		-1.39	0.38	-0.91
	1000	0.24		-0.85	0.96	-1.16
SAM	30		-0.30	-0.11	-0.47	-0.42
	250		0.61	-0.17	-0.71	-0.57
	1000		1.01	-0.71	-0.75	-0.89

The exception is the NAO for which the original solar signal is no longer present. We tentatively conclude that solar variability influences NAM and SAM through its impact in the polar stratosphere, modulated by the QBO, whereas the solar influence on the NAO is the result of a different process. Our previous work suggest this may involve changes in the tropospheric Hadley circulation and storm tracks resulting from solar heating of the tropical lower stratosphere. The mechanisms whereby all these processes take place remain to be elucidated.

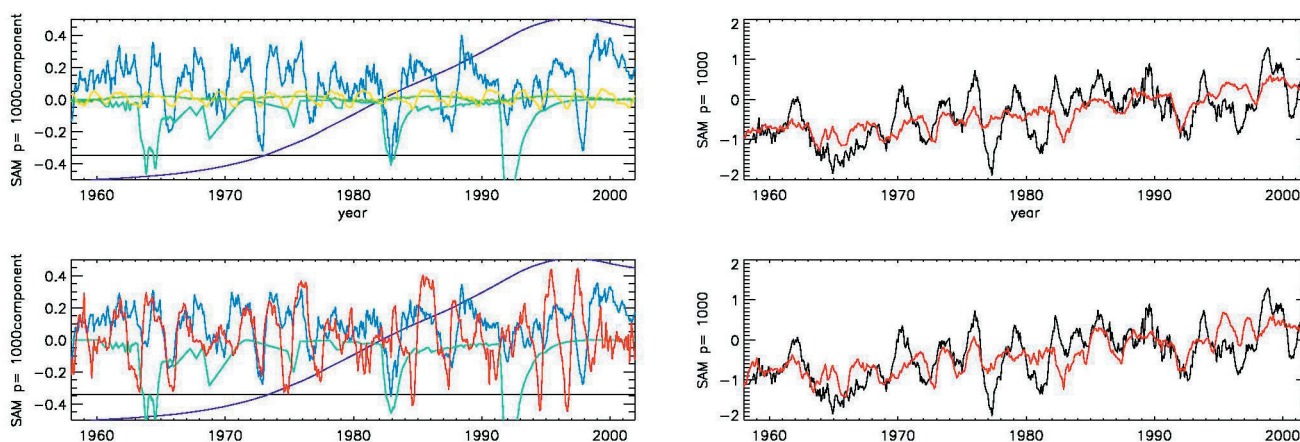


Figure 3: Results of regression analysis of SAM at 1000hPa. Top left: components using standard indices: constant (black), chlorine (purple), ENSO (blue), volcanic aerosol (cyan), solar (green), QBO (yellow). Bottom left: as above but using composite index (red) instead of independent solar and QBO indices. Right: original data (black) and reconstructions, without noise component, (red) both smoothed (after the regression analysis) by a 12-month running mean.

We acknowledge with gratitude Myles Allen for access to the multiple regression code and Mark Baldwin for provision of the NAM and SAM data.

Water Vapour in the Lower Stratosphere: CCM Studies of Increased H₂O

W. Tian and M.P. Chipperfield

Institute for Atmospheric Science, School of Earth and Environment, University of Leeds, England

Introduction

Water vapour plays a key role in the atmosphere through both chemical and radiative interactions. It is the source of HO_x (=OH + HO₂) radicals which directly destroy O₃ in both the lower and upper stratosphere. HO_x species also interact with other chemical families, which in turn also affect O₃ loss. For example, OH reacts with HCl to release Cl. H₂O is also involved in heterogeneous chemistry in the lower stratosphere. It is obviously involved in the formation of liquid and solid aerosol particles but heterogeneous chemical reaction rates can also depend on the aqueous content of liquid aerosols. Water vapour also absorbs infra-red radiation and hence plays a role in the temperature balance of the atmosphere. Clearly, given these many feedbacks, understanding how changes to H₂O may affect the atmosphere requires a detailed, coupled chemistry-climate model.

In this short paper we describe experiments with a 3-D coupled chemistry-climate model (CCM) aimed at diagnosing the chemical and radiative effects of an assumed increase in stratospheric H₂O.

Model set up and integrations

The CCM used in this study has a latitude-longitude resolution of 2.5° x 3.75° and 64 levels extending from the surface to 0.01 hPa (~80 km). The model is based on the Met Office Unified Model (UM) v4.5 [Cullen, 1993] with a detailed, interactively coupled, stratospheric chemistry scheme from the SLIMCAT chemical transport model [Chipperfield, 1999]. The coupled model (UMCHEM) advects 28 chemical tracers with around 42 chemical species including the Ox, HO_x, Cly,

Run	+ 2ppmv H ₂ O	Radiation Coupling
R0		O ₃ , N ₂ O, CH ₄
R1	In chemistry scheme	O ₃ , N ₂ O, CH ₄
R2		O ₃ , N ₂ O, CH ₄ , H ₂ O
R3	In radiation scheme	O ₃ , N ₂ O, CH ₄ , H ₂ O

Table 1: Four 10-year time-slice model experiments

Bry, and NO_y families and source gases. The model includes both gas-phase chemistry and heterogeneous chemistry on liquid and solid aerosols and polar stratospheric clouds (PSCs). The model chemical O₃, N₂O and CH₄ tracers are coupled to the UM's radiation scheme. The chemistry is calculated on 30 levels spanning from -150 hPa to 0.5 hPa. A more detailed description of UMChem can be found in Tian and Chipperfield [2005].

Four integrations of UMChem have been performed for this study and their basic configurations are given in Table 1. Note that in all runs the stratospheric O₃, N₂O and CH₄ values for radiation scheme are taken from the chemistry module. In these experiments we have added an assumed increase of +2ppmv H₂O to the model's chemistry scheme only (R1) or its radiation scheme only (R3). All model diagnostics are 10-year averaged climatologies.

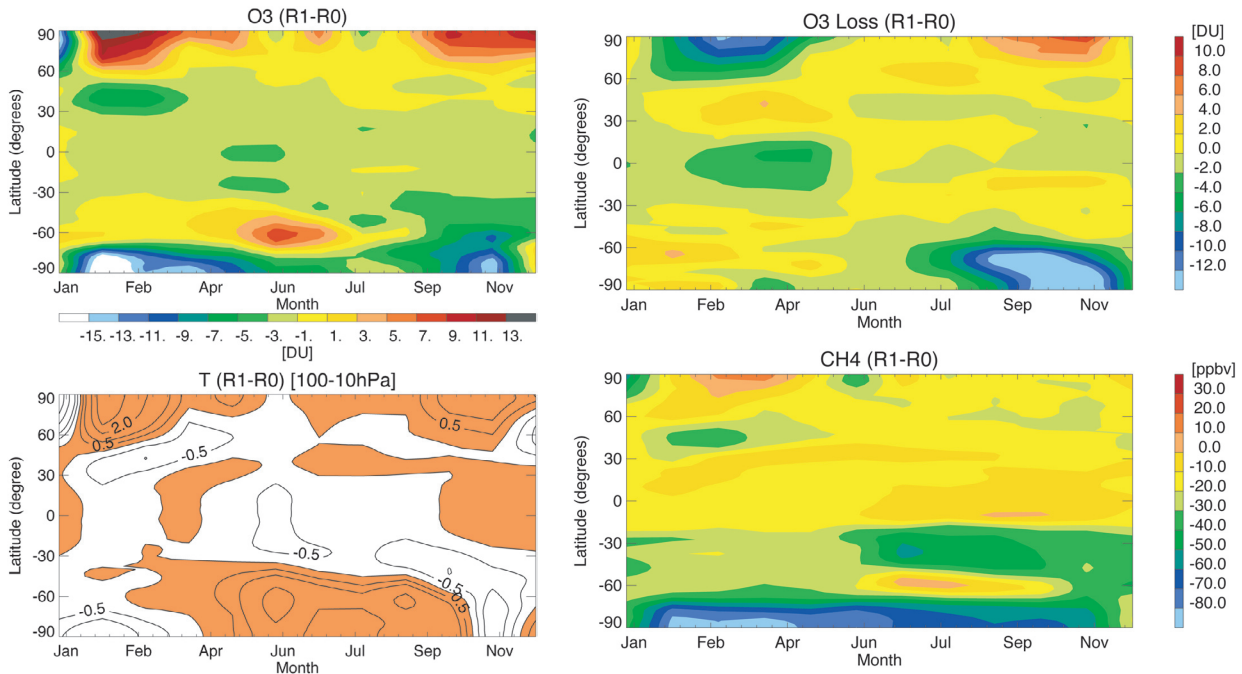


Figure 1: Difference in model fields between runs R0 and R1, showing the effect of +2 ppmv increase in H₂O in the model's chemistry scheme. (a, top left) column O₃ change (DU), (b, top right) change in seasonal column O₃ loss (DU), (c, bottom left) change in mean temperature (K) between 10-100 hPa, and (d, bottom right) change in mean CH₄ (ppbv) between 10-100 hPa.

Results

Chemical effects of water vapour

Figure 1a shows the total column ozone differences between runs R0 and R1. An increase of 2 ppmv H₂O in the chemistry scheme leads to a decrease in total column O₃ at the southern high latitudes (up to 15 DU) and an increase at the northern high latitudes (13 DU). An overall decrease in column ozone (~3 DU) in the tropics is evident. Figure 1b shows the diagnosed seasonal chemical column loss. This is the loss integrated from December 1 and June 1 each year and is useful as measure of polar O₃ loss. This shows that increasing H₂O in the chemistry increases chemical loss in both polar spring periods. Combined with the results in Figure 1a, this shows that the increased chemical loss is masked by increases in column O₃ due to stronger transport in the Arctic. In the Antarctic the net change in O₃ is still negative. The changes to CH₄ (Figure 1d) are consistent with the inferred stronger descent in the Arctic in run R1.

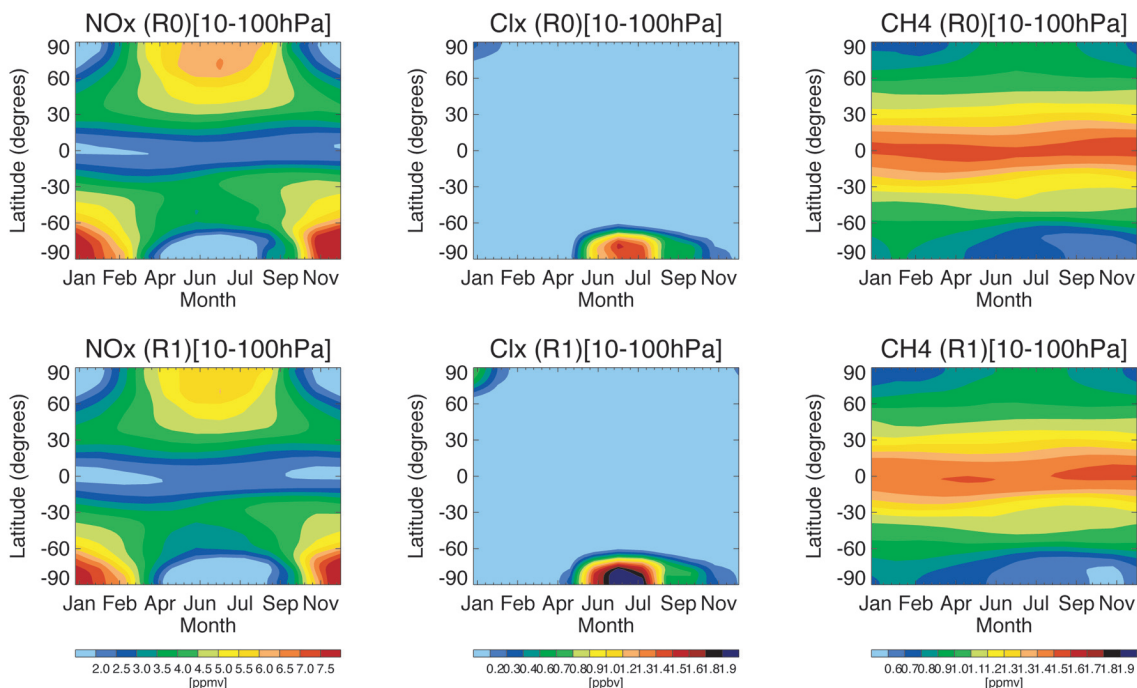


Figure 2: Mean vmrs of NO_x, Cl_x and CH₄ between 10-100 hPa from control run R0 and run with increased H₂O in chemistry scheme R1.

The temperature response to increased H_2O in chemistry is mainly forced by changes in the solar heating as a result of O_3 changes. In the southern high latitude winter, the water vapour increase results in a warming of the stratosphere by 1-2 K. Significant warming of the stratosphere is modelled at the northern high latitudes with a maximum of 2 K in January (Figure 1c). In the tropical stratosphere, the temperature decreases by 0.5 K due to 1% decrease of the column ozone.

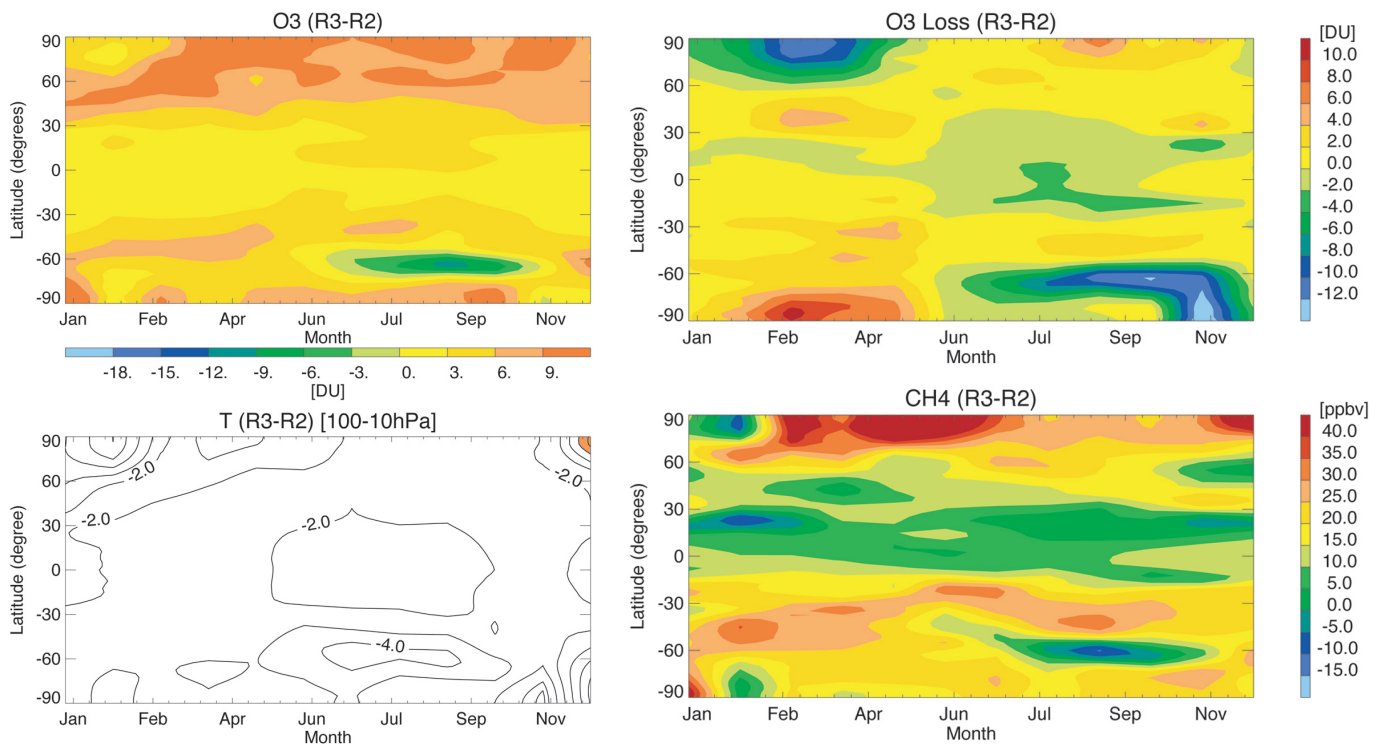


Figure 3: As Figure 1 but for differences between runs R2 and R3, with increase H_2O in the radiation scheme.

Figure 2 shows fields of NO_x , Cl_x and CH_4 from runs R0 and R1. The run with increased H_2O shows larger values of active chlorine (Cl_x) in the polar spring regions. This is due to enhanced PSC activity in the run with increased H_2O and is the cause of the increase seasonal chemical loss in Figure 1c.

Radiative effects of water vapour

Figure 3 shows the impact of increasing H_2O in the model's radiation scheme. The direct response is a cooling of the stratosphere by up to 2 K in the tropics and a maximum of 4 K at high latitudes (Figure 3c). Forster & Shine [2002] found that a uniform increase of 0.7 ppmv of water vapour in the stratosphere resulted in a cooling of the polar vortices by 4-6 K in the spring and an overall cooling of the stratosphere by -0.8 K from 5 to 50 hPa.

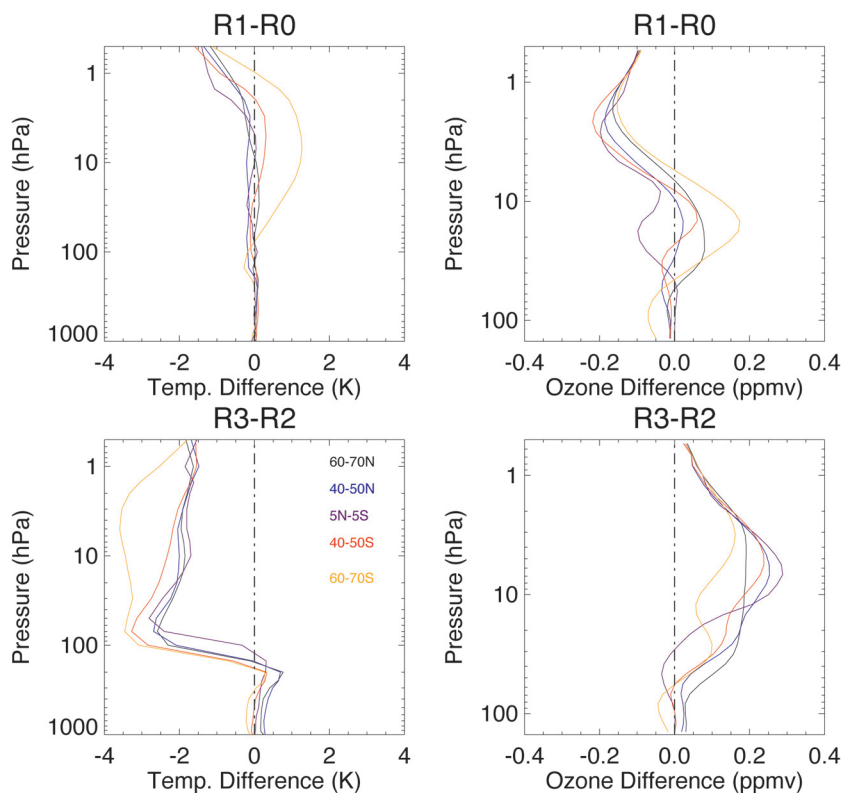


Figure 4: Vertical profiles of the differences in temperature (K) and ozone (ppmv) (top) between run R0 and R1 (top) and runs R2 and R3 (bottom). The results are averaged over five different latitude bands and are 10-year annual averages.

Generally column O_3 increases everywhere with the notable exception of the edge of the Antarctic polar vortex in spring. Figure 3b shows that the seasonal chemical O_3 loss has increased in the polar spring regions due to the stratospheric cooling. In particular, there is a prominent increase in chemical O_3 loss at the edge of the Antarctic vortex which drives the overall column decrease. The H_2O -induced cooling has allowed the occurrence of PSCs to extend to lower latitudes.

Overall Effects

Increasing water vapour leads to a cooling of the stratosphere and modifies the stratospheric circulation. The cooling of the stratosphere slows down the temperature-dependent stratospheric ozone depletion processes on one side but increase polar stratospheric clouds formation resulting in large ozone losses in cold polar winters on the other. Increasing water vapour also has a large impact on chemical processes which destroy and produce ozone in the stratosphere even without its direct cooling effects being taken into account.

Figure 4 shows the vertical profiles of the temperature and O_3 changes between runs R1-R0 and R3-R2 as an annual average. Both the chemical and radiative effects of stratospheric H_2O are significant although their effects on O_3 are reversed

in the upper stratosphere, i.e., the chemistry-related effects tend to decrease O₃ while the radiative effects lead to an increase. The net effect would be to further increase ozone in the middle stratosphere at middle-high latitudes while chemical and radiative effects are likely to cancel in the upper stratosphere. The temperature responses to increasing water vapour in chemistry and radiation scheme are different. The radiative cooling of increasing water vapour is much more significant, ranging from 1 K to 4 K, over all latitudes. The indirect chemical effect (via O₃) gives rise a cooling in the upper stratosphere at all latitudes, but in the Antarctic middle and upper stratosphere significant warming of about 1 K occurs. The combined effects of water vapour may lead to less cooling at southern high latitudes than separately.

Acknowledgements

This research was supported by: That Natural Environment Research Council's Upper Troposphere and Lower Stratosphere Ozone (UTLS OZONE) Programme and the UK Universities Global Atmospheric Modelling Programme (UGAMP).

References

- Chipperfield, M.P., Multiannual simulation with a three-dimensional chemical transport model, *J. Geophys. Res.*, 104, 1781-1805, 1999.
 Cullen, M.J.P., The unified forecast/climate model, *Meteorol. Mag.*, 122, 81-94, 1993.
 Forster, P.M. de F. and K.P. Shine, Assessing the climate impact of trend in stratospheric water vapor, *Geophys. Res. Lett.*, 29, doi:10.1029/2001GL013909, 2002.
 Tian W. and M. P. Chipperfield, A new coupled chemistry-climate model for the stratosphere: The importance of coupling for future O₃-climate predictions, *Q. J. R. Meteorol. Soc.*, 131, 281-303, 2005.

Emissions of Water Vapour from a Supersonic Fleet: Impact on the UTLS

O. Dessens¹, H.L. Rogers¹, V. Grewe², G. Pitari³, I.S.A. Isaksen⁴, C. Marizy⁵ and J. Pyle¹

¹Department of Chemistry, University of Cambridge, England; ²Institut für Physik der Atmosphäre, DLR, Germany; ³Department of Physics, University of L'Aquila, Italy; ⁴Centre for International Climate and Environmental Research/University of Oslo, Norway; ⁵Acoustic and Environment Department, AIRBUS, France.

The objectives of the Scenario of Aircraft Emissions and Impact Studies on Chemistry and Climate (SCENIC) programme were to examine the impact on atmospheric chemistry and climate of new scenarios for civil supersonic aviation.

The scenarios have been developed by the consortium within the project. Subsonic and mixed fleets (sub + supersonic) have been produced for the years 2025 and 2050 (500 supersonic aircraft in the 2050 reference fleet). For 2050, several "perturbed" scenarios have also been produced to study different configurations for the supersonic aircraft or fleet to determine a design for minimal impact of the fleet on the atmosphere.

The impact of water vapour emission from the reference supersonic scenario for 2050 is plotted Figure 1. Three model results are presented: University of L'Aquila, University of Oslo and University of Cambridge. The impact on the water vapour concentration within the stratosphere varies between the models. All the models produce a maximum in water vapour in the source region of aircraft emissions, of 0.3 to 0.4 ppm, with equatorward advection, followed by transport aloft within the tropical pipe. The maximum increase can reach 8 to 12% in comparison with the background water vapour concentration; in the rest of the stratosphere the impact is between 1 and 3%.

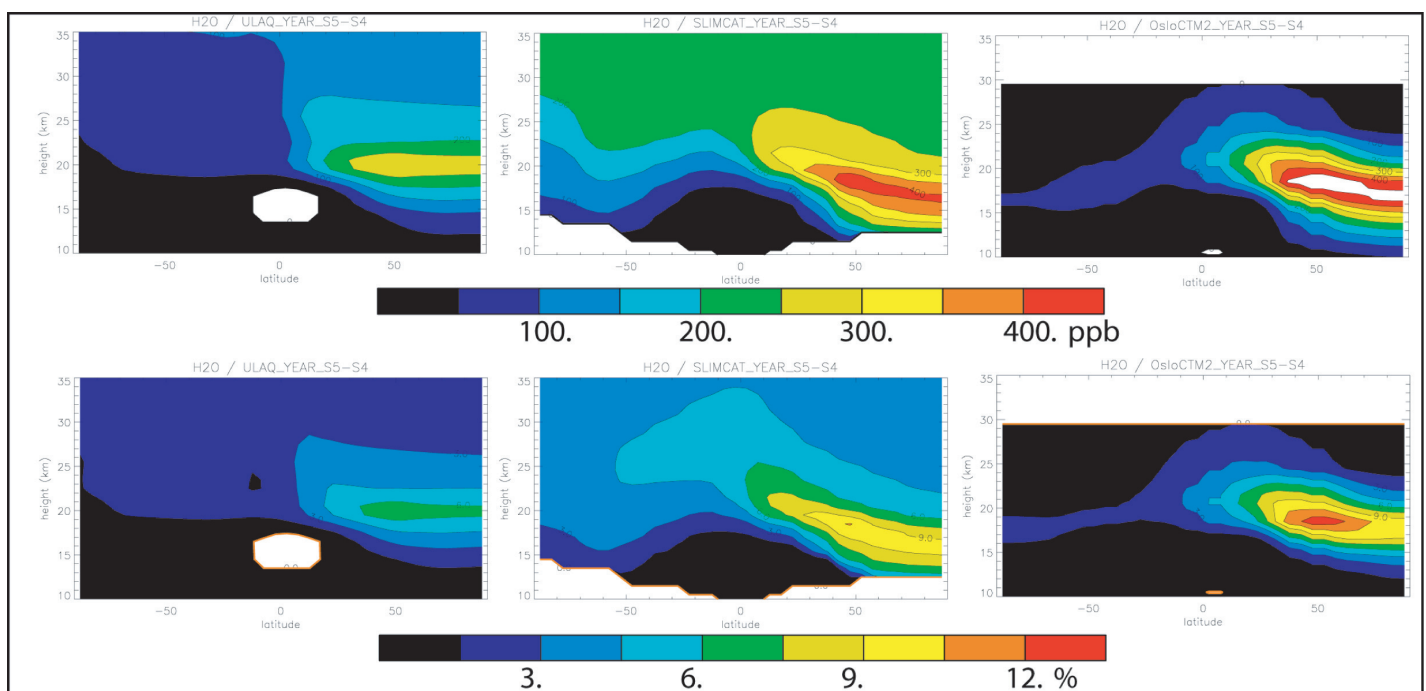


Figure 1: annual-zonal mean water vapour perturbations due to a reference 2050 supersonic fleet, as calculated by Universities of L'Aquila, Cambridge and Oslo models (left to right). Units: mixing ratio (top) and percentage (bottom).

The impact of water vapour on chemistry is driven by the production of HOx radicals from H₂O (Figure 2). The models give a reduction of ozone (-0.2%) in the upper troposphere lower stratosphere region due to a direct effect on the ozone catalytic cycle by HOx. In the middle stratosphere this catalytic cycle is overwhelmed by a similar cycle involving NOx. The impact here of the HOx on the NOx family (via HNO₃ production) is to slow down the ozone destruction which leads to a slight increase in the ozone concentration (+0.2%). These results have to be compared to the direct effect of NOx emissions on ozone which can reach 3 to 4%.

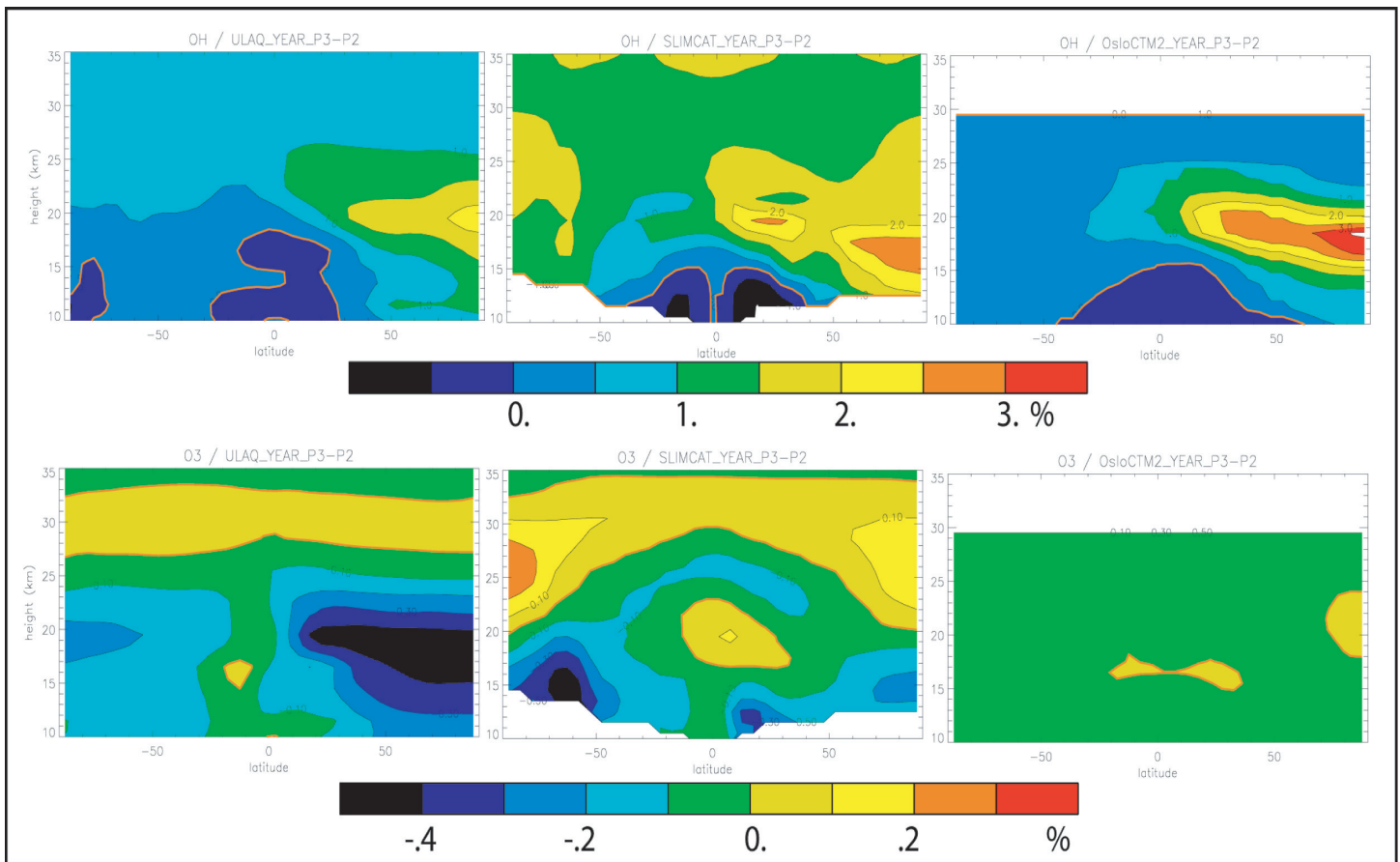


Figure 2: annual-zonal mean OH (top) and ozone (bottom) perturbations due to a reference 2050 supersonic fleet, as calculated by Universities of L'Aquila, Cambridge and Oslo models (left to right). Units: percentage.

The increase in water vapour concentrations within the stratosphere modifies the radiative forcing of the atmosphere. With supersonic emissions (CO₂, NOx, H₂O) the modification of the stratospheric concentration of water vapour has the largest impact on radiative forcing (+25 mW/m², see table below) followed by ozone (via NOx emissions). The change in surface temperature has been calculated based on the changes in radiative forcing. In 2100, for the reference supersonic fleet, surface temperature increases by +40 mK due to the water vapour contribution alone, with a decrease of approximately -10mK due to the ozone.

The results of calculations using three "perturbed" scenarios are presented Figure 3. These scenarios include (1) doubling the number of supersonic aircraft in the fleet, (2) increasing the supersonic aircraft maximum range and (3) reducing the Mach speed. In terms of the fuel consumption (and consequently water vapour emissions) the scenario (1) has twice the 2050 reference consumption, scenario (2) only 20% higher and scenario (3) a reduction of around 40%. From the perturbation scenarios calculations, it can be seen that reducing the quantity of emissions (by reducing the fuel consumption) and lowering the altitude of the emissions (by reducing the supersonic speed) results in a weaker impact on the stratospheric water vapour concentration.

During the project the importance of the transport schemes within the models has, yet again, shown to be significant especially in experiments designed to examine the impact of anthropogenic activity on the atmosphere. In conclusion the direct impact of water vapour emissions from a supersonic fleet on stratospheric chemistry are weaker than those due to NOx emissions, by a factor of 10, however in terms of radiative forcing, the increase in stratospheric water vapour is the main contributor to climate change from supersonic fleet emissions.

Table: change in radiative forcing due to the reference 2050 supersonic fleet emissions (in mW/m²).

	CO ₂	H ₂ O	O ₃	CH ₄	TOTAL
L'Aquila	3.26	15.8	-4.70		14.3
Oslo	3.26	23.0	-7.4	-0.11	18.7
Cambridge	3.26	35.9	-8.6	-1.32	29.2
TOTAL	3.26	24.9	-6.9	-0.71	20.7

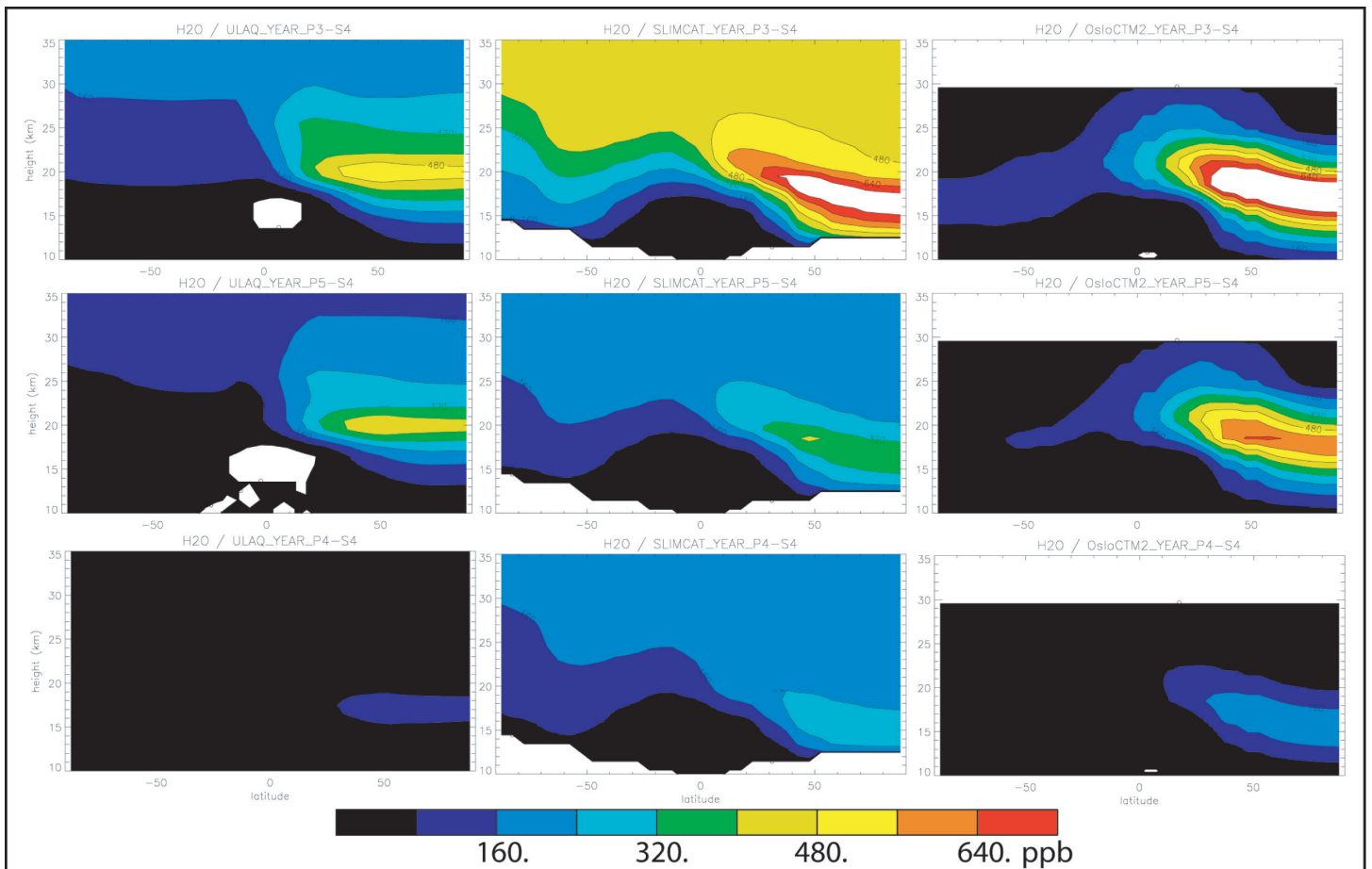


Figure 3: zonal-annual mean impact of water vapour emissions from three perturbed supersonic scenarios ((1) doubling of fleet size; (2) increase in range and (3) reduction of Mach speed from top to bottom) calculated by models from the Universities of L'aquila, Cambridge and Oslo. Units: mixing ratio.

Radiation and Chemistry, and Chemical Impacts

Rapporteur: H. Pumphrey, School of GeoSciences, University of Edinburgh, Scotland

Five talks were presented in the "Radiation and Chemistry" sessions, three on radiation, on Wednesday afternoon, and two on Chemistry, on Thursday morning.

Prof. J. Harries reported on progress with the TAFTS instrument, a far-infrared interferometer. The driving idea behind this project is that climate models need to model the radiative heating rate in each part of the atmosphere, but that no-one has been out and measured it in detail. This is particularly true in the far IR, where the Planck function for the Earth has its peak, and where the rotation band of water vapour controls the emission of radiation to space.

TAFTS measures the upwelling and downwelling radiance. If we can measure how this changes with height, then we can infer the heating rate. The aims are

- To determine the FIR properties of both clear and cloudy atmospheres.
- Compare to radiative properties of the hadel Centre model.
- Assess whether it would be useful to fly an instrument like TAFTS on a satellite.

Prof. Harries reported that instrument calibration had been completed and that TAFTS has been flown successfully on the FAAM BAe 146 and on the Egret aeroplane. Earlier attempts to fly the instrument on the C130 were unsuccessful owing to the excessive vibration to which this aircraft submits its payload. A great deal of data has been taken and the team are now analysing it. Prof. Harries showed some early results for both clear and cloudy atmospheres. He noted that there was a great deal of data processing to be done and that comparisons with climate models had not yet been started. Finally, he noted that the spectral region between the 15 μ m CO₂ band and the pure rotation band of water vapour should become an atmospheric window under dry conditions. He therefore plans to operate TAFTS on the ground at a high latitude or altitude site in order to observe this.

The second talk of the session was prepared by W. Zhong but presented by Prof J. Haigh. In this talk, it was explained that cirrus clouds are important to the Earth's radiation balance, and that to model the flow of radiation through a cloud, the effects of the detailed 3-D structure of the cloud had to be taken into account.

To demonstrate this, artificial 3-D clouds were constructed, using 2-D measurements and statistical information. The radiation flow through three such clouds was calculated using the SHDOM program and a simple approximation called IPA. (The EVENT model mentioned in the abstract was not yet ready for use.) The results demonstrate that:

- Long-wave heating / cooling is large and not at all uniform.
- The simple IPA approximation differs from the full 3-D SHDOM results by as much as 20K/day in places.
- IPA can differ from the 3-D calculations by up to 40%, averaged over the cloud.
- IPA and SHDOM agree much better for shortwave heating.

Questions were asked about:

- Whether it would be valuable to make 3-D measurements of cirrus structure (Prof Haigh thought that it would)
- Whether the 3-D calculation is slow (Yes it is.)
- How the results could be incorporated into a GCM (Difficult!)

In the final talk of the day, Prof. Haigh described a series of regression analyses with which she attempted to quantify any effects of solar variability on the atmosphere's polar and angular modes of variability. A variety of predictors (solar flux, ENSO index, CI loading, volcanic aerosol loading, QBO, etc.) were used in order to predict the zonal mean zonal wind. The regressions suggest that solar variability affects the North Atlantic Oscillation, but not the annular modes. The regression was then re-done using a new predictor: the product of the QBO and the solar variability. The southern annular mode depends strongly on this new predictor, even though it depends only very weakly on both its two factors.

Questions were asked about the provenance of the winds used (all from the satellite era of ERA40) and on the mechanism by which volcanos affect the results.

The audience were too stunned to participate in a general discussion and departed to prepare for the conference dinner. Later in the evening, the atmosphere laid on a display of noctilucent clouds, reminding late stragglers that water vapour is a significant-constituent at altitudes well above the upper troposphere.

Next morning, in the "chemistry" part of the session, Martyn Chipperfield gave a detailed review of the chemistry of water vapour in the stratosphere and how it interacts with Ozone. He pointed out that water is the source of HOx radicals, which are the main ozone destroying species at both the top and bottom of the (non-polar) stratosphere. (The NOx and ClOx groups of species are more important in the middle stratosphere.) In the polar regions, water vapour is a major component of polar stratospheric clouds.

Several runs of the SLIMCAT model were described. One run demonstrated that if one changes the dehydration threshold so that H₂O is removed earlier in the winter, then there are less PSCs later on in the winter and less Ozone loss overall. It was noted that the northern winter of 2004/05 was a record cold winter and that some dehydration occurred - an extremely rare event. The SLIMCAT model shows extensive dehydration for that winter as it is driven by ECMWF temperatures which have a known cold bias.

Water is also a significant contributor to mid-latitude ozone trends. These trends are not large and modelling them is therefore not easy.

The tropical tape-recorder is a stringent test for 3-D models. It was shown that a model with potential temperature as the vertical co-ordinate does a better job than one which uses pressure levels.

CTMs such as SLIMCAT are good for explaining and understanding, but to predict the future behaviour of the atmosphere, a coupled chemistry-climate model is required. The HadAM3 model (one variant of the Met Office Unified Model) is one such model. Several HadAM3 runs were shown, to demonstrate that water has both chemical and dynamical effects on ozone loss.

Dr Chipperfield was asked a variety of questions. Most of these concerned the methodology behind the HadAM3 runs: were they long enough, was the perturbation applied to the water vapour too large, or too small, and so on. There was also some discussion about why potential temperature levels gave a better tape recorder.

In the final talk of the session, Olivier Dessens described how emissions of water from a fleet of supersonic aircraft would affect the upper troposphere and lower stratosphere region. Beginning with the effect of a standard reference fleet, he investigated the effects of doubling the number of aircraft, lowering their speed and using them for longer flights. It was shown that changes in water vapour are the main mechanism by which the aircraft would perturb the radiation balance.

In the general questions at the end of the session, most of the questions were addressed to Martyn Chipperfield. Bob Harwood asked whether the effect of mid-latitude aerosols on Ozone was still an active research topic. Dr Chipperfield thought that chemistry on the highest cirrus clouds was an under-investigated subject. Peter Haynes asked how expensive the chemistry calculations were, compared to the rest of the UM. Dr Chipperfield thought that it added perhaps 50% to the CPU time, noting that the Unified Model was pretty expensive to run anyway.

Stratosphere Troposphere Exchange

Trajectory-Based Studies of Dehydration in the Tropical Tropopause Region

P.H. Haynes

Department of Applied Mathematics and Theoretical Physics, University of Cambridge, England

Since the pioneering paper by Brewer [1949] it has been accepted that stratospheric water vapour concentrations are broadly explained by assuming that most transport from troposphere to stratosphere takes place in the tropics, where tropopause temperatures are significantly lower than at other latitudes (and therefore freeze drying to the saturation mixing ratio implied by tropopause temperatures implies lower concentrations of water vapour). However there has been less broad agreement on details. One continuing question has been whether dehydration as air moves from troposphere to stratosphere is determined by large-scale temperature distributions, or whether it depends on details of small-scale, i.e. convective and mesoscale, dynamics [e.g. Rosenlof, 2003 and references therein]. Whilst it is now accepted (or re-accepted) that in an average sense the frequency of convection penetration decays with height over a region ('the tropical tropopause layer') from about 13 km to 17 km (the latter being the typical height of the coldest temperatures - the 'cold point'), this does not preclude the possibility that occasional penetration of convection to the cold point has a significant effect on the water vapour budget. Nonetheless, this paper will focus on the implications of large-scale processes for stratospheric water vapour.

One particular concern has been that large-scale average temperatures are not cold enough to explain (assuming dehydration to the corresponding saturation mixing ratios) observed stratospheric water vapour concentrations. Thus Newell and Gould-Stewart [1981] noted that observed stratospheric water vapour concentrations are lower than those expected from zonal-mean tropical tropopause temperatures and proposed a "stratospheric fountain" hypothesis, that ascent through the tropopause must be concentrated at locations and times where tropopause temperatures are coldest (particularly over the Indonesian and Western Pacific region in the period October-March). However the observation of the "tropical tape recorder" signal suggests that transport through the tropical tropopause region is taking place throughout the year. Furthermore the "stratospheric fountain" picture is very much based on a one-dimensional view of the tropical tropopause region emphasising vertical transport. In fact simple order-of-magnitude arguments that air parcels move significant horizontal distances as they move through this region. Thus, in contrast to the "stratospheric fountain" view, Holton & Gettelman [2001] argued that horizontal transport through the coldest regions might effectively reduce stratospheric water vapour concentrations from those expected from some average measure of temperatures. They illustrated this effect using a simple model in which, in particular, wind and temperature distributions were prescribed by simple formulae.

A leading question arising from the Holton & Gettelman [2001] paper is the implication for stratospheric water vapour of transport by the actual large-scale wind fields through the actual temperature field in the real atmosphere. Operational analysis and re-analysis datasets such as those from European Centre for Medium Range Weather Forecasts (ECMWF) now provide quantitatively useful information on these fields. A set of recent investigations [Bonazzola & Haynes 2004 - hereafter BH04; Fueglistaler et al., 2004; Fueglistaler et al., 2005a - hereafter F05; Fueglistaler & Haynes, 2005 - hereafter FH05] have used ECMWF analysis fields to undertake trajectory-based investigations of transport through the tropical tropopause region and the implications for stratospheric water vapour. Recalling the 'large-scale' vs 'small-scale' distinction above, the ECMWF-analysis-based investigations can be considered to be taking account of large-scale processes, where large-scale means in practice greater than 100 km or so in the horizontal. A corresponding approach using wind and temperature fields from a general circulation model is described by Hatsushika & Yamazaki [2003]. A summary of the results of these investigations and their implications has recently been given by Fueglistaler et al. [2005b].

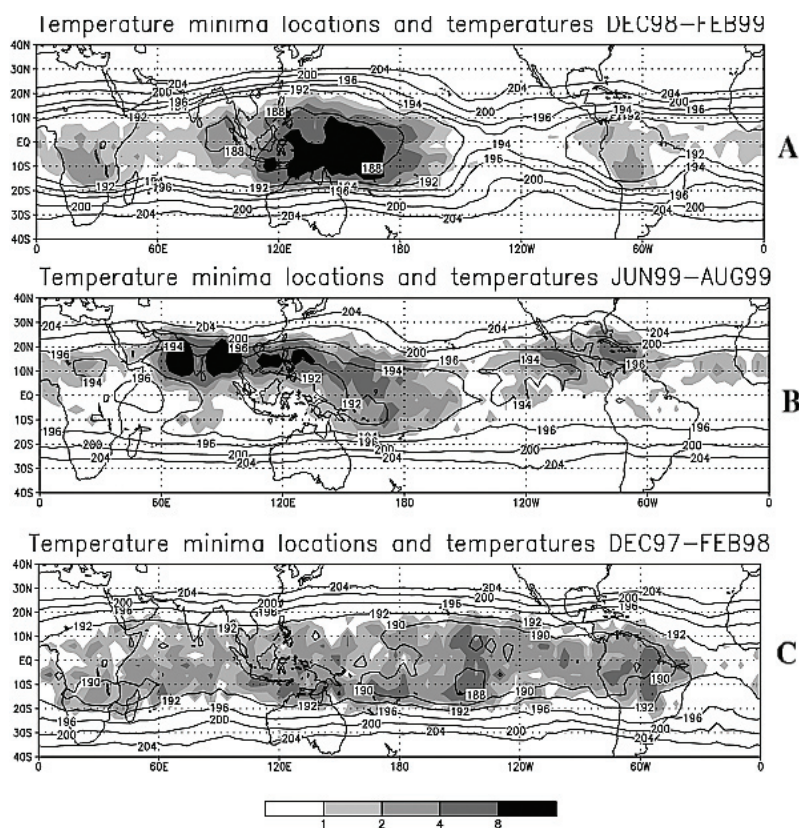


Figure 1: (Figure adapted from BH04.) Contours show average temperature field (K) as experienced by all trajectories in the 'cold point layer' (CPL) defined by BH04. Shading gives density of Lagrangian cold points (with value 1 corresponding to uniform distribution over tropics). Recall that these results are for back trajectories initialised with uniform distribution on 400 K potential temperature surface. Panel A shows NH winter 1998/99. (CPL was bounded by 360 K and 380 K potential temperature surfaces.) Panel B shows NH summer 1999. (CPL was bounded by 361 K and 381 K potential temperature surfaces.) Panel C shows NH winter 1997-98 (corresponding to strong El Niño conditions, Panel A corresponds to La Niña conditions). Note the concentration of Lagrangian cold points in the West Pacific region in Panel A. The extended F05 study over the period 1979-2002 shows the concentration over the West Pacific to be typical, except in the NH summer season (e.g. Panel B) and under strong El Niño conditions (e.g. Panel C).

A systematic way in which these investigations have been used to link temperatures and velocity fields on the one hand and stratospheric water vapour on the other is to calculate ensembles of back trajectories, typically 2 or 3 months in duration, from points evenly distributed in the horizontal on some suitable isentropic surface in the lower stratosphere. Some back trajectories reach the tropical troposphere - the troposphere-to-stratosphere (TS) ensemble while others (as expected) reach the extratropical stratosphere. The 'entry' value of water vapour concentration for the stratosphere is taken to be defined by the Lagrangian time history of temperature along TS trajectories. Under the assumption that microphysical processes dehydrate instantaneously to the saturation mixing ratio, the entry value is determined by the average over all TS trajectories of the minimum saturation mixing ratio experienced along the trajectory. This motivates the idea of a 'Lagrangian cold point' (F05) - the location of the minimum temperature experienced along the trajectory. (To good approximation the minimum saturation mixing ratio is determined by the minimum temperature.) Of particular interest is the geographical distribution of Lagrangian cold points and the corresponding temperatures. A common feature of the results of all the investigations noted above is that for the TS ensemble the distribution of Lagrangian cold points is significantly concentrated in the geographical regions where temperatures are lowest. This is illustrated in Figure 1, taken from BH04, showing distributions of Lagrangian cold points for Northern Hemisphere winter 1998/99, Northern Hemisphere summer 1999 and Northern Hemisphere winter 1997/98. The implication is that air parcels arriving in the lower stratosphere have sampled the cold temperature regions efficiently. BH04 quantify this efficiency in various ways and argue that it is in part due to the geographical distribution of vertical transport - the 'stratospheric fountain' effect suggested by Newell & Gould-Stewart [1981] - and in part due to the effects of horizontal advection - the effect suggested by Holton & Gettelman [2001].

The efficient sampling of the cold temperature regions implies that the average value of Lagrangian cold point temperature is significantly lower than an Eulerian space-time average (over the tropics) of conventional cold point temperature (i.e. the instantaneous coldest point in a vertical column). The corresponding water vapour concentrations predicted by the Lagrangian calculation are also significantly lower (by 2-3 ppmv depending on season) than those that would be predicted from Eulerian averages of the conventional cold point temperatures. F05 use a large set of Lagrangian calculations covering the period 1979-2002 and based on the ERA-40 analysis dataset to show that the predicted water vapour concentrations in good agreement with measurements both on a time-average basis over particular observation periods and on the basis of the predicted annual cycle. Figure 2 shows relevant results from F05.

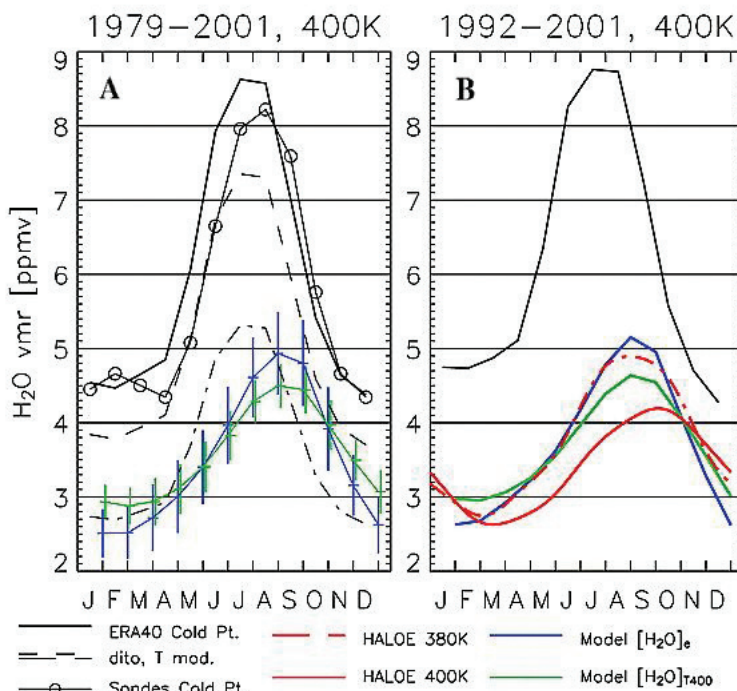


Figure 2: (Figure adapted from F05.) (A) shows seasonal variation of various predictions of stratospheric vapour concentrations for the period 1979-2001: blue - entry value calculated from Lagrangian cold point calculations (based on ERA-40 data), green - corresponding prediction of tropical lower stratospheric value using combination of entry value (for points from which back trajectories belong to TS ensemble) and climatological values (for other points) - see F05 for further details, solid black - entry value predicted from Eulerian average of ERA-40 cold point temperatures along with prediction based on artificial lowering of temperatures by 1 K (dashed) and 3 K (dash-dot), open circles - entry value predicted from radiosonde cold points taken from Seidel et al. [2001]. (B) shows corresponding quantities for 1992-2001 with HALOE measurements averaged 30°N-30°S interpolated to 400 K (solid red) and 380 K (dash-dot red).

Satellite instruments - particularly the HALOE instrument [Randel et al., 2004] - now provide a detailed quantitative picture of interannual variation in stratospheric water vapour. The trajectory calculations suggest that interannual variations in the entry value of stratospheric water vapour concentrations might be affected not only by variations in average temperatures in the tropical tropopause region, but also by geographical changes in the distribution of Lagrangian cold points. Certainly Bonazzola & Haynes [2004] show that there is significant difference between the geographical distribution of Lagrangian cold points between NH winter 1997/98, which was a strong El Niño year, and NH winter 1998/99, which was a strong La Niña year (see Figure 1). However, perhaps surprisingly, over the 1979-2002 period considered by FH05 the year-to-year variations in Eulerian average tropical temperature serve as a very good predictor of the average Lagrangian cold point temperatures. (However it should be emphasised that Eulerian average cold point temperatures are an inaccurate predictor of the absolute values of Lagrangian cold point temperatures - recall Figure 2.) Some of the results obtained by FH05 are shown in Figure 3. The major result (Figure 3a) is that during the period 1995-2002 when the water vapour measurements are most reliable and are available from two independent instruments, SAGEII and HALOE, the interannual variation in water vapour concentrations is very well predicted by the Lagrangian calculations (in the sense that the correlation between the predicted time series and one of the instrument time series is as good as that between the two instrument time series). Figure 3b shows some interesting details of the interannual variability in temperatures. The height-time temperature cross-section indicates a strong role for the quasi-biennial oscillation (QBO) with perhaps a secondary role for El Niño/La Niña variations. The level of the Lagrangian cold point is typically 90-100 hPa, which is at the very lowest limit of the QBO. It is interesting that from late 2000 onwards both SAGE

and HALOE show low water vapour concentrations, with the temperatures and the predicted water vapour consistent with this until the end of the ERA-40 data record in August 2002. Randel et al. [2004] note the upward propagation of the low concentrations into the middle stratosphere in a similar manner to the upward propagation of the 'tropical tape recorder' signal. The ECMWF operational analysis dataset suggests that cold temperatures continue at least to early 2005 and the height-latitude structure of the temperature anomalies indicates that the persistent cold temperatures over the period 2001-2004 at the cold point level may in part be interpreted as the failure of the warm phase of the QBO, visible in Figure 4 as descending from 10 hPa to 50 hPa during

2001-2002, to reach 100 hPa in late 2002/early 2003. It is clear more generally from Figure 3 that at the 100 hPa level relevant to Lagrangian cold point temperatures there is significant variation in the temperature field from one QBO cycle to the next (and hence significant variation in the implied water vapour field). Whether or not this variation is driven by tropical phenomena, or whether it is driven from the extratropics (e.g. through variation in the wave-driven upwelling) remains to be determined.

The results of the trajectory-based studies shown in Figures 2 and 3 suggest that transport and dehydration associated with the large-scale wind and temperature fields (with large-scale here meaning that resolved by ECMWF or similar analysis datasets) can account rather accurately for observed concentrations of lower stratospheric water vapour, including seasonal and interannual variation, provided that the Lagrangian character of the process is properly taken into account.

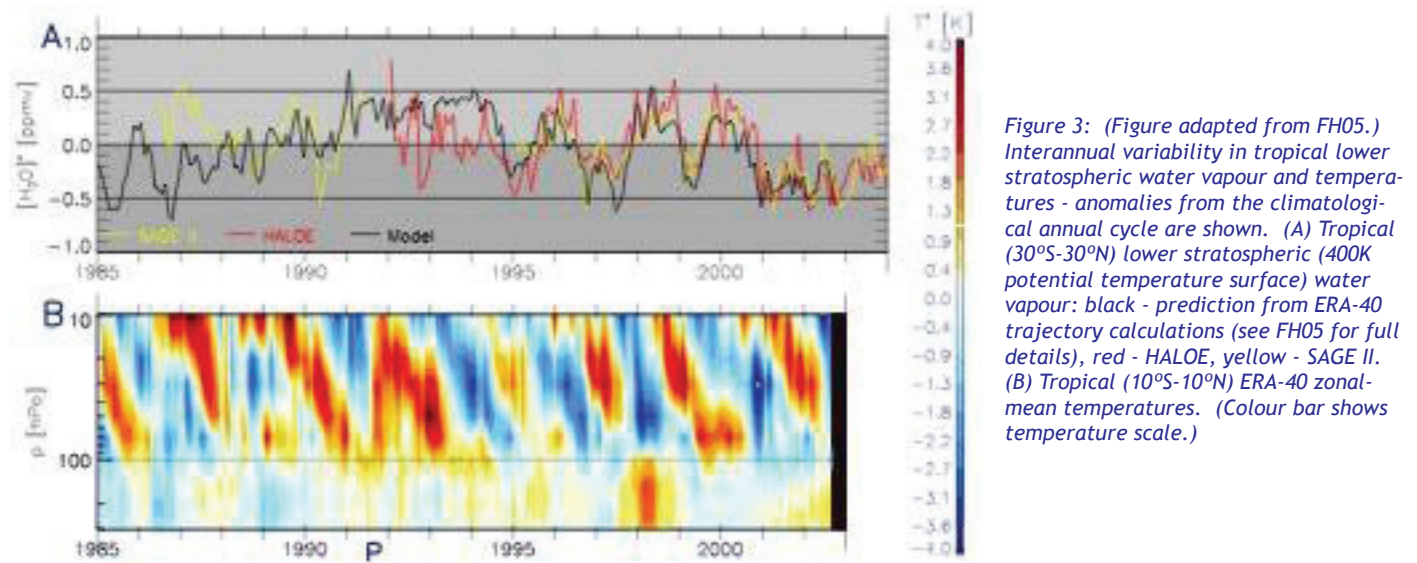


Figure 3: (Figure adapted from FH05.) Interannual variability in tropical lower stratospheric water vapour and temperatures - anomalies from the climatological annual cycle are shown. (A) Tropical (30°S-30°N) lower stratospheric (400K potential temperature surface) water vapour: black - prediction from ERA-40 trajectory calculations (see FH05 for full details), red - HALOE, yellow - SAGE II. (B) Tropical (10°S-10°N) ERA-40 zonal-mean temperatures. (Colour bar shows temperature scale.)

Some lines of future investigation of this conclusion might include the following:

(i) Does a more realistic representation of microphysical processes change this conclusion? The BH04 study considers a very simple microphysical model and find differences of 0.3-0.6 ppmv from the 'instantaneous dehydration' case. Jensen & Pfister [2004] report results from a more sophisticated model and discuss many aspects of the interplay between small-scale temperature fluctuations and microphysical processes.

(ii) What is the role of convective processes in dehydration and more generally in transport in the tropical tropopause layer? Notwithstanding the trajectory results summarised above, Webster & Heymsfield [2003] argued on the basis of isotopic measurements that both convective dehydration and gradual dehydration (the latter presumably associated with large-scale processes) played a significant role in the tropical upper troposphere.

(iii) What are the physical processes determining vertical transport in the tropical tropopause layer? The trajectory calculations suggest significant geographic variations in temperature at levels where the direct role of convection might be expected to be small. Is this consistent with radiative transfer calculations, taking account of realistic temperature structure, geographical variations in underlying cloud decks and, perhaps, thin clouds arising in the dehydration process?

Acknowledgements

The University of Cambridge component of the work described above was funded by a grant from NERC under the Clouds, Water Vapour and Climate programme (grant GST/02/2892) and by the Isaac Newton Trust. The author is grateful to M. Bonazzola, A.R. Mackenzie and C. Ren for their various contributions and, particularly, to S. Fueglistaler for his generous approach to collaboration.

References

- Bonazzola, M. and P.H. Haynes, A trajectory-based study of the tropical tropopause region, *J. Geophys. Res.*, 109, D20, D20112, 10.1029/2003JD004356, 2004.
- Fueglistaler, S., M. Bonazzola, P. Haynes and T. Peter, Stratospheric water vapor predicted from the Lagrangian temperature history of air entering the stratosphere in the tropics, *J. Geophys. Res.*, 110, doi:10.1029/2004JD005516, 2005.
- Fueglistaler, S., M. Bonazzola, H. Hatsushika, P.H. Haynes, T. Peter, H. Wernli and K. Yamazaki, Tropical Troposphere-to-Stratosphere Transport: A Lagrangian Perspective, *SPARC Newsletter* no. 25, 20-22, 2005.
- Fueglistaler, S. and P.H. Haynes, Control of interannual and longer-term variability of stratospheric water vapor *J. Geophys. Res.*, (submitted), 2005.
- Fueglistaler, S., T. Peter and H. Wernli, Tropical troposphere-to-stratosphere exchange inferred from trajectory calculations. *J. Geophys. Res.*, 109, doi:10.1029/2003JD004069, 2004.
- Hatsushika, H. and K. Yamazaki, Stratospheric drain over Indonesia and dehydration within the tropical tropopause layer diagnosed by air parcel trajectories, *J. Geophys. Res.*, 108, D4610--doi:10.1029/2002JD002986, 2003.
- Holton, J.R. and A. Gettelman, Horizontal transport and dehydration in the stratosphere, *Geophys. Res. Lett.*, 28, 2799-2802, 2001.
- Newell, R. E. and S. Gould-Stewart, A stratospheric fountain, *J. Atmos. Sci.*, 38, 2789-2796, 1981.
- Randel, W.J., F. Wu and S.J. Oltmans, Interannual changes in stratospheric water vapor and correlations with tropical tropopause temperatures, *J. Atmos. Sci.*, 61, 2133-2148, 2004.
- Rosenlof, K.H., How water enters the stratosphere, *Science*, 302, 1691-1692, 2003.
- Seidel, D.J., R.J. Ross, J.K. Angell and G.C. Reid, Climatological characteristics of the tropical tropopause as revealed by radiosondes, *J. Geophys. Res.*, 2001, 7857-7878, 2001.
- Webster, C.R. and A.J. Heymsfield, Water isotope ratios in and out of clouds map dehydration pathways, *Science*, 302, 1742-1745, 2003.

Trajectory Studies of Water Vapour Transport in the Upper Troposphere and Lower Stratosphere during the LAUTLOS Campaign

A. Lukyanov¹, A. Karpechko², M. Müller³, E. Kyrö², H. Vömel⁴, R. Kivi², V. Yushkov¹, L. Korshunov¹, S. Khaykin¹ and A. Paukkunen⁵
¹Central Aerological Observatory, Dolgoprudny, Russia; ²Arctic Research Centre (FMI/ARC), Finland; ³Alfred Wegener Institute for Polar and Marine Research, Germany; ⁴Climate Monitoring and Diagnostic Laboratory, NOAA, USA; ⁵Vaisala Oy, Finland

The main objective of LAUTLOS campaign held in Sodankylä, Finland (January-February 2004) was an intercomparison of different types of the world known balloon humidity sensors. The obtained water vapour profiles provide a good opportunity to study the distribution and variability of water vapour in the upper troposphere and lower stratosphere. Figure 1 shows the water vapour profile (blue colour) obtained by FLASH hygrometer on the 17th February 2004, which demonstrates a laminated vertical structure. We applied reverse domain filling (RDF) trajectories to analyze such a structure using ECMWF potential vorticity (PV) and specific humidity as the passive tracers. RDF trajectories revealed that water vapour laminae are caused by differential advection of air masses sampled by hygrometer. In the stratosphere air masses from the polar vortex interior and exterior were observed at adjoining vertical levels. Figure 2 shows the presence of the vortex filaments with enhanced water vapour just above Sodankylä at the levels 460 K, 530 K, 630 K corresponding to the layers of observed profiles. The layer just above the tropopause at 330 K is caused by filamentation of the tropospheric anticyclone containing a moist air. The development of anticyclone was followed by generation of thin filaments possessing larger fraction of tropospheric air than surroundings. Figure 1 also shows profiles of ECMWF water vapour (red colour) and modified PV (green colour), both directly interpolated (thin curves) and reconstructed by reverse trajectories (thick curves). The Figure demonstrates the ability of reverse trajectories to reproduce the laminated structure of tracers similar to observed one. ECMWF humidity revealed a dry bias about 1-1.5 ppmv above hygropause, which was found for every observed profile during LAUTLOS campaign.

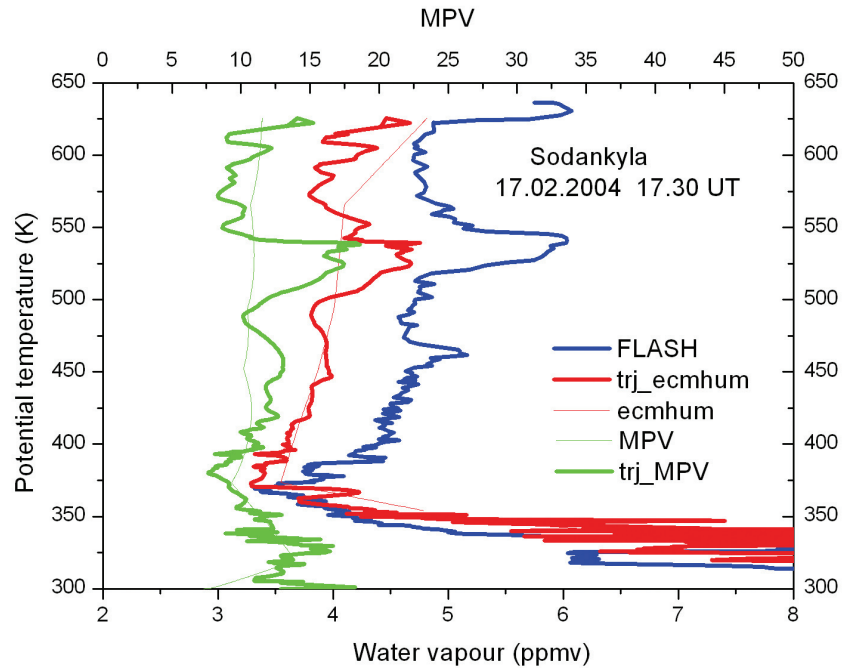


Figure 1: Vertical profiles of water vapour (FLASH -blue colour, ECMWF-red colour) and modified PV (green colour), 17th February 2004, 17.30 UT.

LAUTLOS Sodankylä 17.02.2004 10-day RDF PV

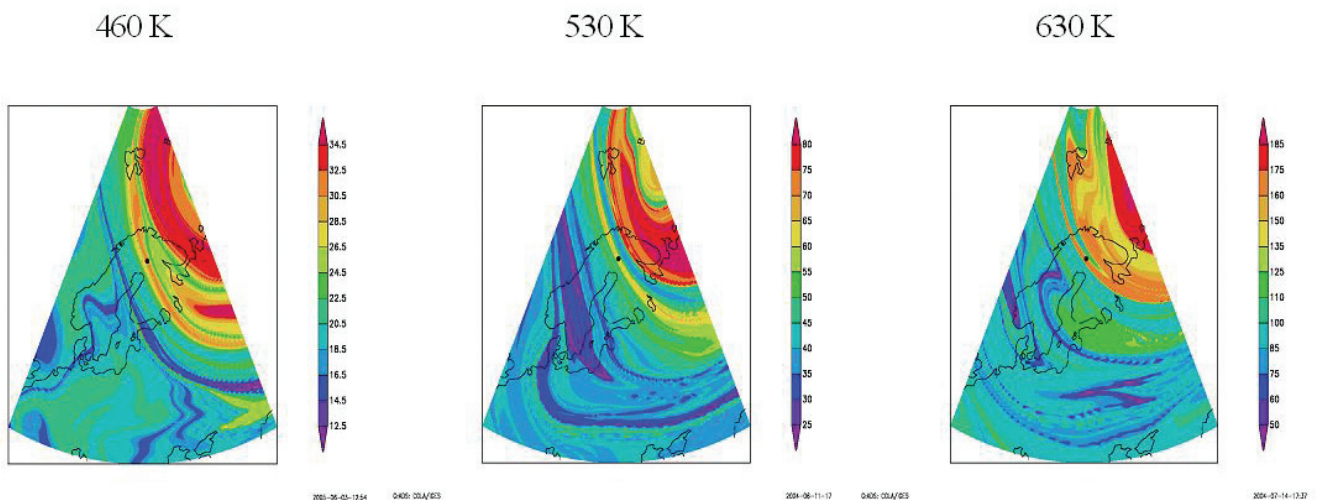


Figure 2: RDF calculations of PV at 460K, 530K, and 630K potential temperature levels, 17th February 2004, 18 UT. Sodankylä is marked with a black dot.

Also we estimated the local and instantaneous air mass fluxes through the tropopause using two methods. The first method based on Wei-formula with PV adopted as a vertical coordinate provides the quantitative estimates of air mass fluxes. The second method is fully Lagrangian based on the calculation of forward trajectories during 6 hours. Trajectories were initiated below and above the dynamical tropopause (3.5 PVU) on several pressure levels. PV was calculated along each trajectory and a location where it reached value of 3.5 PVU was considered as exchange point. Such regions of two-way transition (troposphere-stratosphere trans-

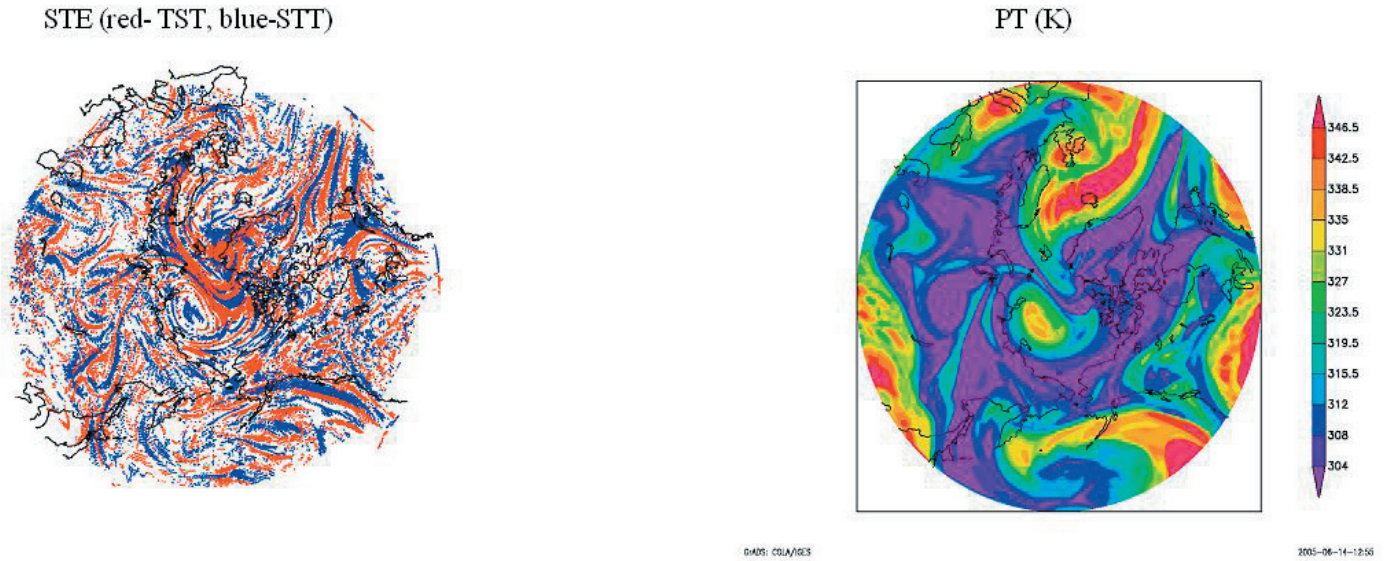


Figure 3: Locations of trajectory's transition across the tropopause (left), potential temperature level of the tropopause, 18th February 2004, 12 UT (right).

port (TST) and stratosphere-troposphere transport (STT)) on the 18th February 2004 over Northern hemisphere are shown in Figure 3 jointly with the potential temperature level of the tropopause. Figure 3 demonstrates that cross-tropopause mass exchange primarily occurs at the tropopause-slope regions. It is more clearly presented in Figure 4 where the mass fluxes in both directions have a maximum near the troughs and ridges of the tropopause and reproduce its wavy structure. Although the mean net air mass flux in Figure 3 is about zero, for ozone and water vapour the downward and upward fluxes are not equal. The Figure shows the regions where a moist tropospheric air enters to the stratosphere and ozone-rich stratospheric air goes to the troposphere. Such a thin structure of mass exchange was obtained by using ECMWF data with horizontal resolution 0.50 x 0.50. Calculations based on data with resolution 2.50 x 2.50 give completely different and unrealistic results.

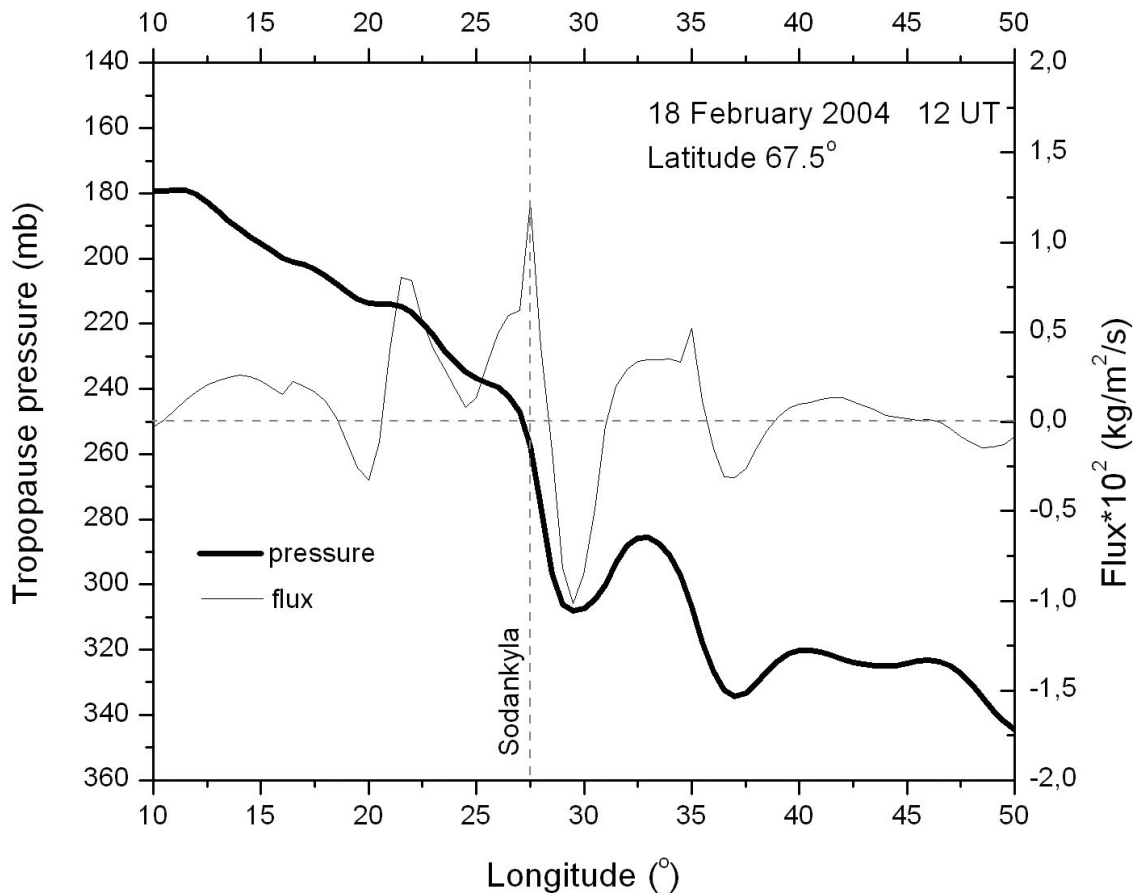


Figure 4: Pressure level of the tropopause (thick curve) and air mass flux (thin curve) along the latitude 67.50°N, 18th February 2004, 12 UT.

A Trajectory-Based Investigation of Tropopause Moistening in the Asian Summer Monsoon Region

N. Patmore and R. Toumi

Space and Atmospheric Physics, Blackett Laboratory, Imperial College, London, England

Using satellite and reanalysis data, we investigate the source of an extensive moist pool, which spans the tropopause layer over the arid regions to the west of India from June to August (JJA). The pool is a dominant feature of the global upper troposphere and lower stratosphere water vapour distribution, extending from ~ 150 to 70 hPa. Using HALOE data, Jackson et al. [1998] and Randel et al. [2001] demonstrate that its formation is associated with diabatic water vapour transport. However, the source of the moistening remains speculative.

We show that the moist pool is present in the ERA-40 reanalysis and use trajectories to reveal large-scale source regions. Finally, we analyse the water vapour budget to ascertain the importance of smaller-scale processes. We find that in the upper troposphere there are two dominant source regions: one over north-west India and another over the Middle East. At higher levels, sources are less localised. Through the budget analysis, we show that smaller scale processes may also be important.

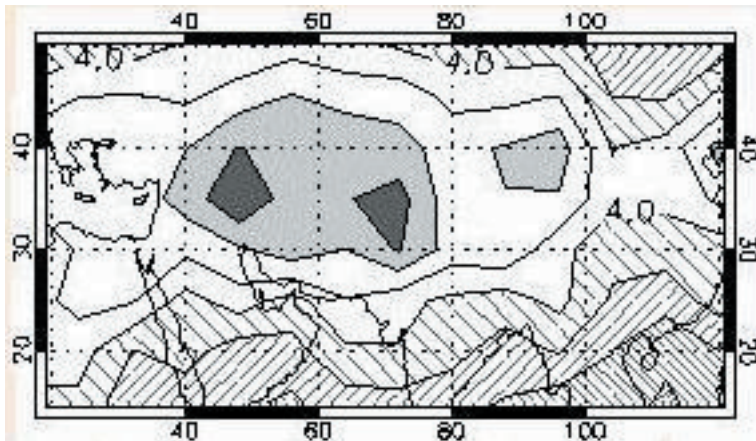


Figure 1: HALOE water vapour (July-August 1993-2000) at 395K. Contour interval: 0.2ppmv.

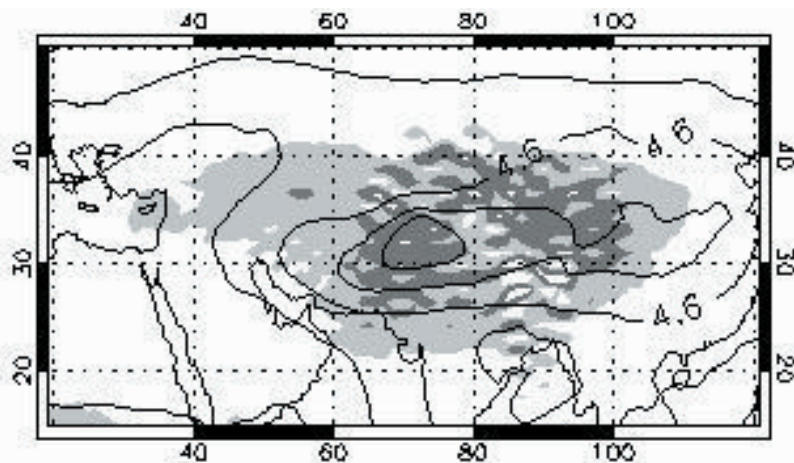


Figure 2: ERA-40 water vapour (contours) and PV (shading) July-August 1993-2000. Contour interval: 0.2ppmv, shaded $<6, 6.5$ p.u.

launched from isentropic levels across the tropopause layer over southern Asia. These were filtered to give a sample with initial locations within the pool (defined as those with an initial PV less than derived criteria).

We find that:

- The majority of trajectories experience significant cross-isentropic motion (up to 25 K in 8 days at 375 K).
- Over 70% of trajectories ascend cross-isentropically from a lower level.
- Over 70% of trajectories remain trapped in the anticyclone during the experiment.

In summary, the majority of trajectories arrive at the moist pool by circulating around the monsoon anticyclone through the upper troposphere and lower stratosphere, experiencing significant diabatic heating and cooling within its boundaries.

To locate specific source regions, we trace backward along the moist pool trajectories and record where they first cross certain isentropic surfaces. Figure 3 shows the densities of trajectories ascending through a surface 10 K below two of the launch levels.

HALOE and ERA-40 Climatologies

The moist pool is clearly visible in HALOE observations up to 430 K; Figure 1 shows the pool at 395 K. Previous authors assume that the pool is formed from the moist outflow of the monsoon convection (around the Bay of Bengal and south-east Asia), but this region remains relatively dry in the upper troposphere and lower stratosphere.

HALOE ozone observations show minima in the moist pool region. The vertical gradients of both tracers suggest that air is being advected from below. Unexpectedly, we find that a region of high ozone overlies the main monsoon convection.

Figure 2 is the equivalent ERA-40 water vapour climatology (contours). The presence and general consistency in location of the pool suggests that ERA-40 is adequately representing the processes involved in its formation. The shading shows areas of low potential vorticity (PV); here indicating the core of the monsoon anticyclone. The moist pool is clearly constrained by the strong PV gradient of the anticyclone. The isentropic gradient in PV between the moist pool and the monsoon convection is consistent with the gradients of water vapour and ozone shown by HALOE. The presence of this PV gradient implies that, on average, the outflow from the monsoon can not stir directly into the moist pool. If this is the case: where does the moisture come from?

Trajectory Study

To reveal the sources of the moist pool, we analyse the paths of trajectories entering the low PV core of the anticyclone. Trajectories are calculated from an offline model that uses ERA-40 reanalysis 3D winds.

Over 400 thousand 8-day back-trajectories were

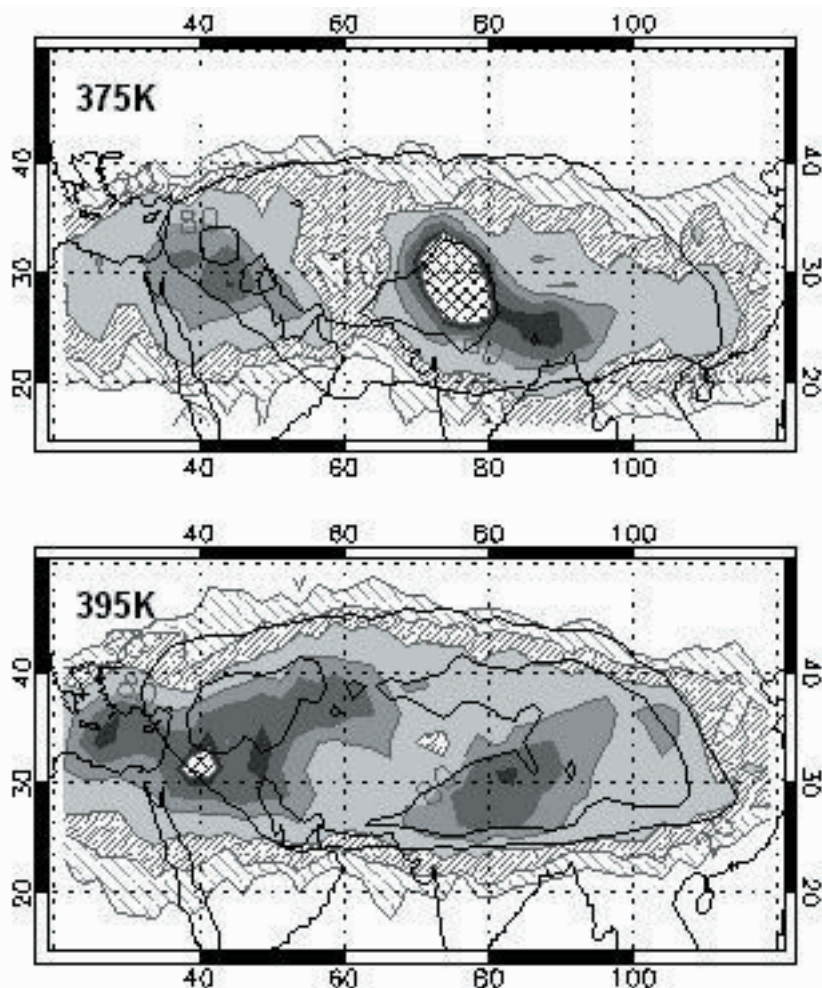


Figure 3: Densities of trajectories ascending through surfaces 10 K below the 375 K and 395 K launch levels. Contours: 5, 10, 20, 40, 60, 80, 120 crossings per 2.5° grid-box. Hatched shading < 20, cross-hatched shading >120.

The 375 K result is most significant, as this shows the source regions of moistening coming from outside the tropopause layer (365 K). Here, there are two dominant source regions: one over the Himalayas and another over the Middle East. Very few trajectories originate from the main monsoon convective regions (consistent with the PV barrier hypothesis), however the Himalayan source could be regarded as the monsoon outflow in the upper troposphere and lower stratosphere. This air tends to be slightly dryer, possibly due to convective dehydration. At higher levels, the source regions become more diffuse, spreading around the anticyclone. We also find significant descent (not shown): dry air diabatically cools almost vertically through the centre of the anticyclone. At all levels, descent tends to be dominant, suggesting that, contrary to observations, the large-scale fields are acting to dehydrate the pool.

The Reanalysis Water Vapour Budget

An investigation of the reanalysis water vapour budget confirms that the large-scale fields are acting to dehydrate the moist pool. We calculate that small-scale processes must balance over 25% of the vertical flux to sustain the moist pool in the anticyclone's core. These could include microphysical processes or sub-grid scale transport, such as vertical diffusion. Further analysis is required to quantify these sources.

Acknowledgements

Thanks to J. Methven for providing the offline trajectory model and to NERC for funding this research. ECMWF ERA-40 and HALOE data were obtained via the British Atmospheric Data Centre.

References

- Jackson, D.R., S.J. Driscoll, E.J. Highwood, J.E. Harries and J.M. Russell III, Troposphere to stratosphere transport at low latitudes as studied using HALOE observations of water vapour 1992-1997, *Q.J.R. Meteorol. Soc.*, 124, 169-192, 1998.
- Randel, W.J., F. Wu, A. Gettelman, J.M. Russell, J.M., Zawodny and S.J. Oltmans, Seasonal variation of water vapour in the lower stratosphere observed in Halogen Occultation Experiment data, *J. Geophys. Res.*, 106, D13, 14313-14325, 2001.

Upper Troposphere Lower Stratosphere Water Vapour Budget from Mesoscale Simulations in the frame of the HIBISCUS Project

V. Marécal¹, E.D. Rivière¹ and G. Durry²
¹LPCE, Orléans, France; ²GSMA, Reims, France

Introduction

The RAMS-Chemistry model [Cotton et al., 2001; Marécal et al., 2005] was run in the frame of the HIBISCUS project in order to understand the chemical, microphysical and dynamical processes that govern the distribution of chemical species and water vapour in the Tropical Tropopause Layer (TTL). The RAMS-Chemistry model is a limited-area atmospheric model coupled on-line with a chemistry model. The present modelling work was done in coordination with the balloon-borne measurements carried out during the HIBISCUS field campaigns that took place in Bauru (Brazil, 49° W 22.3° S). Two case studies have been modelled: a large scale system associated with a surface cold front and a heavy tropical convective system. Vertical water vapour fluxes have been calculated from both simulation outputs as a first attempt to study the stratosphere/troposphere exchanges of water vapour for these two different meteorological systems.

Large Scale System

The large scale frontal system was observed on 13th and 14th February 2004. The locations of the front and the associated cloud bands simulated by the model show a fairly good agreement with satellite observations at the different stages of the front evolution. Balloon-borne measurements of water vapour were obtained from the micro-SDLA (Spectromètre à Diode Laser Adjustable) [Durry & Mégie, 1999] around 23UT on 13th February 2004 near Bauru. The model results for water vapour mixing ratio and temperature have been compared to the balloon-borne observations (Figure 1). The model provides realistic results up to 13.5 km altitude. In the 13.5 to 16 km altitude layer, the model is significantly moister than micro-SDLA. This is related to a too warm air temperature in the model compared to observations (see Figure 1b) leading to insufficient dehydration by ice condensation. In

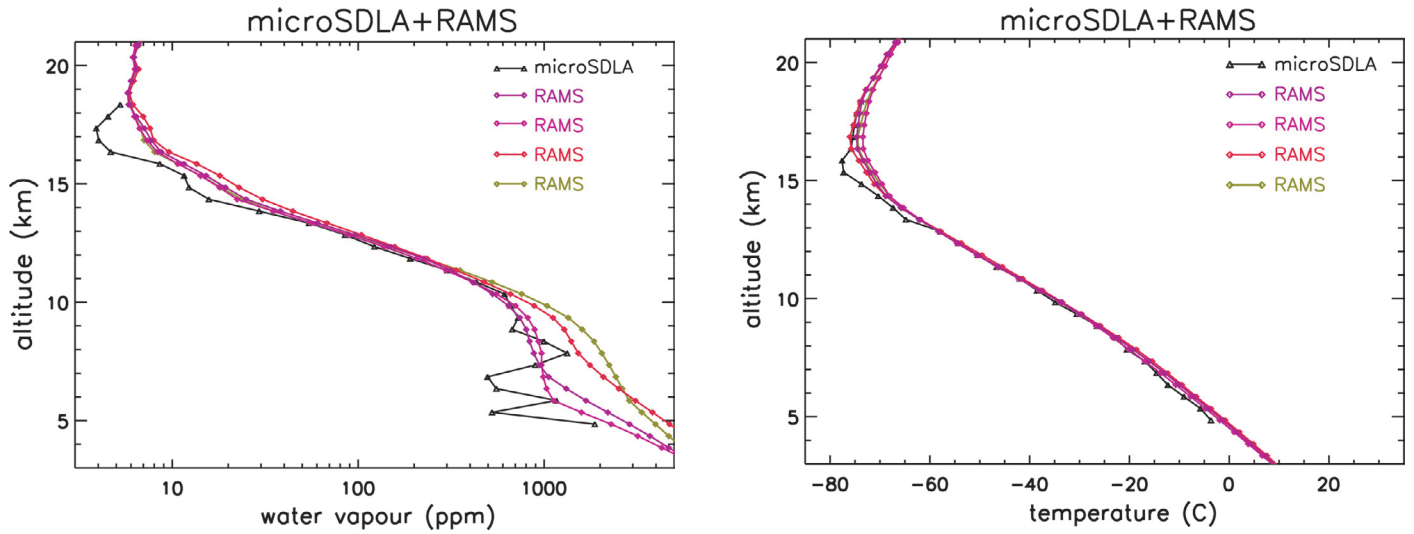


Figure 1: Comparison between micro-SDLA measurements and 4 RAMS model profiles at the time and location of the balloon-borne measurements. The observations are averaged on the model vertical grid. Left: water vapour in ppmv; Right: temperature in °C.

the 16-18.5 km layer, the model is moister than microSDLA measurements while simulated temperatures are realistic. In this layer, the model water vapour field depends on the ECMWF analyses used to constraint the mesoscale model.

The water vapour flux averaged over the domain were the system develops is shown as a function of time for different altitude levels in Figure 2. The mean flux is positive at any level and any time, meaning that there is an upward flux of water vapour on average which is due the large scale slow ascent associated with the frontal system. There is a correlation with time between the different altitude levels, with smoother variation as altitude increases. These two last results are consistent with the off-line trajectory analysis. A first qualitative analysis have shown that the variations with time of the fluxes seems to be related to the variations of intensity of both the large scale slow ascent and downward motions associated with the frontal system.

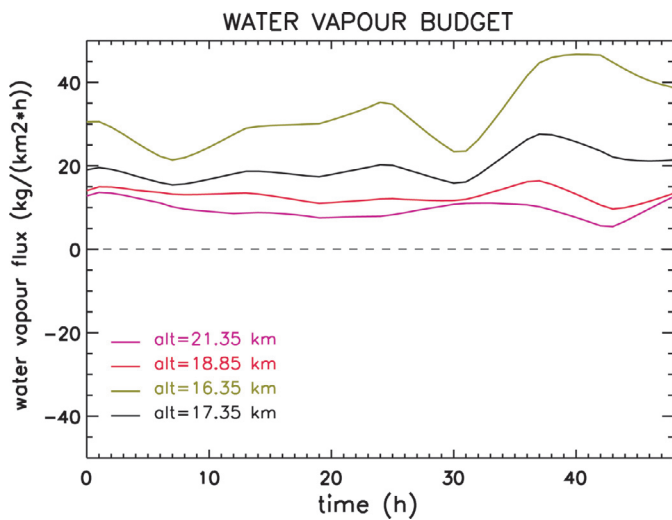


Figure 2: Mean water vapour flux as a function of time. Time=0 corresponds to the 13th February 2004 at 00UT.

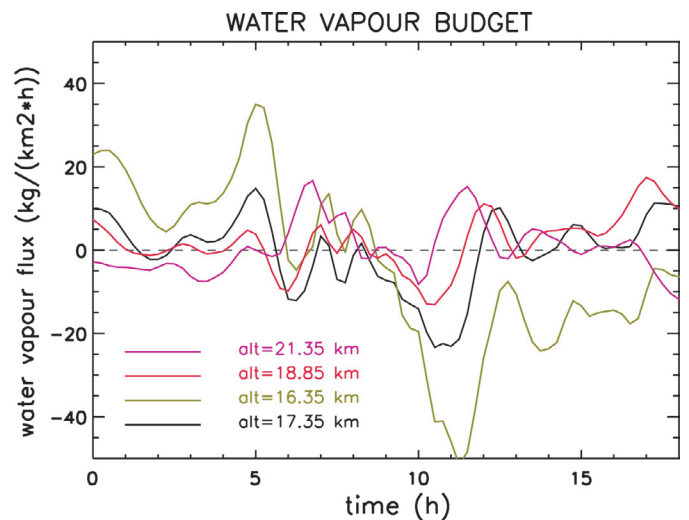


Figure 3: Mean water vapour flux as a function of time. Time=0 corresponds to the 8th February 2001 at 12UT.

The Convective System

The convective system observed on 8th February 2001 was a very intense precipitating system composed of a cluster of individual convective cells. The convective system started to develop around 15UT with a maximum of convective activity around 22UT. Model simulation results for rainfall rates and cloud tops are in agreement with the Bauru radar observations. The water vapour flux averaged over the convective area is shown in Figure 3. The main difference with the large scale system is that for the convective system there are both upward and downward mean fluxes. In particular, mean downward fluxes are obtained for a period of several hours when the convection intensity is at its maximum. This could be possibly explained by wave breaking due to the interactions between the different convective cells. The off-line trajectory analysis do not shown evidence of such a process but this is possibly due to the rapid evolution of the convective system that may not be captured by the off-line trajectory technique. A complementary study is currently done at LMD (CNRS, France) on the analysis of the wave energy from the model outputs.

Conclusions and Discussion

The RAMS-Chemistry mesoscale model has been run to simulate two different meteorological systems observed during the HIBIS-CUS field campaigns. The present work has shown that Eulerian calculations of water vapour fluxes provide information on the stratosphere/troposphere exchanges. But these fluxes calculations cannot be interpreted unless other tools are used. In particular, a trajectory analysis is a complementary tool for analysing the model results. These trajectories can be calculated off-line for precipitating systems that develops slowly but for convection that evolves rapidly, an on-line trajectory calculation as proposed by

Gheusi et al. [2004] seems more appropriate. Also, for convection studies a complementary wave analysis can be of importance since convection generates.

The objective of meso-scale simulations is a better understanding of the dynamical/microphysical/chemical processes that influences tropical upper troposphere and lower stratosphere air composition and that are associated to tropical meteorological systems and in particular to convection. This is made possible because:

- the model horizontal and vertical resolutions can be modified and adapted to the considered meteorological system;
- the model outputs can be compared to the balloon-borne observations for validation purposes. These comparisons are meaningful since a fine resolution is used for simulating precipitation systems; and
- the microphysics can be explicitly resolved by the model avoiding the use of convective parameterisation.

The analysis of processes at small/mesoscale by meso-scale models such as RAMS-Chemistry is a necessary step to improve the global model parameterisations.

References

- Cotton, W.R., R.A. Pielke Sr., R.L. Walko, G.E. Liston, C.J. Tremback, H. Jiang, R.L. McAnelly, J.-Y. Harrington, M.E. Nicholls, G.G. Carrio and J.P. McFadden, RAMS 2001: Current status and future directions, Meteorol. Atmos. Phys., 82, 5-29, DOI 10.1007/s00703-001-0584-9, 2003.
- Gheusi, F., J.-P. Cammas, F. Cousin, C. Mari and P. Mascart, Quantification of mesoscale transport across the boundaries of the free troposphere: a new method and applications to ozone, Atmospheric Chemistry and Physics Discussions, 4, 8103-8139, 2004.
- Marécal V., E. Rivière, G. Held, S. Cautenet and S. Freitas, Modelling study of the impact of deep convection on the UTLS air composition. Part I: analysis of ozone precursors, Accepted for publication in Atmospheric Chemistry and Physics Discussion, 2005.

The Influence of Future Climate Change on Tropospheric Ozone

D.S. Stevenson and the ACCENT modelling team*
Department of Meteorology, University of Edinburgh, Scotland

In terms of radiative forcing of climate since the pre-industrial era, tropospheric ozone (O_3) is the third most potent greenhouse gas, with a forcing roughly one quarter of that due to increases in carbon dioxide. Ground-level O_3 is also a ubiquitous and toxic air pollutant, causing damage to plant and animal tissues. These twin roles of O_3 - influencing both climate change and air quality - make it a key gas for policymakers to understand and control, in terms of both its present-day and future distributions. The major driver of increases in tropospheric O_3 to date has been rising levels of anthropogenic emissions of its precursors, in particular nitrogen oxides (NO_x), carbon monoxide (CO), methane (CH_4) and other volatile organic compounds (VOCs). These emissions will continue to evolve in magnitude and distribution - partly through increases in the rapidly developing parts of the world (e.g., S.E. Asia) - but also through decreases brought about by the implementation of air pollution legislation (e.g., the introduction of catalytic converters on motor vehicles), particularly in the relatively highly developed parts of the world (e.g., Europe, N. America, Japan). Whilst future emissions are likely to be the major control on O_3 , as the physical climate changes, there are also likely to be several important climate-related mechanisms that will affect O_3 .

In order to perform an up-to-date assessment of the influences on future tropospheric O_3 (and other important species), two major model inter-comparison exercises have been co-ordinated within the framework of ACCENT ('Atmospheric Composition Change: the European NeTwork of excellence'; <http://www.accent-network.org>). In the first experiment [Gauss et al., submitted], the focus was on radiative forcing from O_3 changes in both the stratosphere and the troposphere, and the time frame considered was 1860-2000-2100. In the second experiment [Dentener et al., submitted; Stevenson et al., submitted], the time frame considered was 'the next generation' (2000-2030), and there were several foci: O_3 air quality; nitrogen and sulphur deposition; model validation using satellite data; O_3 radiative forcing; and chemistry-climate feedbacks. In this second experiment, we evaluated three 2030 emissions scenarios, ranging from 'optimistic', through 'likely', to 'pessimistic', and for the central emissions case, also assessed the influence of climate change. This article presents results from the second experiment, and in particular the effects of climate change on tropospheric O_3 in 2030.

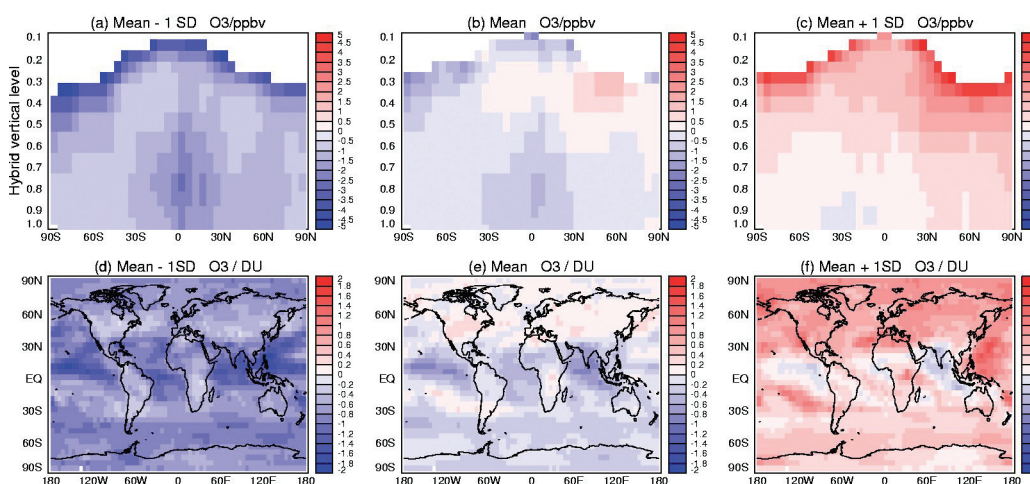
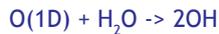


Figure 1: Ozone changes due to climate change 2000-2030. The central panels show the ensemble mean change from 9 models - panels either side show the mean plus/minus 1 standard deviation.

Over twenty models performed simulations of the 2000 and 2030 emissions scenarios; a subset of nine models performed the climate change simulation. Figure 1 shows the impact of climate change in 2030 on annual zonal mean O_3 and tropospheric column O_3 for the ensemble of nine models, and also shows the results one standard deviation either side of the mean. Figure 1b shows that the mean impact of climate change is to increase O_3 in the tropical and Northern Hemisphere (NH) upper

troposphere (UT); decreases occur elsewhere, particularly in the Southern Hemisphere (SH) upper troposphere and the tropical lower troposphere (LT). Ozone budgets (not shown) reveal that the upper troposphere increases are mainly related to enhanced influx of O₃ from the stratosphere, associated with an increased Brewer-Dobson circulation - on average, this mechanism has a stronger impact in the Northern Hemisphere. The budgets also reveal that the O₃ decrease in the tropical lower troposphere is associated with an enhanced loss of odd oxygen (O₃ plus oxygen atoms) through the reaction:



This reaction is the major mechanism for tropospheric O₃ destruction, and water vapour concentrations rise with temperatures in climate models, broadly following the Clausius-Clapeyron equation.

Figure 1 also illustrates the large degree of uncertainty concerning the overall sign of the climate feedback on tropospheric O₃, as illustrated by the left- and right-hand panels, which show the mean model \pm one standard deviation. The negative water vapour feedback is evident in all three zonal mean plots, but is largely swamped by positive feedbacks (predominantly increases in the stratospheric influx) at one standard deviation above the mean response. Towards the other end of the model responses (one standard deviation below the mean), the water vapour feedback dominates over the whole troposphere. Other regionally important climate-ozone feedbacks include changes in the magnitude and distribution of lightning NO_x and biogenic VOC emissions.

To summarise, this study has shown that there is currently no consensus amongst models on the overall sign for the feedback of climate change on global tropospheric O₃. Nevertheless, two competing processes appear crucial: (i) the increase in water vapour associated with warming, and its impact on O₃ destruction; and (ii) increases in the stratospheric influx of O₃. Improved understanding of these two mechanisms is required to further constrain the likely impacts of future climate change on tropospheric O₃.

References

- Dentener, F.J., D.S. Stevenson, K. Ellingsen, et al., The global atmospheric environment for the next generation, submitted to *Geophys. Res. Lett.*, 2005.
- Gauss, M., G. Myhre, I.S.A. Isaksen, et al., Radiative forcing since pre-industrial times due to ozone change in the troposphere and the lower stratosphere, *Atmos. Chem. Phys. Discuss.*, 5, 5751-5807, 2005.
- Stevenson, D.S. F.J. Dentener, M.G. Schult et al., Multi-model simulations of present-day and near-future tropospheric ozone, submitted to *J. Geophys. Res.*, 2005.

*The ACCENT modelling team (Experiment 2):

D.S. Stevenson¹, F.J. Dentener², M.G. Schultz³, K. Ellingsen⁴, T.P.C. van Noije⁵, O. Wild⁶, G. Zeng⁷, M. Amann⁸, C.S. Atherton⁹, N. Bell¹⁰, D.J. Bergmann⁹, I. Bey¹¹, T. Butler¹², J. Cofala⁸, W.J. Collins¹³, R.G. Derwent¹⁴, R.M. Doherty¹, J. Drevet¹¹, H.J. Eskes⁵, A.M. Fiore¹⁵, M. Gauss⁴, D.A. Hauglustaine¹⁶, L.W. Horowitz¹⁵, I.S.A. Isaksen⁴, M.C. Krol², J.-F. Lamarque¹⁷, M.G. Lawrence¹², V. Montanaro¹⁸, J.-F. Müller¹⁹, G. Pitari¹⁸, M.J. Prather²⁰, J.A. Pyle⁷, S. Rast³, J.M. Rodriguez²¹, M.G. Sanderson¹³, N.H. Savage⁷, D.T. Shindell¹⁰, S.E. Strahan²¹, K. Sudo⁶, and S. Szopa¹⁶

¹University of Edinburgh, School of Geosciences, Edinburgh, United Kingdom; ²Joint Research Centre, Institute for Environment and Sustainability, Ispra, Italy; ³Max Planck Institute for Meteorology, Hamburg, Germany; ⁴University of Oslo, Department of Geosciences, Oslo, Norway; ⁵Royal Netherlands Meteorological Institute (KNMI), Atmospheric Composition Research, De Bilt, the Netherlands; ⁶Frontier Research Center for Global Change, JAMSTEC, Yokohama, Japan; ⁷University of Cambridge, Centre of Atmospheric Science, United Kingdom; ⁸IIASA, International Institute for Applied Systems Analysis, Laxenburg, Austria; ⁹Lawrence Livermore National Laboratory, Atmospheric Science Division, Livermore, USA; ¹⁰NASA-Goddard Institute for Space Studies, New York, USA; ¹¹Ecole Polytechnique Fédérale de Lausanne (EPFL), Switzerland; ¹²Max Planck Institute for Chemistry, Mainz, Germany; ¹³Met Office, Exeter, United Kingdom; ¹⁴rdscientific, Newbury, UK; ¹⁵NOAA GFDL, Princeton, NJ, USA; ¹⁶Laboratoire des Sciences du Climat et de l'Environnement, Gif-sur-Yvette, France; ¹⁷National Center of Atmospheric Research, Atmospheric Chemistry Division, Boulder, CO, USA; ¹⁸Università L'Aquila, Dipartimento di Fisica, L'Aquila, Italy; ¹⁹Belgian Institute for Space Aeronomy, Brussels, Belgium; ²⁰Department of Earth System Science, University of California, Irvine, USA; ²¹Goddard Earth Science & Technology Center (GEST), Maryland, Washington, DC, USA.

Stratosphere Troposphere Exchange

Rapporteur: A. Waterfall, Rutherford Appleton Laboratory, Oxfordshire, England

The final session of the meeting consisted of five presentations on the topic of 'Stratosphere Troposphere Exchange'. An initial 45 minute presentation was given by P. Haynes, from the University of Cambridge, entitled 'Trajectory-Based Studies of Dehydration in the Tropical Tropopause region'. This outlined a trajectory based approach to studying dehydration and discussed results pertaining to the seasonal climatology and interannual variability of stratospheric water vapour, and the seasonal and interannual variability in tropical tropopause temperature, and highlighted various outstanding issues.

In a number of recent studies a trajectory based approach has been used to study dehydration. The basic theory outlined in the presentation was that the 'Lagrangian cold point' sets the entry value of water vapour into the stratosphere, and that therefore by using back trajectories and the temperature history of the air parcel it is possible to build up a picture of stratospheric water vapour which agrees much better with observations than that obtained using a conventional Eulerian approach. The contributions of different transport processes to dehydration were also estimated, and it was found that those of horizontal transport and the stratospheric fountain were of similar magnitude. In climatological studies using back trajectories from 1979-2001 from ERA 40, it was found that in most seasons the Lagrangian cold point was centred on the Western Pacific (where temperatures are coldest). One exception to this was the Northern Hemispheric winter of 1997/98, a strong El Niño year, in which the region where the trajectories experienced their minimum temperature was much more evenly spread. During the Northern Hemisphere summer, there was also a region over SE Asia, and a worse match was seen between where the trajectories experienced their minimum temperatures and where the coldest temperatures were located.

Results were then presented on the interannual variation in the absolute values of stratospheric water vapour. It was found that from 1995 onwards the anomalies from the average seasonal cycle gave as good a match to HALOE data as was found between HALOE and SAGE. However in 1993/94, the model predicted significantly larger values than HALOE. The variation in the model was driven by the temperatures around the 100 mb level; the temperature anomalies at this level were said to be a good predictor of the Lagrangian cold point anomalies. Finally, the seasonal and interannual variation of the tropical lower stratosphere temperature was discussed. A drop in temperature has been seen since 2000, and work currently in progress was presented with the aim of investigating whether this could be explained by changes in the stratospheric wave driving. Some evidence for a drop in temperature was seen using a simple model.

The second presentation was given by A. Lukyanov from the Central Aerological Observatory, in Russia on 'Trajectory studies of water vapour transport in the UTLS during the LAUTLOS campaign'. The LAUTLOS campaign took place in Sodankylä, Finland during January and February 2004, with the main objective being the intercomparison of different types of balloon humidity sensors. In this presentation, water vapour measurements from the FLASH-B instrument taken during the campaign were utilised, and the results of trajectory studies looking at stratosphere-troposphere exchange and cross-tropopause fluxes were described. It was found that the laminar vertical structure of water vapour during the campaign was mainly caused by differential advection between air masses with different origins present at adjoining vertical levels. A dry bias in the ECMWF data of the order of 1 - 1.5 ppmv was seen in comparison to the measurements.

The next presentation was given by N. Patmore, from Imperial College, entitled 'Muddling Processes in the UTLS over the Asian Summer Monsoon'. This described the results of trajectory analyses to study the origin of an extensive tropopause moist pool overlying the desert region of South-East Asia, to the west of the main monsoon region. The authors showed that the moist pool is constrained within the core of an anticyclone by a PV barrier. This prevents outflowing air from the monsoon convective regions contributing directly to the moist pool as had been previously thought. Ascending trajectories spiral upwards around the edge of the anticyclone, whilst air descends through the centre of the anticyclone. Dominant source regions were identified, although the mechanisms involved are unclear. Analysis of the ERA 40 water vapour budget suggested that sub-grid scale processes may also be important in maintaining the moist pool.

The fourth presentation was by V. Marécal, from CNRS, France on the 'UTLS water vapour budget from mesoscale simulations in the frame of the HIBISCUS project'. This described the results of a modelling study with the 3D mesoscale model, RAMS, for two case studies from the HIBISCUS field campaigns that took place in Bauru, Brazil in 2001 and 2004. The first case study concentrated on a large scale driven precipitating system which occurred on the 13th-14th February 2004, whilst the second case study focussed on heavy convection around Bauru on the 8th February 2001.

There was found to be a difference in the water vapour fluxes in the upper troposphere and lower stratosphere between the two cases. In the first there was an upward flux for water vapour related to large scale slow ascent, consistent with the trajectory analysis. In contrast the mean flux of water vapour for the convective system in the second case study had both positive and negative values. Correlations observed between tropospheric and stratospheric levels related to wave activity.

The final presentation in the session was by D. Stevenson from the University of Edinburgh, and was entitled 'Climate feedbacks on tropospheric ozone'. Tropospheric ozone is the third largest greenhouse gas, is closely coupled to OH and CH₄ lifetime and at ground level is an air pollutant. Most studies of future ozone concentrations focus on emission trends but climate feedbacks may also be important. Results from an intercomparison of the tropospheric ozone distributions predicted for a set of future climate scenarios by twenty five models, as part of the ACCENT project, were shown. The results showed that there are two important feedbacks of the climate on tropospheric ozone; a negative feedback due to water vapour via an increased ozone loss, and a positive feedback due to an increase in the stratospheric influx of ozone. However, there was no consensus between the models on which process dominated. Feedbacks from lightning and isoprene emissions seemed to be less important globally, whilst other potential feedbacks have not yet been analysed.

